Nanometer-Scale Surface Modification Using the Scanning Probe Microscope: Progress since 1991

R. M. Nyffenegger and R. M. Penner*

Institute for Surface and Interface Science, The Department of Chemistry, University of California, Irvine, Irvine, California 92697-2025

Received September 27, 1996 (Revised Manuscript Received February 6, 1997)

Contents

I.	Introduction	1195
II.	Principles of SPL	1196
	A. Mechanical Modification	1196
	B. Electrical Modification	1196
	C. Optical (or Optically Assisted) Modification	1197
III.	Experimental Considerations, and Instrumentation	1198
	A. Instrumentation	1198
	B. Sample Preparation	1199
	C. Probes	1199
IV.	Results	1200
	A. Electrical SPL Methods	1200
	1. Direct Modification of the Surface	1200
	2. Organic Materials as Lithographically Active Layers	1205
	3. Material Transfer Between Tip and Surface	1209
	4. Chemical Vapor Deposition	1211
	5. In Situ SPL in Liquids	1212
	6. Atomic-Scale Modification Processes	1215
	7. Applications	1216
	B. Mechanical SPL Methods	1217
	1. Direct Modification of the Surface	1217
	2. Organic Materials as Lithographically Active Layers	1219
	C. Optical SPL Methods	1221
	1. Laser-Assisted Lithography	1221
	2. Near-Field Optical Microscopy (NSOM)	1222
V.	Conclusions and Outlook	1223
	A. Summary of Experimental Observations	1223
	B. Performance of the Different Techniques	1224
	1. Device Fabrication	1224
	2. Data Storage Fabrication	1225
	C. SPL Applications and the Future	1225
VI.	Glossary	1226
VII.	Acknowledgments	1226
VIII.	References	1226

Ralph Nyffenegger was born in 1965 in Bern, Switzerland, where he grew up and received his masters diploma in 1990 and his Ph.D. in 1994, both in chemistry from the University of Bern. Since, he has been a post-doctoral fellow at UCI with Professor Penner. At UCI he is currently involved in the development of novel SPM techniques and in the synthesis and characterization of zinc-based semiconductor nanoparticles.

Reg Penner was born in 1960, grew up in rural Minnesota, and attended Gustavus Adolphus College in Saint Peter, MN, graduating in 1983. He received a Ph.D. in Chemistry from Texas A&M University in 1987, and held postdoctoral appointments at Stanford and Caltech prior to moving to UCI in 1990 where he is currently Associate Professor of Chemistry. At UCI, his research group focuses on the development of methods for electrochemically synthesizing nanometer scale materials and on characterizing these materials using electrochemistry, microscopy, and spectroscopy.

I. Introduction

Soon after the invention of the scanning tunneling microscope (STM)[1] and the scanning or atomic force microscope (SFM/AFM),[2] researchers found that subsequent images of an area sometimes revealed different topography. This observation indicated that scanning could alter the surface. After recognizing this fact, only a small step was required in order to undertake these modifications in a controlled way.[3−5] In recent years, scanning probe-based lithography (henceforth SPL[6]) has attracted the attention of a large number of research groups, as evidenced by the fact that this review encompasses over 300 publications. Current work in the area of SPL has tremendous scope both in terms of the distance scales which are involved, which range from the atomic scale, e.g., single atom manipulation[7,8] to line drawing in the 50 μm range,[9] and in terms of the variety of instrumen-

* Address correspondence to this author at rmpenner@uci.edu.

S0009-2665(96)00069-6 CCC: $28.00 © 1997 American Chemical Society

tation which have been employed. The objectives of research in the area of SPL are equally diverse—atomic scale experiments have been aimed primarily at extending the current understanding of the physics of the *surfaces themselves*, while nanometer scale SPL work has either been driven by technological applications for this science, such as high-density memories, or by fundamental interest in the chemistry and physics of the *modified regions* or the nanometer-scale materials which are produced.

Several trends are recognizable in the SPL literature published since 1991. First, the five year period under consideration has witnessed the emergence of entirely new scanning probe microscopy (SPM) methods including the widespread introduction of noncontact and lateral (or frictional) atomic force imaging modes in commercial instrumentation, and near-field optical microscopy (NSOM).[10] Concurrently, new SPL methods, based on the unique capabilities of these instruments, have also appeared. Secondly, SPL is beginning to take on some of the characteristics of a mature area of scientific inquiry. Specifically, in the recent literature, greater emphasis has been focused on fundamental investigations of modification mechanisms—work aimed at achieving an understanding of the chemical or physical mechanism operating in modification experiments of various types. Finally, the capabilities of SPL methods introduced in the late 1980s have been dramatically improved in several instances. Examples include the STM-based CVD deposition of metals, the field-emission mode STM modification of polymer resist films, and the STM-based electrochemical deposition of materials.

Although the historical record for SPL spans just 10 years, a large volume of papers have appeared during this period (over 500 papers). SPL advances during the first half of this period have been reviewed.[6,11,12] Therefore, to avoid redundancy, we focus here on work published in the last five years (1991 publication date or later). SPM investigations encompass distance scales ranging from 0.1 nm (e.g., single atom deposition or removal) to 1.0 μm (involving perhaps 10^6-10^9 atoms). At the extremes of this range, the methodologies which are employed are substantially different: Atomic-scale SPL typically requires an ultrahigh vacuum environment and/or cryogenic sample temperatures, whereas for SPL modification at the $\sim$10−100 nm scale, it is frequently possible—even necessary—to operate in liquid solvent or in clean gaseous ambients containing reactant species. Because of the divergent nature of the SPL at these two extremes, previous reviewers of SPL have usually concentrated attention on one or the other. Experts in the area of atomic-scale SPL have recently authored several excellent reviews,[13−16] for example, and for this reason the discussion of atomic-scale and single atom manipulation presented here is abbreviated. Finally, to further define the scope of the reviewed literature, it is useful to delineate an operational definition for SPL. For the purposes of this review, then, SPL will be taken to include any experiment in which an SPM was used to locally modify the surface of the substrate—whether these modifications are geometrically well-defined structures or irregular pits or dots. Within the confines defined above, we have endeavored to achieve complete coverage of the SPL literature.

We have organized this review as follows: In section 2, we briefly discuss the principles which underlie nanometer-scale SPL modification experiments. In section 3, experimental aspects of SPM are discussed. In these first two sections, no attempt has been made to write in a review style. Section 4 contains the actual review of the SPL literature. In this section we report on the appearance of the fabricated features, specific experimental parameters and—if provided by the authors—mechanistics of the lithographic process. This section has two levels of organization: First, SPL contributions during this period have been classified as either electrical, mechanical, or optical on the basis of the mechanism of the observed modification process. In the case of electrical and mechanical classifications, the published work has been further grouped according to the identity of the "lithographically active layer" in or upon which modifications have been produced. Finally, the review is concluded in section 5. Here we summarize the experimental procedures and compare SPL methods in terms of the utility of these methods for fundamental and applied research. Finally, we speculate on the future of SPL.

II. Principles of SPL

We have organized the SPL literature in this review according to classifications of the mechanism as *mechanical*, *electrical,* or *optical*. A general description of each of these three modification modes is attempted next.

A. Mechanical Modification

At least two mechanical modification SPL schemes can be delineated: *Scratching*—in which the probe tip of an SFM (typically) is employed to mechanically displace material on a sample surface, and a mode which, for lack of a better name, we shall refer to as *"pick-up-and-put-down"*. As the name implies, weakly adsorbed particles on a surface can sometimes be encouraged to reversibly adhere to an SPM probe tip. In this case, these particles can be picked up from one region of a surface (or can be attached to the tip *ex situ*) and subsequently transferred to another region of the surface. Relative to scratching, pick-up-and-put-down has been infrequently demonstrated, but recent advances may improve the feasibility of this method. Figure 1 shows schematically the principle of mechanical lithography. This process creates holes or trenches that are often surrounded by walls consisting of the removed material. An example of this type of lithography is shown in Figure 2.

B. Electrical Modification

In Figure 3, the principle of "electrical" lithography is displayed. For applied voltages above a certain threshold, material on the sample surface exposed to the electric field undergoes chemical or physical changes. These changes may be either reversible or irreversible, and mechanistically, they can derive

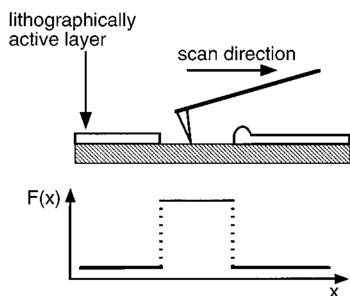

Figure 1. Schematic diagram illustrating the principle of "scratching". The high applied force on the SPM tip causes the tip to plow through the sample. The excess material is usually pushed to the sides of the scan line or window resulting in walls of debris.

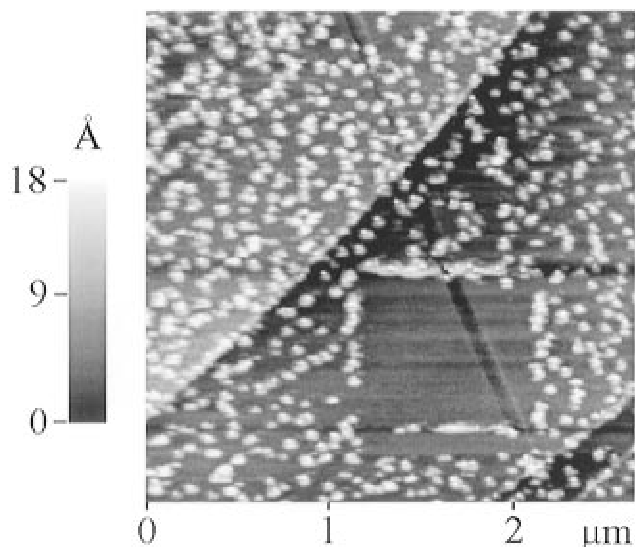

Figure 2. An example of a mechanical lithographic process. NC-AFM scanning with large forces displaces material from the center of the scan window to the edges. Reimaging at lower magnification and using a lower applied force reveals the modified area. The "modification" image was scanned with the set point of the noncontact mode close to "0", i.e., close to continuous contact mode, the subsequent image shown here was then taken in noncontact mode.

from electric field effects directly, as a consequence of the increased current flow induced by the higher bias voltage (e.g., ohmic heating), or, in liquid ambients, because of electrochemistry at either the tip or sample which occurs at the higher applied biases. In general, electrical modifications are induced by the application of short (microsecond to millisecond) tunneling current or bias pulses which help to spatially limit the lateral dimension of the modification on the surface. These changes frequently do not produce profound changes in the topography, however, using contrast enhancing techniques such as force modulation,[17] lateral force,[18] conductance,[19] dI/ds or dI/dV[20] can distinguish more clearly between the modified and unmodified areas of the substrate. A typical example is shown in Figure 4.

C. Optical (or Optically Assisted) Modification

Two discrete types of optical modification schemes can be distinguished. In methods based on the near-field optical microscope (NSOM), the SPM tip functions either as a detector of light or as a light source.

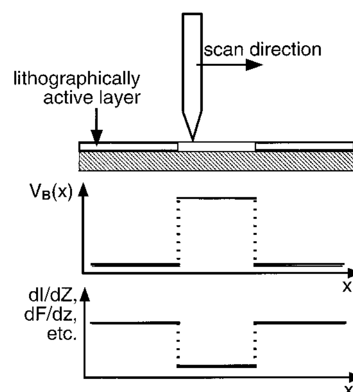

Figure 3. Schematic diagram illustrating the principle of electrical lithography. Upon the application of an electrical field, a modification of the sample surface is obtained. This modification can be derived from the transfer of atoms from the tip to the sample, the removal of atoms from the sample surface, or it may be represent a modification of the chemical or physical nature of the surface (polymerization, crystallization). Often, modified regions are not readily visible in a topographic image and only became clear either by postprocessing of the latent pattern (etching) or through the use of image modes that reveal either chemical or electronic structural differences of the surface.

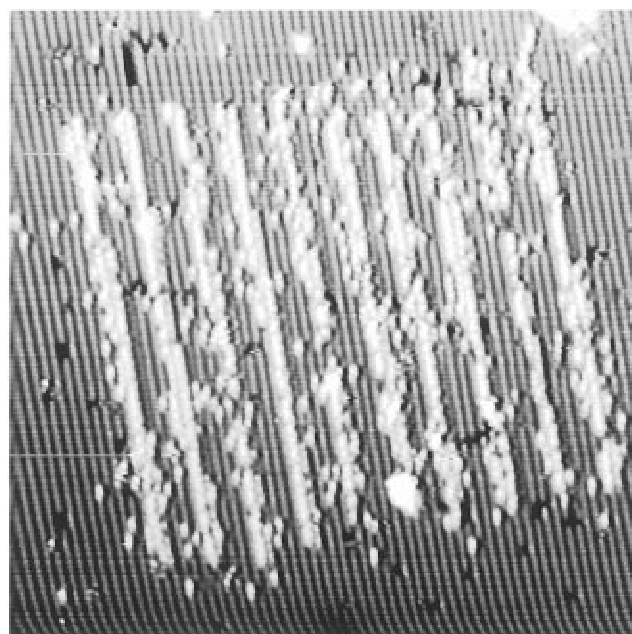

Figure 4. High-resolution patterns written in hydrogen passivated Si(100)-2×1:H using an STM with a −4.5 V tip bias and 2.0 nA tunneling current. The line width is 1 nm, and the line spacing is 3 nm. Patterned areas appear brighter (i.e., 0.15 nm higher) since the removal of hydrogen restores the clean Si surface, thus increasing locally the efficiency of electron transfer. (Reproduced with permission from ref 356. Copyright 1994 American Institute of Physics.)

In either case, if the tip is sufficiently close to the surface ($d < \lambda/50$[21]) the coupling of light can involve a region of the surface which is considerably smaller in diameter than the far-field diffraction limit (i.e., $\lambda/2$). SPL schemes involving the NSOM have recently been reported involving, for example, the exposure of conventional photoresist films. Alternatively, the tip−sample gap can be illuminated using an external source. This external illumination can, for example, activate or sensitize a reactive species

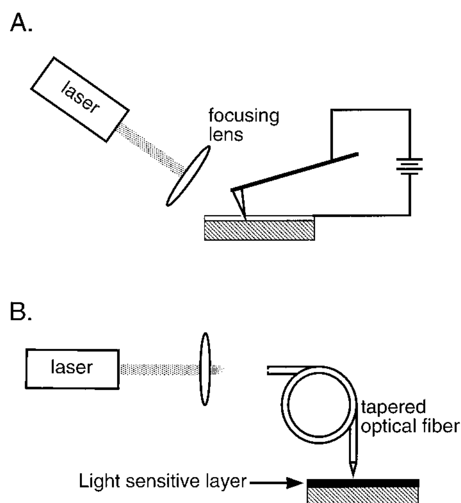

Figure 5. Schematic diagram illustrating the principle of optical or optically assisted SPL. Light is channeled to the surface either through the tip or by focusing the light at the tip–sample gap. Several types of modification have been demonstrated: Local melting, light-induced polymerization, and light-assisted field evaporation, the last usually obtained with a simultaneously applied voltage pulse.

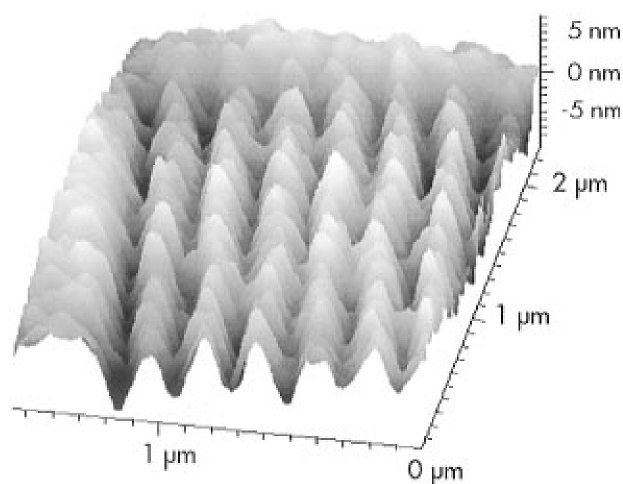

Figure 6. AFM image of a line pattern (spacing 164 nm) created by NSOM-based lithography. Lines were obtained by irradiating a photoresist (Hoechst Novolack AZ 6612) through an optical fiber tip. A solution of the resist with 10% of a photosensitive complex were spin cast onto a polished silicon wafer and subsequently annealed to remove any solvents, resulting in a film which was insoluble in bases. Irradiation of this resist restores the solubility in base and a pattern can thereby be formed. (Reproduced with permission from ref 334. Copyright 1995 Elsevier Science S. A., Switzerland.)

to electron bombardment and thereby trigger a reaction of the activated species on the sample surface under the tip. A schematic setup for this technique is shown in Figure 5, and a typical example is given in Figure 6.

III. Experimental Considerations, and Instrumentation

In this section, the principles and instrumentation which are associated with various SPL modification modes are reviewed. Literature references to the implementation of these methods, as well as specifics regarding the implementation, are reserved for section IV.

A. Instrumentation

Despite the existence of a variety of commercial scanning probe microscopes, home-built instrumentation continues to play an important role in experiments involving lithography. A survey of the 1995 SPL literature, for example, reveals that 25% of this work involved home-built SPMs while the remaining 75% was performed using commercial instrumentation. In contrast, for experimental work involving only SPM imaging, these percentages are 17% home-built and 83% commercial. One possible interpretation of these statistics is that commercial instruments are not yet well adapted to SPL. In the following paragraphs, we briefly discuss the instrumental requirements associated with some of the most common SPL experiments, and review recent innovations in SPL instrumentation.

At a minimum, electronics including a pulse generator and an oscilloscope are required in addition to the conventional imaging electronics of an SPM in order to perform a lithography experiment involving pulsed bias, current, or tip position. The patterning of a surface with many modified regions also requires that a trigger signal be output from the $x-y$ scan controller (typically a computer) so that the pulse generator can be fired repeatedly as the tip is stepped between the predefined locations on the surface which define the pattern to be generated. The electronics of the SPM must be sufficiently "open" to permit the generation of this triggering pulse, and the synchronization of the pulse in time with the motion of the probe tip. In most commercial instruments, the movement of the probe (or the sample) in the $x-y$ direction is controlled by software. Commercial software that (at least partially) fulfills the requirements for convenient SPL patterning is presently available.[22]

Also desirable is the ability to analyze the patterns which are obtained using a variety of other techniques including optical microprobe methods, scanning electron microscopy (SEM), X-ray photoelectron spectroscopy (XPS), and scanning auger microprobe (SAM) analyses. "Finding" the previously produced structures can be very difficult, and a locating system—which permits a particular micrometer-scale region of a surface to be revisited by these other spatially selective probes, or by another scanning probe microscope—would be extremely useful. To enable the transfer of a sample from a SPM to a far field optical microscope, for example, both instruments would have to be equipped with translation stages having better than micrometer-scale precision which permit predetermined positions on the sample to be located and relocated. For producing larger structures, or larger arrays of nanostructures, on a surface an additional requirement are scanners with the ability to scan laterally over regions of up to 100 $\times$ 100 μm^2.

SPM imaging usually involves tip velocities on the order of micrometers per second. If it is assumed that comparable tip velocities can be employed in a

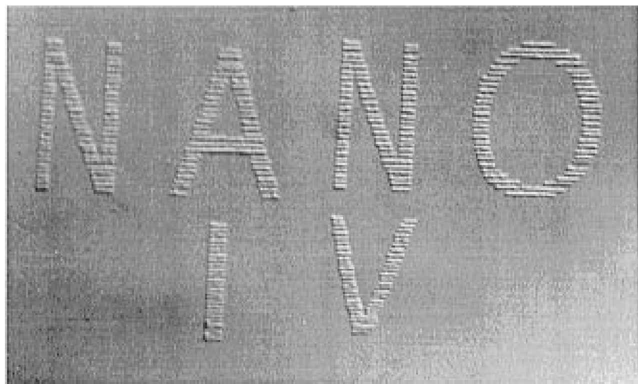

Figure 7. An example of parallel lithography. An array of two cantilevers fabricated the message "NANO IV" in one run. The left cantilever patterned "NA" and "I", the right one "NO" and "V". The pattern was written in hydrogen-terminated silicon, and the latent image was subsequently transferred into the sample with a KOH etch. The height of the letters is approximately 50 μm, the depth of the etched profile 50−80 nm. (Reproduced with permission from ref 24. Copyright 1996 American Vacuum Society.)

SPL writing experiments, then data transfer rates during writing are the product of this velocity and the reciprocal bit length. For example, a bit dimension of 10 nm (which is the sum of a 5 nm diameter for a modification and a 5 nm boundary region), yields data transfer rates during writing of 100 bits s^{-1}. It is needless to say that for practical applications, this writing speed must be increased by many orders of magnitude. It is worthwhile recognizing that the time required to generate the actual surface modification (usually microseconds to milliseconds), is generally not rate limiting. Instead, the movement of the probe and the response time of the feedback system impose an upper boundary on the rate at which the modification step can be attempted while the stability of the system is maintained within acceptable limits. Several approaches to increasing data transfer rates during writing and reading have been recently investigated: Mamin and co-workers[23] used a rotating sample—in analogy to a hard disk—instead of rastering the probe in the more conventional line-by-line fashion.

An implicit problem with SPL-based memory is that with a single tip, data must be transferred to a surface in a serial mode. The Quate group has overcome this limitation by effecting SPL in parallel using an array of cantilevers operating independently.[24−26] An example of this application is shown in Figure 7. Novel probe designs having high-speed capabilities and built-in actuators have been developed, for example, by Minne *et al.*,[24,27−30] Fujii and Watanabe,[31] or MacDonald *et al.*[32,33] A variety of other instrumental refinements which are relevant to increasing the speed of the SPL experiment have also been reported[34−37] as follows: (i) implementation of stacked piezoceramic plates as actuators in place of conventional piezoelectric tubes, (ii) designs for faster electronics such as I/V converters[38] and feedback circuits,[39] and (iii) application of high-performance computers (e.g., with parallel processing capabilities) for independent scan (pattern) generation and image acquisition respectively.[40]

B. Sample Preparation

In most of the experiments discussed in this review, the substrate surface which is subjected to modification is structurally distinct from the bulk of the sample. That is, a thin layer of "lithographic active" material on the sample surface is actually altered. This layer can consist of a Langmuir−Blodgett (LB) film, a self-assembled monolayer (SAM),[41] standard lithographic resist materials,[42] or thin layers of sputtered metal.[43] At hydrogen-terminated silicon (111) surfaces, prepared by etching in concentrated HF solutions, the lithographically active layer can be the chemisorbed hydride monolayer: This adsorbed hydrogen can be locally stripped in an STM experiment by applying a bias pulse. In a corrosive ambient such as air, areas where the hydride layer have been removed are susceptible to oxidation to SiO_2 (see examples in section IV, under silicon).

LB films and SAMs are prepared following standard procedures. Details can be found in the respective papers or in reviews e.g., by Gaines[44] or Roberts[45] for LB films and by Ulman[46] or Dubois and Nuzzo[47] for SAMs. Resists are often polymers films (e.g., polymethyl methacrylate or PMMA) that undergo a chemical transformation such as cross-linking during exposure to light, electrons, etc. Exposed regions of the polymer film exhibit different chemical and/or physical properties as compared with the nonexposed polymer. From the exposed film, a positive or negative mask is obtained by selectively removing only nonexposed or exposed polymeric material, respectively. This removal process relies on the different solubilities of exposed and nonexposed regions of the film produced by cross-linking. An overview of resist materials is given by Moreau.[42] In contrast to optical lithography where films of roughly 1 μm thickness are used, with SPL, much thinner films in the range from 10 to 50 nm, often prepared by spin coating, may be used.[48]

C. Probes

For most STM-based SPL experiments, standard electrochemically or mechanically etched metal wires have been used as tips. However in experiments in which the STM tip is used to mechanically modify a surface, relatively soft metal tips have been replaced with tips composed of harder materials in a few cases. For example, Kaneko *et al.*[49] have described the application of conductive, boron-doped diamond tips for such applications. If, as is more likely, the mechanism of the STM lithography is electrical, the tip must resist oxidation, field evaporation, and shape changes; effects which can be induced either by resistive heating or by the high electric fields imposed by an applied voltage pulse.

Similar considerations apply for AFM-based SPL experiments: Sumomogi *et al.* have employed single diamonds as tips,[50,51] whereas tips with a high quality diamond coating[52] have been prepared by Niedermann *et al.* The durability of these tips for mechanical modification experiments is apparently superior to that of either silicon or silicon nitride. Tips and cantilevers of nearly degenerate silicon have recently become commercially available[53] and these exhibit

sufficient electrical conductivity for many SPL experiments involving bias pulse-induced modification of surfaces. However, it is very common to sputter a thin film of metal, usually gold, onto the AFM probe to further increase the conductivity. Recently, Thomson and Moreland[54] investigated a variety of different tip coatings for point-contact studies and concluded that gold indeed gives the most reproducible and stable coatings for this purpose in air.

IV. Results

This section is organized into three subsections on the basis of the classification of an SPL experiment as having a mechanism which is predominantly electrical, mechanical, or optical. Because the mechanism operating in some of the reviewed experiments is uncertain, this classification scheme is somewhat arbitrary and some misclassification is probably inevitable.

A. Electrical SPL Methods

In the context of this review, electrical experiments are defined as those in which the imposition of an electric field is required for modification of the surface. In general, this field is either obtained by the application of a large dc voltage between sample and tip, or by the application of voltage pulses.

The literature in this section has further been classified according to whether the method operates directly at a clean surface—that is, a surface on which no intentionally added lithographically active layer is present. We have classified all such methods as "direct". As mentioned earlier, atomic resolution lithography experiments (SPL experiments involving the manipulation of single atoms), most of which fall into this category, are only very briefly reviewed. Applications of electrical lithography to the modification of silicon surfaces, because of the technological significance of this material, are given special emphasis: Because of the large volume of papers, work with clean silicon and hydrogen-terminated silicon (Si:H) surfaces are discussed separately. A large volume of papers report the SPL modification of surfaces on which a thin resist layer is present. The objective in these experiments has been to generate a chemical modification of the resist layer which permits the preferential removal of this layer, or of the surrounding unmodified resist, in order to obtain a mask.

Experiments involving a lithographically active layer have been organized according to the *method of formation* (e.g., LB monolayer, self-assembled monolayer), of this layer. This format is employed despite the *chemical* similarity of these layers in order to highlight the specific instrumental parameters associated with the modification of the layers prepared by these various methods. Because of their unique characteristics, SPL experiments conducted in an electrolytic environment are summarized separately at the end.

1. Direct Modification of the Surface

a. Silicon. *1. Si:H.* Dagata *et al.*[55,56] patterned hydrogen terminated n-Si(100) for use as a negative mask for the selective epitaxial growth of GaAs. This approach was also investigated by Snow *et al.*[57] These workers epitaxially deposited 5 nm of silicon on the GaAs and passivated the resulting silicon surface by etching in HF. This sample was then patterned with a STM and the structures which were obtained were transferred to the underlying GaAs using a two-step etch procedure. Snow *et al.*[58] also attempted to passivate GaAs with sulfur and to subsequently remove this passivation layer locally using the STM. However, the chemical homogeneity of the modified regions and the thickness of the passivation layer were difficult to control resulting in poorer reproducibility as compared with the Si:H system. Patterning parameters for the GaAs:S system were as follows: $E_B = 1.2$ V sample-(−), $I_T = 0.4$ nA; for imaging the bias was held at 2.8 V.

Sugimura, Nakagiri, and co-workers have investigated many aspects of SPL based on Si:H surfaces.[59−75] Si:H surfaces were prepared by etching cleaned Si(111) wafers in 1.0 wt % HF solution for 30−60 s; unetched wafers with thick native oxide layers were also employed. The patterning of these surfaces involved the application of a 5.0 V bias [sample-(+)], and currents between 0.1−0.5 nA for the patterning. These SPL experiments were usually performed in a glovebox in order to achieve controlled humidity.[61,63,65,66,68−70] Following SPM patterning, samples were subjected to various etching procedures in order to amplify the relief produced by the modification step, see also Figure 8. The authors proposed a modification mechanism involving the electrochemical oxidation of the surface in humid air, or by field-enhanced oxidation in a dry environment.[61,74] The obtained structures consisted of protrusions, 1−2 nm high. An explanation for this height change from the unpatterned Si to the patterned SiO_2 areas can be given in terms of the different densities, 12 and 19.8 $cm^3\ mol^{-1}$ for Si and SiO_2, respectively. Smaller and better defined etch patterns were obtained when tetramethylammonium hydroxide (TMAH) was used instead of the more common KOH solutions.[69] This was possible due to the reduced roughening of the surface during the etching process. Surface roughness measurements revealed a 10-fold decrease when TMAH was used instead of KOH. Grooves 40 nm deep and 50 nm wide were obtained. Even though especially suited for etching Si(100), TMAH also etches Si(111) at least 100 times faster than SiO_x, it is therefore also applicable for this surface.

Several applications of these patterned silicon surfaces were proposed and experimentally tested by Sugimura and Nakagiri: The electroless deposition of gold and other metals occurs preferentially on the unexposed, Si:H surface, whereas metal deposition was inhibited at exposed SiO_x lines.[68] A positive gold pattern was obtained as follows: An oxidized silicon surface was covered with a monolayer of trimethylsilizane by CVD.[71] This monolayer was then locally degraded or removed by means of anodization with the SPM tip. Finally, treatment of the modified surface with the electroless plating solution resulted in the deposition of gold only at regions of the surface patterned with the STM.[74] Ultimately, these gold patterned surfaces could be functionalized as fol-

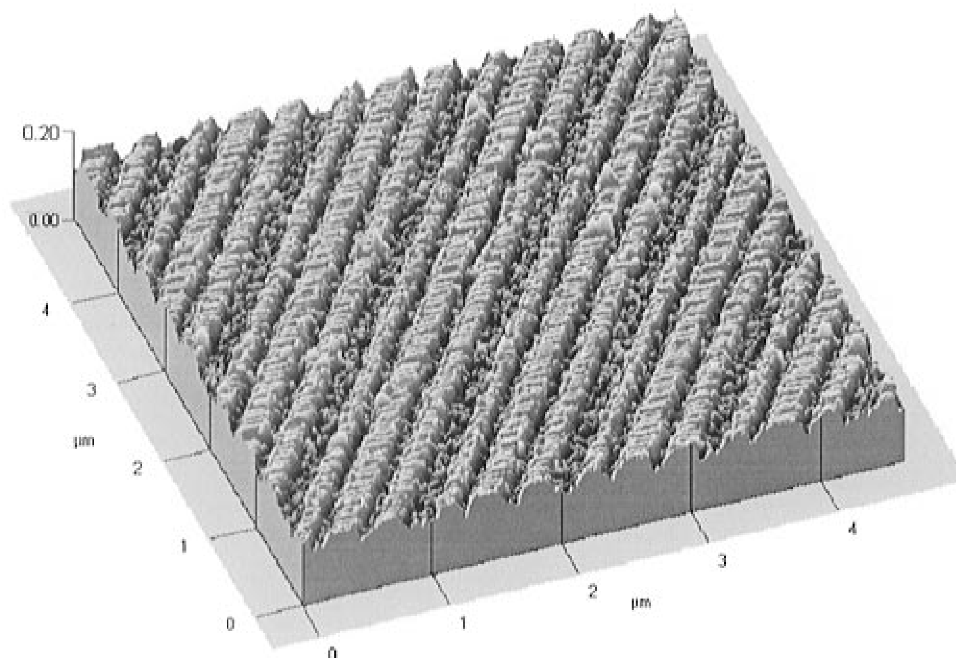

Figure 8. AFM image of gold patterns on silicon. The patterning was performed as follows: Hydrogen-terminated Si was locally oxidized by STM at a sample bias of 5 V and 0.2 nA current. The sample was then etched for 1 min in aqueous tetramethylammonium hydroxide and subsequently immersed in an electroless plating bath for 7 min. (Reproduced with permission from ref 65. Copyright 1995 American Vacuum Society.)

lows: The patterned samples were immersed into a solution of an alkanethiol (*n*-hexadecyl mercaptan) that formed a self-assembled monolayer on the gold patterns but not on the silicon. This was confirmed experimentally using Auger electron spectroscopy. Such functionalized patterns might be useful in sensor applications.[67,72] A second similar application involved the use of the same organosilane layer as a protective mask: Si etching reagents such as $NH_4F/H_2O_2/H_2O$ are effective on both Si and SiO_x but do not etch the monolayer-modified surface. In this way, grooves 30−60 nm wide and 5−10 nm deep respectively, were created on SPM-patterned surfaces.[75]

Fay *et al.*[76] used both n- and p-type Si(100) in their studies. Gratings with periodicities between 80 and 500 nm were fabricated. Whereas for the 80 nm grating a maximum tunneling current of 2 nA could be applied, 500 nm gratings could be fabricated with 20 nA currents using the same bias (1−2 V). The latter modifications were visible in a SEM even after the thermal growth of a 70 nm thick SiO_2 layer and subsequently sputtering 16 nm of Au on top of the substrate. Using AES, the authors demonstrated that within the modified areas, the oxygen content was increased, thus supporting the transformation of Si into SiO_2. Even though reactive ion etching in HBr greatly increases the roughness of Si, it was found suitable for pattern transfer.

Urban *et al.*[77] pointed out that the (110) surface is well suited for this patterning scheme due to the observed strong anisotropy of the surface structure which is obtained by etching.

Instead of rinsing Si(111) surfaces in water following an HF etch, Pérez-Murano *et al.*[78−81] dried etched surfaces in an N_2 gas stream, thereby obtaining fluorine surface concentrations of up to 10^{14} cm^{-2}. These authors hypothesize that this lithography is electric field driven. In addition to topographic images, spectroscopic images were also recorded, i.e., current images at different biases. The contrast for an SPL-patterned region was a sensitive function of bias, indicating that the modification is not purely topographical but also electronic in nature.

Kramer *et al.*[82] applied the same method to amorphous silicon (a-Si) surfaces. A drawback of a-Si is that anisotropic etching is not possible, and extremely smooth surfaces cannot, therefore, be easily obtained. Amorphous silicon, however, can easily be deposited on a variety of smooth substrates and can be used as a mask for the patterning of the underlying substrate. This approach may be useful for the patterning of materials which, like GaAs, do not have a robust passivation chemistry. Kramer *et al.* investigated the influence of scan rate, current, and bias on pattern formation. In air, no marked influence of the tunneling current was observed (range 2−100 pA). The authors therefore rejected the possibility that electron-induced desorption of hydrogen was solely responsible for pattern formation and, on the basis of a bias amplitude study, concluded that field-induced oxidation may be an important contributing process as well. Thin films of amorphous and hydrogenated silicon were deposited using CVD on a thin metal film of TaIr. This silicon layer was further passivated and patterned with a STM. In a two-step etch the not-oxidized silicon is removed and the pattern transferred into the metal film. Lines with lengths of 2 µm and widths of 40 nm were obtained.[83] Following this principle, a 100 nm thick layer of amorphous Si layer was used by Minne *et al.*[25] to pattern an underlying 500 nm thick oxide film.

Lithography on Si:H was performed by Snow and Cambell[84,85] using AFM with an electrically conducting tip. As the AFM is operated in contact mode, special considerations were given to the coating of the Si_3N_4 tip. The authors found that Ti remained both mechanically and electrically stable, the tip−sample gap exhibits a high resistance likely due to the native oxide on Ti. A 100 nN force and a bias between 1.5 and 2.5 V was employed for the writing process. Scanning with the same force but without the applied bias did not alter surface morphology. The writing patterns were visible to the AFM after exposure but could also be used as a mask for subsequent etching by KOH. Rather high speeds of up to 1 mm s^{-1} and line width down to about 15 nm were obtained. An improvement of the etch selectivity between silicon and silicon oxide was reported by the same authors when an electron cyclotron resonance (ECR) source was used: A Cl_2 plasma generated by this source showed higher efficiency than typical reactive ion etching techniques. This fact allows lower pressures of the plasma which produces less scattering, resulting in deeper and smoother etch profiles.[86]

Teuschler *et al.*[87,88] patterned a Si(100) surface with a conductive AFM tip (7 V bias) and measured frictional forces on these patterns. The oxidized patterns revealed a 20% increase in the friction force compared with unmodified hydrogen terminated areas.

Gordon *et al.*[89] proposed a chemical model for the mechanism of field-enhanced oxidation on Si(111): A hydrogen-terminated silicon surface prepared by etching in HF will exhibit some Si−F bonds. In air, F can easily be replaced by OH. These OH terminals eventually can bridge and form an monolayer of oxide. Growth does not stop at this point but an oxide layer up to 0.7 nm in thickness can be formed. This can be explained in terms of field effects across the interface between Si and the oxide layer which promote the diffusion of oxygen-bearing ions. The application of an electric field between the tip of an AFM and the substrate causes this oxide layer to grow further to a thickness of 8 nm for 7−8 V biases. These workers further demonstrated that the best lithographic performance was obtained using the AFM in contact mode and a 100 nN loading force. In noncontact mode, incomplete line drawing was observed, see also Wang *et al.* below.[90]

2. SiO_2. Field enhanced oxidation on SiO_2 was observed by Tsau *et al.*[91] They showed that oxide lines can be formed by applying a high bias (several volts, sample-(+)) between a silicon sample and the doped cantilever tip. No patterning was observed with sample-(−) pulses. The patterns consist of lines roughly 1 nm high and could be transferred into grooves after a short dipping into HF, thus suggesting that the fabricated lines indeed consist of SiO_2. The authors also showed that noncontact AFM can be employed for lithography.[90] The minimum observed feature size was 10 nm, a size that the authors attribute to the chemical reaction "bandwidth". This explanation also accounts for the fact that this resolution limit is also observed with STM and contact AFM. The observed features were not due to deposited charge as the structures could still be imaged after several hours. The formation of silicon dioxide is thought to be electrochemical as these experiments were performed in an air ambient. Compared to experiments with contact AFM, the writing time was longer, likely due to the fact that the effective writing time, i.e., when the tip very is close to the surface, is shorter due to tip oscillations.

Hattori *et al.*[92,93] also investigated the field-assisted oxidation of Si. A clear relationship between the observed height of the fabricated structures and the applied bias (2−10 V) as well as the scan speed (0.1−10 μm s^{-1}) was observed. By etching with HF, the produced structures could be transformed into grooves. The depths of these grooves correlated with the height of the original structures, indicating that they are composed entirely of SiO_2. By analyzing the dependence of the structure size upon scan rate, the authors suggest that the fabrication process is mainly limited by the diffusion of oxidizing species. Similarly, Whidden *et al.*[94] used 5 nm thick oxides for pattern generation. Sample-(+) biases were varied between 2 and 8 V; currents, between 80 pA and 1 nA. However, the authors suggest that the generated features consist of hydrocarbon deposits and are not a product of further oxidation of the sample. The latent patterns were transferred into the oxide by HF vapor etching (10 nm deep, extending into the silicon substrate) and further into the underlying Si by reactive ion etching in a CF_4/O_2 flow.

Porous silicon was patterned by Enachescu *et al.*[95] in a UHV chamber. Modifications in the form of parallel lines were obtained by applying a 7 V bias (sample-(+)) with the feedback "on" at a tunneling current of 27 pA. The fabricated structures exhibited a lower conductivity (attributed to the formation of defect states) and a lower barrier height as compared with unmodifed porous silicon regions. Both effects will cause the tip to be driven closer to the surface in order to maintain the set point current. Thus the apparent depth of the fabricated structures was attributed partially to these electronic effects and the real dimensions were difficult to assess. These authors also investigated phosphorus-doped, hydrogenated amorphous silicon and observed two different types of modifications, both apparently electronic in nature. E_B values of 9 −10 V and I_T > 100 nA caused compressive modifications of the surface and grooves having a width of 10−20 nm could be written. In contrast, E_B values of 5−9 V and I_T in the range from 1 to 100 nA resulted in the formation of raised regions and, under these conditions, lines were formed. Both effects were explained in terms of electronic effects associated with the reduction of electronically active P-dopant sites (compression) or to the formation of additional surface states (conductivity increase).[96]

3. Si. Ostrom *et al.*[97] showed that upon applying a pulse between a tungsten tip and a Si surface, small "columns" could be grown on the sample surface. Although the authors preconditioned the tip by means of a tip−sample contact in order to transfer Si to the tip, they suggested that the formation of the structures was based upon the diffusion of surface

atoms rather than a transfer of atoms from the tip. Preconditioning was necessary in order to obtain a sharper tip to induce a radial electric field rather than a parallel field underneath a blunt tip. It was observed that sample-(+) pulses (7 V, 1−10 s) produced significantly larger structures than negative pulses; 10−20 nm compared with 3.5 nm.

In UHV using STM, Yau *et al.*[98,99] produced small structures on a Si surface when a bias above 5 V (sample-(+)) was applied. They proposed that adsorbed contamination on the Si sample was polymerized during the voltage pulse. IV spectroscopic characterization was used to show that the observed mounds were topographic rather than electronic structures. These workers further noted the spotty appearance of the lines, and speculated that freshly formed nanostructures might provide channeling (focusing) of the current between the tip and sample. Thus the field strength surrounding the structure might be too small to allow for the growth of a new structure. Only at some minimum distance from the first structure would the field strength be sufficient to support the polymerization reaction.[100]

b. Layered or van der Waals Materials. An abundance of prior work involving the modification of layered materials such as highly oriented pyrolytic graphite (HOPG), MoS_2, $NbSe_2$, WSe_2, or $Bi_2Sr_2CaCu_2O_x$ exists. The attraction to these materials is obvious: The basal planes of these compounds are frequently atomically smooth, these surfaces are renewable by cleaving, and because the basal plane is coordinatively saturated, these surfaces are extremely unreactive and therefore stay free of chemisorbed impurities even in air or liquid ambients. An additional characteristic of the layered metal dichalcogenides and graphite is the anisotropic bonding in these materials which has facilitated the "quantized" removal of material in a layer-by-layer fashion in some previous work. Possibly because of the weak interlayer forces in these materials, the SPL modification on these surfaces typically requires only mild conditions of applied force or tip−sample bias.

HOPG is one of the earliest and best studied materials for scanning probe-based lithography, e.g., Albrecht *et al.*[101] showed in 1989 that an STM could be used to write entire words with 30 nm sized letters in the surface of HOPG. Terashima *et al.*[102] reported in 1990 that STM-generated pits acted as perfect nucleation sites for evaporated gold. The mechanism of the hole formation, however, is not yet fully understood. Several authors have investigated the different parameters affecting this hole formation, the reported values e.g., for threshold bias vary markedly: Moriarty and Hughes[103] investigated the pit formation at very high resolution and showed the smallest structural formation consisting of the displacement of 4 atoms. Abe *et al.*[104−106] investigated 30 nm thick arc evaporated carbon films and found similar behavior as generally observed for HOPG. The depth of the pits was the same as the nominal film thickness, suggesting that all material was removed until the substrate was exposed. Upon applying a sample-(+) pulse having an amplitude larger than 4 V, mound formation was observed. Auger analysis showed that these mounds were composed of carbon and of the underlying metal (Au or Pt). On carbon films directly evaporated onto Si, no mound formation was observed. Kondo *et al.*[107,108] found a threshold value of 2.5 V in air and 8.5 V under UHV conditions. The authors explain this difference in terms of two different mechanisms: In UHV sublimation is believed to be responsible for removal of atoms, and the threshold voltage should be related to the binding energy, for graphite 7.43 eV. In air, humidity effects play a major role and the important reaction is an electrochemical one forming CO_x and H_2 at energies below 2 eV. These values are in agreement with the observed threshold bias voltages. Differences can be discussed in terms of activation energies. The same behavior of threshold values in air and in UHV was also observed for MoS_2, $NbSe_2$, and $Bi_2Sr_2CaCu_2O_x$. Uesugi and Yao[109] observed both pit and structure formation on graphite. Pits were observed e.g., in air. Small structures on the graphite surface were formed in a mixture of hydrogen and acetone at 20 Torr and are believed to be composed of carbon either from contamination or by decomposition of acetone. Parameters were sample-(+) 4 V pulse for 50 μs. The authors did not observe deposition in vacuum and therefore excluded the Pt tip as a possible source for the dots. Lines on graphite were also fabricated by Wang *et al.*[110] An example of SPL on graphite is depicted in Figure 9. For SPL on graphite in electrolytes see subsection 5.

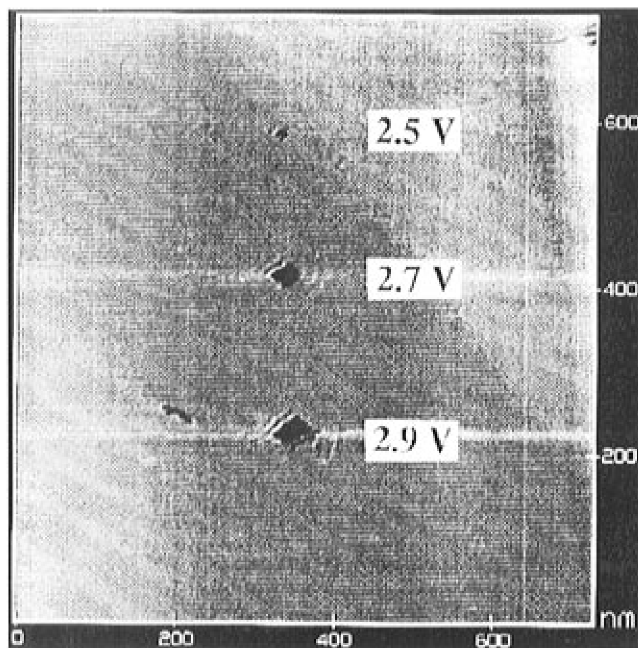

Figure 9. An STM image of a modified graphite surface in air showing pits produced by the application of tip−sample bias pulses. A bias pulse threshold of 2.5 V was observed for pit formation, and for larger pulse amplitudes, larger pits were formed. For the three pulses 2.5, 2.7, and 2.9 V, diameters of 10, 20, and 30 nm were obtained in this experiment. The pulse width was ~1 s. (Reproduced with permission from ref 107. Copyright 1994 Elsevier Science, The Netherlands.)

Following the observation by Parkinson[111] in 1990 that the layer-by-layer etching of metal−dichalcogenide crystals (specifically $SnSe_2$, $TiSe_2$, and $NbSe_2$)

is induced by STM imaging, the SPM-induced modification of these materials has captivated the interest of several groups, and several new phenomena have been observed.

Using an STM, Dransfeld and co-workers[112] reported that the application of bias pulses (tip-(−) 5 V × 10−400 ns) to the van der Waals surface of a WSe_2 single crystal caused the etching reaction of this surface to be nucleated and, with continued STM imaging, an etched region—one monolayer in depth and having a triangular shape—was formed and continued to grow with time. In more recent work with WSe_2, this research group[113−115] has been able to generate more subtle modifications of the basal plane surface which apparently did not involve the removal of material from the surface as in earlier etching experiments. In these experiments the modifications appeared either as mounds or as ringlike structures. Qualitatively similar structures have been seen previously by STM on the nominally nonmodified surfaces of natural MoS_2 crystals.[116,117] High-resolution STM imaging revealed that no material was removed from the surface during the modification operation. Relaxation of these structures was not observed for periods of several hours following their generation. While the origin of these modifications was not apparent, the authors went on to demonstrate that these features could be removed by mechanical means: The tip sample distance was lowered by increasing the current and decreasing the tunneling bias. Then, with the feedback strongly damped, the tip was scanned at a high rate over a modified region of the surface. When this "ironing" procedure was repeated twice, modified regions were removed.[118]

$SnSe_2$ and MoS_2 were investigated under UHV conditions by Huang *et al.*[119] Vacancies of 3−4 atoms could be formed in these materials when pulses in a STM configuration were applied. Voltage amplitude thresholds of 3.5 V for MoS_2 and 1.4 V for $SnSe_2$ were seen. The larger threshold for MoS_2 was ascribed to the fact that the Mo−S bond strength is greater than that for Sn−Se.

c. Bulk Metals or Metal Films. Silver films were employed in the STM modification experiments of Rabe and Buchholz.[120] These workers showed that very short voltage pulses of ∼50 ns and 5 V in amplitude were sufficient to modify the surface of thin silver films. The modification consisted of pits for sample-(+) pulses, and of pits and/or hillocks in the case of pulses having a sample-(−) polarity. Prior to the application of a pulse, the tunneling current was reduced to 2 pA. This low current set-point combined with the short duration of the pulse restricted the total number of electrons involved in these processes thereby eliminating the possibility of modification due to heating effects. Consequently, it was concluded that these modification processes were most likely brought about by the field evaporation of metal at either the tip or sample.

Titanium surfaces have been patterned by Sugimura *et al.* using a strategy similar to that which this group has employed for Si:H surfaces (*vide supra*). The oxidation of Ti to TiO_2 is observed under the influence of a +5 V bias between the sample and tip in an N_2 atmosphere with controlled humidity. The observed modifications appear as protrusions because of the lower density of TiO_2 as compared with Ti. The reaction of Ti to TiO_2 is described as an electrochemical process in the water-filled gap between sample and tip.[59,60,62,64] As was seen for silicon surfaces,[63] on TiO_2 the humidity was found to be very important: Size as well as etching rate were increased at higher humidity.[60,64] However, humidity had no influence on the lithographic process on an organosilane-modified Ti substrate. In this case the pattern size depended uniquely on the tip size. This difference was explained in terms of the hydrophobicity differences between these two surfaces.[75]

In other SPL experiments with Ti, a thin layer of the metal (7.5 nm) was deposited on Pt and then selectively removed with a STM in tunneling mode by ramping the bias voltage between ±2 V for 0.25 s at 80 V s^{-1}. In this way, Pt disk ultramicroelectrodes having radii between 5 and 36 nm were fabricated. The authors suggest that surfaces patterned using this procedure might be employed for electrochemical investigations of nanoelectrodes.[121]

Chromium films on Si (30−50 nm) were investigated by Song *et al.*[122] with STM both in air and in N_2. A native oxide film of 1 nm thickness was assumed to exist at the chromium surface in all experiments. Upon applying elevated tunneling bias, structures as small as 25 nm were observed. Two different types of modifications were observed: With a large bias (sample-(+) 3.5 V) and using a stationary tip, patterns were formed which were water soluble, producing a positive mask. With a smaller bias and a scanning tip, patterns were formed that were almost insoluble in water and stable in NaOH or standard Cr etchant solutions. These observations are consistent with the formation of CrO_3 in the "high dose" patterning experiments (involving a stationary tip) and the water insoluble Cr_2O_3 in the "low dose" experiments.

A 10 nm film of Cr was modified by Wang *et al.*[123] using AFM. These experiments were carried out under conditions of controlled humidity. No modification of the Cr surface was obtained when working in dry air or when applying sample-(−) pulses. In humid air and with sample-(+) pulses, mounds could be formed having dimensions which depended on the pulse duration (varied between 10 ms and 1 s) and amplitude (2−10 V). The smallest structures which were observed were 20 nm in diameter and 3.5 nm high. The fabricated structures were stable in dry air; however, in humid air these structures disappeared within half an hour, suggesting that the composition of these structures was water soluble CrO_3. Auger spectroscopic results were consistent with the formation of a chromium oxide species on the surface, also supporting the hypothesis that these modification result from a tip induced oxidation of the chromium surface.

Fukuzawa and co-workers[124] investigated the system of a Pd STM tip and a thin Pd film on Si in air. These workers observed that the application of bias pulses having either polarity caused the formation of mounds on the surface. A threshold voltage of 4 V for sample-(−) pulses and 6 V for sample-(+) pulses

was established and the size was found to increase from 100 to 1000 nm with increasing pulse amplitudes.

On a patterned substrate two previously formed lines were connected with a STM by Welland *et al.*[125,126] A 25 nm layer of gold/palladium was the top layer on this sample. By applying a 4 V, 9 ms pulse mounds could be formed. The authors manufactured an entire row of such mounds to connect two of these preformed lines.

Hosaka *et al.*[127] investigated the possibilities of changing locally the magnetic properties using SPL. A layered Pt/Co film was employed in an UHV chamber with a magnetic force microscope (MFM). A tip with a magnetic layer (PtCoCr) and a outer carbon layer was used for both writing and reading. Pulses (8 V) were applied to form magnetic domains with about 60 nm diameter. The authors describe the process of magnetization resulting from local heating due to the field emission current during the pulse. In an earlier paper, they demonstrated the magnetization using STM. In that case polarization microscopy was used to verify magnetization.[128]

d. Superconductors. $YBa_2Cu_3O_{7-x}$ (YBCO) films were investigated by Yang *et al.*[129] using STM. These workers observed a tunneling induced etch effect, causing the formation of square patterns to be etched in the surface (see also 1). By applying pulses of 150 μs duration and 5.5−8.5 V amplitude, relatively large pits were formed having dimensions of ∼100 nm in diameter and 30−100 nm in depth. These dimensions were pulse amplitude dependent. Furthermore, they observed a threshold of 5.5 V for sample-(+) pulses and 8.5 V for the opposite polarity. By scanning one line up to 300 times, Bertsche *et al.*[130] produced a groove in the YBCO surface. Surface modification was observed with pulse amplitudes of near 4 V, however, only if the tip was placed close to a terrace edge. The pulse removed material leaving a 3 nm diameter structure. No debris could be found indicating that a mechanical process could be excluded. Heyvaert *et al.*[131] found that exposure to moderate electrical fields (1 V bias at 0.2 nA current) could alter the surface of YBCO as well. The rate depended not only on the applied electrical field (varied between 0.5 and 1.2 V) but also on the exposure time. The oberved influence of the electrical field strength and the lack of material accumulation on the border of the imaging windows let the authors conclude that field evaporation and not mechanical milling was reponsible for the observed modifications. Contradictory results have been reported by several groups and are discussed in section B.1.

Thomson *et al.*[132] summarized the influence of tunneling parameters as well as the humidity on the possible mechanisms of modification of YBCO surfaces. SPL at low tunneling resistances was attributed to mechanical milling, whereas at somewhat higher "intermediate" resistances, the process was classified as an e-beam lithography type and finally for very high currents and biases it was speculated that thermal heating of an oxygen-deficient surface led to vaporization and thus the removal of material. A humid and slightly acidic environment was found to enhance material removal, suggesting that electrochemical reactions in the tunneling gap may contribute to the modification of YBCOs. Of the modification regimes explored in this work, the e-beam "mode" was found to be the most reproducible. The tunneling parameters used in this regime were $I > 1$ nA and $4 < U < 5$ V.

On $Bi_2Sr_2CaCu_2O_x$ ($T_c = 80$ K), Terashima *et al.*[133] reported that monolayer deep etch pits which were ∼10 nm in diameter could be obtained by raising the tunneling bias to 4.5 V for 1 s.

e. Other. GaAs surfaces prepared by MBE were employed for SPL investigations by Dagata *et al.*[134] When an arsenic protective layer was grown on top of the GaAs, stable patterns could be written, whereas on Ga-terminated samples no structuring could be performed. A further improvement was observed when a 12 monolayer thick intermediate layer of indium-doped GaAs was grown a few ML below the surface. The authors suggested that indium, in the form of In_2O_3, segregates near the surface thereby stabilizing the structures formed by the modification procedure.

Sinnott *et al.*[135] demonstrated theoretically the feasibility of extracting hydrogen atoms from a diamond(111) surface using a diamond tip terminating in an ethynyl radical (C≡C•). It was further predicted that tip crashes or the binding of the reactive tip to defect sites would cause a loss of the ethynyl group and thus deactivate the tip.

2. Organic Materials as Lithographically Active Layers

a. Organic Resists. Dobisz, Marrian, and coworkers[48,136−143] performed lithography on thin (10−50 nm) resist films (e.g., SAL601 from Shipley) in UHV using a STM and made comparisons to results obtained using e-beam exposure of the same resists: Using STM, circular nanostructures were seen for excursions of the bias above ∼8 V (tip-(+)).[48] A well-defined size dependence on the bias pulse amplitude was also observed: For biases at the 8 V threshold, nanostructures with diameters of 20 nm were obtained and this diameter increased linearly with the applied bias up to 60 nm for 30 V, see Figure 10. In these experiments, no significant dependence of the nanostructure size on the tip composition was found. For purposes of comparison, a negative resist (SAL601) was spin coated onto Si and GaAs substrates and exposured using both the STM (conditions 10−50 V, 10−100 pA, 200 nC cm^{-1}) and electron-beam (conditions 50 kV, 10 nm).[138] The smallest line width for the e-beam technique was found to be 93 nm, however, with STM lines with widths below 25 nm were obtained. Both the quality of the modification and the line width was found to depend on the applied bias, the film thickness (between 30−50 nm) and the substrate: GaAs appears to be less well suited for high-resolution lithography because of the greater surface roughness of GaAs. Another negative resist, P4BCMU (a polydiacetylene with pendant urethane groups) was employed in similar experiments.[143] The smallest features obtainable in this case were larger (55 nm) than on Si, but still smaller than the 80 nm features obtained by e-beam on the same GaAs substrate.

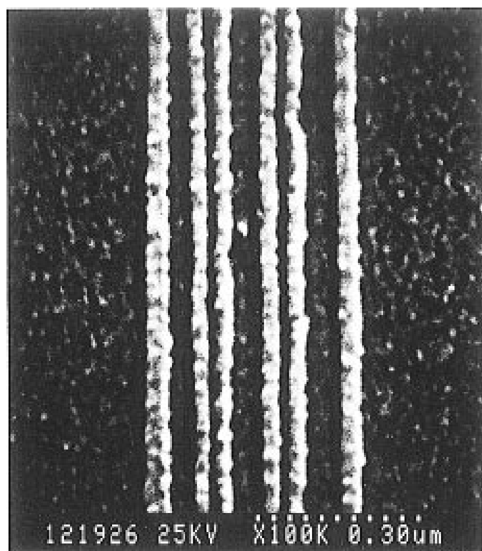

Figure 10. SEM micrograph of lines written with STM in 30 nm thick film of the photoresist SAL601-ER7 (Shipley) on a Si substrate. Lines were written with a bias of 15 V (sample-(+)) and a scan speed of 500 nm s^{-1}. After exposure, the samples were annealed at 107 °C and developed in a commercial reagent. For SEM imaging a 15 nm Au film was sputtered onto the samples. (Reproduced with permission from ref 140. Copyright 1991 American Vacuum Society.)

SAL601, a negative tone polymer resist, was also investigated by Archer *et al.*[144] These workers showed that the application of biases above 10 V (tip-(+)) caused the formation of mounds 20−30 nm in diameter and 1−1.5 nm in height, whereas applied pulses with amplitudes below 9 V caused the formation of grooves in the surface—apparently caused by mechanical contact of the tip with the surface.

A 50 nm thick film of a chemically amplified resist (Si-CARL: chemical amplification of resist lines (with silicon)), spin coated onto a layer of a conductive organic polymer, was investigated by Kragler *et al.*[145] Patterning was performed in air with a STM using biases of ∼50 V (both polarities) and currents in the 10 pA range. A difference between the two polarities was observed in terms of the "damage" imposed on the surface: For tip-(−) biases, larger amplitudes were required in order to mimic the behavior seen at relatively low tip-(+) biases. For example, the modification seen for a tip-(−) 50 V experiment, would only be observed following development of the resist, whereas in experiments involving either larger tip-(−) biases or tip-(+) biases, the modifications which were obtained could be seen by STM even prior to development. The authors reported that the energy required to induce full exposure of the resist using the STM was ∼10 mC cm^{-2}, a value 3 orders of magnitude higher than for high energy e-beam lithography. On the basis of this analysis, it was concluded that the low-energy electrons sourced in the STM experiment are relatively inefficient at transposing the photoactive molecules of this resist.

Park *et al.*[146] used so-called spin on glass—a resist based on a Si−O backbone with methyl groups as organic components—as the lithographically active layer. This resist was spin coated onto Si(111) and modified by applying a high voltage (70−100 V, sample-(+)) pulses between a conductive AFM tip and the surface while in contact. Whereas the latent image could not be imaged with the AFM, after etching in a buffered oxide etch (BOE), the written pattern became visible as grooves with line widths down to 40 nm. The authors noted that they were able to write lines at a rate of up to 3 mm s^{-1} with 100 nm line width.

Dobisz *et al.*[147] simulated STM-based lithography involving resists using a method[148] which was originally developed for modeling field emission. The system which was modeled consisted of a 20 nm diameter sphere operating at a planar surface on which a resist layer having a thickness of 5 nm was deposited. In this simulation, electron scattering by the resist was not considered. For this tip geometry, spot sizes of the emission were found to be between 2 and 11 nm depending on distance between the tip and the surface of the resist layer (5−20 nm) and applied electric fields (1.9−5 V nm^{-1}). Using a self-assembled monolayer as a resist,[149] the authors found 15 nm as the smallest feature size, suggesting that real tip diameters were larger than the 20 nm assumed in the simulation. A counter-intuitive conclusion of these simulations was that a very small tip−resist separation (allowing higher resolution) may not be desirable as tunneling becomes unstable, eventually leading to a tip crash.

b. Langmuir−Blodgett (LB) Films. The system investigated by Stockman *et al.*[150−153] consisted of a Si(111) surface on which a thin (25 nm) gold layer was deposited by vacuum evaporation. On this gold surface, four layers of ω-tricosenoic acid were deposited using the Langmuir−Blodgett (LB) method. A STM, operating in field emission mode with biases of 8 and 10 V (sample-(+)), was then employed to pattern this surface by drawing lines at a speed of 1 μm s^{-1} using currents between 5 and 25 nA. Patterned regions of the ω-tricosenoic acid tetralayer were rendered insoluble in ethanol, presumably due to cross linking involving the terminal vinyl group. Consequently, following a patterning experiment, rinsing of the surface with ethanol removed the ω-tricosenoic acid resist layer only at nonexposed regions producing a negative mask. Argon ion milling was employed to selectively remove the exposed gold; regions underneath the cross-linked polymer were unaffected. In order to test the quality of the remaining gold, electrical resistivity measurements at varying temperatures were performed. These measurements showed a metallic resistivity vs temperature dependence, thus confirming the success of this experiment. The narrowest line width obtained was 15 nm, determined mostly by the tip shape. However, long and continuous lines (10 μm) could not be obtained with this minimum line width. An example of this scheme is shown in Figure 11.

LB multilayers of PMMA (two, four, and six layers) and monolayers of octadecanol ($CH_3(CH_2)_{16}CH_2OH$) were used as resists by Xu and Allee[154] on Au and Ti surfaces. LB film-modified surfaces were exposed in air with an STM using tungsten tips (E_B = 8−10 V

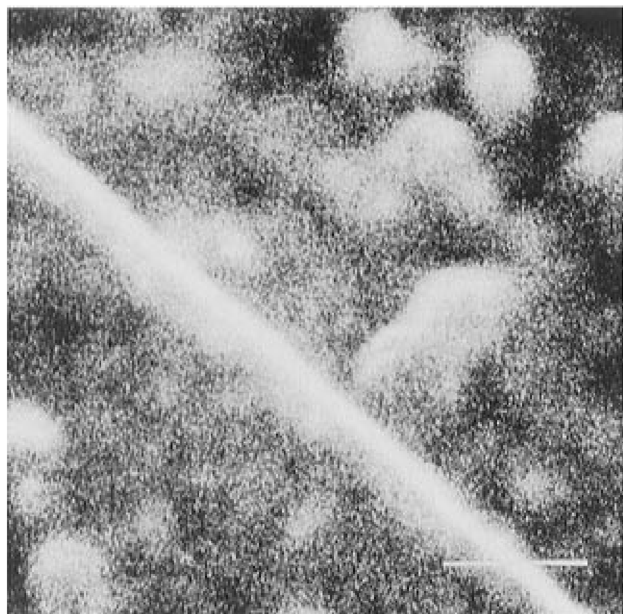

Figure 11. SEM micrograph of a 15 nm wide gold line obtained by patterning a ω-tricosenoic acid monolayer-modified gold surface using an STM. Exposure of this film using an applied bias of −8 to 10 V and 20 nA, cross-linking of the resist occurred rendering it insoluble in ethanol. Following STM patterning, unmodified regions of the LB film were removed by rinsing with ethanol, and argon ion milling was employed to remove gold from regions exposed by the rinsing step. Protruding gold lines, covered with the cross-linked ω-tricosenoic acid monolayer, were thereby obtained. The length of the scale bar is 1 μm. (Reproduced with permission from ref 153. Copyright 1993 American Institute of Physics.)

tip-(+), $I = 0.5-3.0$ nA). Octadecanol monolayers functioned as negative masks in these experiments: Nonexposed regions of the surface could be dissolved by acetone, whereas exposed areas were insoluble. Scanning Auger microprobe analyses revealed that the remaining LB regions (i.e., exposed regions) were covered by a contamination layer. PMMA LB films, in contrast, behaved as positive masks: Etchants (such as cyanide used for Au) caused the preferential removal of areas which were exposed by the STM, suggesting that the exposed and thus fragmented areas were more susceptible to the "attack by etchants". An advantage of PMMA resists patterned in air using the STM (as compared with conventional *in vacuo* e-beam protocols) was that a separate "development" step following the patterning of the surface was not necessary. Development of the PMMA resist causes a proliferation of the damage initiated by the electron beam. The authors attributed the stronger effect of STM patterning to enhanced oxidation of the PMMA resist in the proximity of the tip−sample gap.

Day *et al.*[155] reported that an LB monolayer of stearic acid could serve as a mask for STM based lithography on gold coated Si. The voltage threshold for creating modifications to the monolayer was found to be ±4 V, and a negative mask was created by the modification process: Removal of the LB film in chloroform or acetone left only the patterned structures on the sample.

Penner and co-workers[156,157] investigated the modification of Langmuir−Schaeffer-like bilayers of stearic acid deposited on the graphite basal plane surface using a STM in air. The application of bias pulses (6 V either polarity × 50 μs) caused the formation of lumps and voids having typical dimensions of 10−20 nm in diameter. The mechanism by which these modifications were produced was not apparent. Whereas lumps were persistent for hours, voids were observed to refill with material on the time scale of several minutes. This refilling was interpreted as the viscous flow of molecules from the bilayer and, using equations derived for the circular geometry of this experiment, the time required for the refilling of circular 10 nm diameter voids was used to calculate the viscosity of the bilayer. The viscosity values measured obtained using this method were in good agreement with expected values.

An unusual localized charging effect at LB-modified Au(111) surfaces was reported by Yano *et al.*[158] using a combined STM and AFM approach. Upon application of a triangular voltage pulse of 9 V tip-(+) (3 ms), an enhanced conductivity of the surface was seen by STM, despite the fact that AFM images of the same region showed almost no difference in topography. The reproducibility of this effect was demonstrated by generating 100 nanostructures on a 780 nm^2 area. Although the mechanism of this modification process was not apparent, the authors ruled out the possibility that metal might be field evaporated onto the surface of the LB film from the tip because the resulting metal nanostructures would be visible in an AFM experiment.

c. Self-Assembled Monolayers (SAMs). The selective removal of an alkane thiolate monolayer (*n*-octadecanethiol on Au(111); evaporated on mica) during STM imaging in air was reported by Kim and Bard.[159] The imaging conditions employed to effect removal of the alkane thiol layer involved the imposition of a small gap impedance of 1.0 MΩ obtained using $E_B = 10$ mV, and $I_T = 10$ nA. Under these conditions, it is likely that the STM tip is in physical contact with the monolayer and that a mechanical removal mechanism is operating. More nonperturbative imaging conditions (involving $E_B = 1.0$ V, and $I_T = 1$ nA), however, caused the removal of the thiolate monolayer when the same area of the surface was repeatedly imaged. Pits and mounds could also be formed with voltage pulses "a few seconds long" and having a 3.0 V amplitude and a sample-(+) or sample-(−) bias were applied, respectively.

Crooks and co-workers[160] investigated SAMs of octadecyl mercaptan ($CH_3(CH_2)_{17}SH$) on Au(111) for use in lithographic STM applications. Repetitive scanning of a small area with tunneling conditions of $E_B = 0.3$ V, $I_T = 0.1$ nA caused a visible modification of the substrate involving the sweeping of molecules to the edges of the scan window. At higher E_B values of 3 V, complete removal of SAM material within scanned areas was observed. In addition to scanning probe evidence for this selective removal process, electrochemical experiments independently demonstrated the generation of clean gold "microelectrodes" on the otherwise electrochemically inactive thiol-modified surface following the STM gen-

eration of one or more etched regions. Specifically, this experiment involved the STM etching of several $5 \times 5\ \mu m^2$ "windows" into the SAM, and the subsequent observation of $Ru(NH_3)_6^{3+/2+}$ cyclic voltammetry at the exposed gold surface within these windows in aqueous solutions.

This group also studied the chemical vapor deposition (CVD) of copper onto SAM-modified surfaces. It was observed that CVD copper deposition occurred preferentially at regions of the thiol-modified gold surface from which the thiol monolayer had been removed by STM-"etching"; disproportionation of the copper precursor, (hexafluoroacetylacetonato)copper-(I)−(1,5) cyclooctadiene, did not occur at thiol-modified regions of the surface.[161,162] Copper-filled squares with side lengths between 0.5 and 5 μm were produced using this scheme.

STM was also employed by Xu and Allee[154] to pattern SAMs of octadecyl mercaptan (i.e., octadecanethiol) on GaAs surfaces. Exposure involved imaging with a large E_B of 10 V (current = 0.5 nA) and produced a positive mask: Etchants such as ammonium hydroxide (NH_4OH) and citric acid [HOC-($CH_2COOH)_2COOH$] attacked only regions of the GaAs-modified surface which had been imaged by the STM. An increase in surface roughness of the GaAs surfaces was observed following the etching step-indicating that the SAM provided incomplete protection of the GaAs surface from these etchant solutions.

Marrian, Dobisz, Perkins, and co-workers[163,164] have investigated a variety of SAMs—based both on silane and thiol functionalities—for lithographic applications at Si(100) surfaces. [[[(Aminoethyl)-amino]methyl]phenethyl]trimethoxysilane [$(CH_3O)_3Si(CH_2)_2C_6H_4CH_2NH(CH_2)_2NH_2$, PEDA], [4-(chloromethyl)phenyl]trichlorosilane ($Cl_3SiC_6H_4CH_2Cl$, CMPTS), and octadecyltrichlorosilane ($C_{18}H_{37}SiCl_3$, OTS) were self-assembled onto native silicon oxide surfaces and patterned in UHV using an STM (see conditions below). After patterning, both types of resists were treated with Pd catalyst and a Ni-electroless plating solution. Only in unexposed areas did Ni deposition occur−indicating that the SAM layers function as negative masks. In contrast, OTS is a positive resist when used in combination with 50 keV e-beam lithography. The authors further established threshold values for the applied tunneling bias necessary to perform the lithography: For OTS this threshold was 10 V (sample-(+)), for PEDA, 8 V, and for CMPTS, 4V. These voltage threshold values did not correlate with the known photochemical sensitivity of these materials. In this initial work, the smallest transferred feature sizes were 20 and 25 nm; however, recent refinements of the method by these authors have permitted an improvement of the resolution to 15 nm.[149] This higher resolution was made possible by improvements to the level of dispersion of the Pd catalyst on the surface. An additional refinement involved the use of hydrogen-terminated silicon in place of surfaces terminated with a native oxide which were used in earlier studies. A lowering of the threshold from 8 to 6 V for PEDA was observed on such samples, likely contributing to the narrower lines obtained following exposure.

A modified STM was used by Müller *et al.*[165] to perform lithography on both SAMs of *n*-hexadecanethiol ($CH_3(CH_2)_{15}SH$) and *n*-docosanethiol ($CH_3(CH_2)_{21}SH$). The STM was equipped with a high voltage power supply (which enabled the application of bias pulses up to 200 V) and a fast $x-y$ scan generator. The monolayers were formed on polycrystalline Au films and patterned using an STM in UHV. During patterning the tip was operated in field emission mode with biases at around 100 V and currents between 0.1−2.0 nA. These imaging conditions produced a tip−sample distance of ~30 nm which, in turn permitted scan rates of 30 $\mu m\ s^{-1}$ to be employed. Gratings were obtained consisting of 50−100 nm high lines having a period of 0.2 to 1.6 μm. The smallest line width observed was 70 nm, and a threshold dose for patterning under these condition was established at 300 $\mu C\ cm^{-2}$—comparable to the thresholds seen for PMMA in e-beam lithographic work.

Lercel *et al.*[166,167] studied SAMs of octadecanethiol both on evaporated gold on Si(11) and GaAs(100) substrates. As had previously been demonstrated, this C_{18} thiol monolayer was found to be very stable on gold and protective for 24 h against oxidation in air even on GaAs surfaces. The localized modification of this monolayer was accomplished by applying a large imaging bias (4 V threshold) in a STM configuration. Minimum line widths between 15 and 25 nm were obtained, see Figure 12. On gold surfaces, the patterned SAM was used as a positive mask for a KI/I_2 etch. On patterned SAM-modified GaAs, an etchant containing NH_4OH, H_2O_2, and H_2O was found to be suitable. At applied biases below 4 V, modifications to the thiol-modified surfaces were also observed; however, these modifications were interpreted as mechanical in nature; apparently caused by the proximity of the tip to the resistive thiolate layer. Patterning in this low bias mode yielded irreproducible results—in particular, continuous lines could not be obtained.

d. Other Polymeric Materials. Polymers which are not conventional resist materials have nevertheless been found to have useful properties for SPL experiments involving electrical modification mechanisms.

A thin film of a very hygroscopic polymer, polyvinyl alcohol (PVA), was prepared on a graphite basal plane surface. By applying a pulse between the tungsten tip and the coated sample in a STM configuration in UHV and in air ambients, Tang *et al.*[168] fabricated structures with sizes between 0.5 and 2 nm. A pronounced effect of the relative humidity (RH) during PVA film preparation on the resolution of the modification process was observed. Apparently the polymer film could retain water even when loaded into a UHV chamber as nanostructures obtained in UHV resembled those seen in air and in low humidity air ambients (1−2 nm). At 100% RH, 0.5 nm structures were observed. The threshold voltage for structure fabrication increased from 2.9 V at 100% RH to 5 V in UHV conditions, suggesting that electrochemistry may play a role in the mechanism of the modification process.

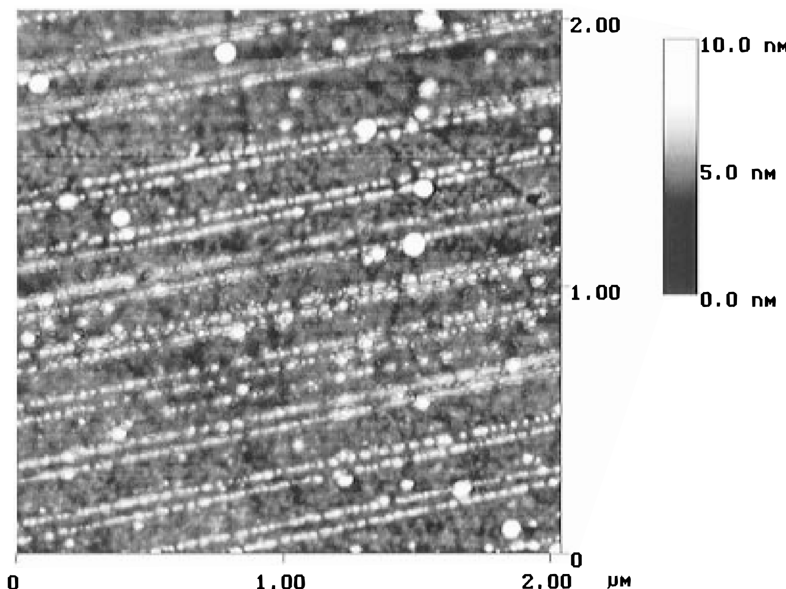

Figure 12. NC AFM image of lines, written with an STM, in a self-assembled monolayer of octadecanethiol on GaAs. The lines were produced using an imaging bias of 10 V (sample-(+)) and a tunneling current of 100 pA. The features shown are 2−4 nm in height. (Reproduced with permission from ref 166. Copyright 1994 American Institute of Physics.)

Bashkin *et al.*[169] reported the modification of thin layers of hexamethyldisilazane (HMDS, $[(CH_3)_3Si]_2NH$) on graphite. Hillocks were formed when a sample-(−) pulse between 4 and 6 V and 0.1 ms duration was applied. Also on an additional LB monolayer of barium stearate $[(C_{17}H_{35}COO)_2Ba]$ on top of the HMDS layer the same hillock formation was observed. Pulsing with amplitudes higher than 6 V also altered the surrounding substrate.

3. Material Transfer Between Tip and Surface

Material can be locally transferred from a probe tip to a surface (or vice versa) by a process which bears a resemblance to the field evaporation of materials seen in the field ion microscope (FIM).[170] SPL experiments of this type have been the focus of much prior research. Particularly in air ambients, however, other mechanisms (e.g., tip contact, electrochemistry) have been found to contribute to material transfer in addition to the field evaporation mechanism which is important in UHV. This is indicated, for example, by experimental findings that the threshold field strength required to effect transfer of several metals are uncorrelated in SPM-induced versus FIM-based experiments. Several reviews of the SPM literature in this area have been published by Tsong,[171] Lang,[172] and recently by Gratzke and Simon,[173] see below.

Gratzke and Simon[173] have focused attention on the mechanisms which might contribute to the transfer of metal atoms between a metal tip and surface during the application of a bias pulse in UHV. An early example of such an experiment was the deposition of gold mounds on a gold surface using a gold STM tip by Mamin *et al.*[174,175] Gratzke and Simon asserted that field evaporation cannot supply the necessary number of Au atoms (that is, the number required by the size of the mounds which are experimentally obtained) in the requisite time (i.e., the duration of the bias pulse). For example, Binh and Garcia[176] have calculated that an ion current of 10^6 s^{-1} is induced by a field of 10 V nm^{-1} (approximately equal to the field present in the STM experiment). This flux is insufficient to supply ~500 Au atoms in 10 ns as seen, for example, in the experiments of Chang *et al.*[177] Other mechanisms can also be ruled out either based on the results of calculations, or because experimental data does not provide evidence for the operation of these mechanisms: Joule heating-induced melting of the tip and tip deformations caused by electrostatic forces are two such mechanisms which are given consideration in that review. On the basis of the improbability of these other mechanisms, Gratzke and Simon proposed a new mechanism based on the Nottingham effect: The energy difference between electrons which leave the tip during tunneling and the electrons from an external circuit which replace these electrons is dissipated as phonons in the tip causing heating. The calculations of the authors' confirm that the rise time of the temperature to the melting point (of gold, for example) is of the same order of magnitude as the experimental pulse width. However, further experiments are necessary to decide the validity of this hypothesis, and further refinement of this model is also necessary. Joule heating and the Nottingham effect have been discussed also by Xu *et al.*[178]

As already noted, since the original work of Mamin *et al.*,[174,175] material transfer between a gold tip and a gold sample has been the subject of several studies: Chang *et al.*[177] found that in UHV STM experiments, tip-(−) pulses produced both pits and mounds with the same probability. This result is consistent with evaporation from both the tip and the sample with approximately equal probability, and leads to the expectation that similar statistics should be seen using a tip-(+) pulse polarity. However, a quick degradation of the tip was observed in this case. The different behavior seen with pulse polarity was explained in terms of the "regeneration" of the tip. If the tip is negatively biased, electrons are sourced by a relatively small area of the tip very near the apex.

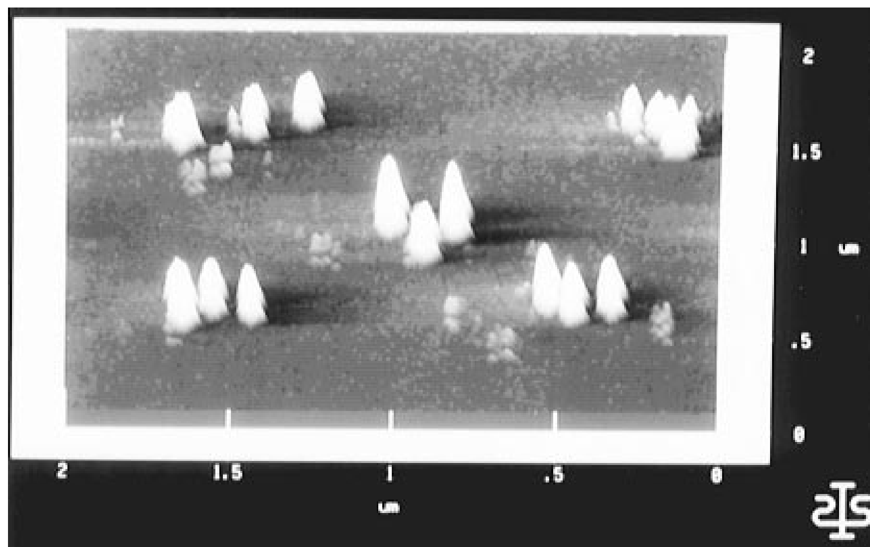

Figure 13. STM image of gold structures on silicon. The mounds were obtained by applying voltage pulses (12 V amplitude, 50 μs duration) between a gold STM tip and the hydrogen terminated Si(111) substrate resulting in material transfer from the tip to the sample. The structures in the corners of this image were produced with the tip biases negative with respect to the surface during the pulse; the center structures with the tip positive. Typical dimensions are 100 nm in diameter and 20 nm in height. (Reproduced with permission from ref 186. Copyright 1994 American Institute of Physics.)

With a positive tip bias, on the other hand, the "blunt" sample surface generates a relatively diffuse stream of electrons which impact the tip over a relatively large area. Consequently, the current density in this geometry can be too small to cause the level of tip heating required for melting and regeneration. The authors also observed a broad size distribution for both pits and mounds, and a sharp threshold for the modification process with tip-(−) bias: A 100% efficiency of modification was seen with a 3.9 V pulse height, whereas 3.2 V pulses almost never created a pit or mound.

These conclusions were substantially confirmed in the work of Ohi *et al.*[179] However, these workers did not report pits for pulses having a sample-(−) bias. The broad distribution of mound sizes, however, is explained as follows: The rapid transferal of atoms from the tip to the surface results in the formation of a gold "bridge" or "neck" from the surface to the tip because the rate of the deposition exceeds the time response of the feedback circuit. The current transient associated with this momentary short eventually (in a few ns) causes the retraction of the tip and the breaking of the gold bridge. The shape of the tip and the amount of atoms transferred in this process are obviously determining of the final shape of the generated structure and can also explain, qualitatively, a large fluctuation in the shape and size. Related work involving quantum point contacts has been reported by Pascual *et al.*[180]

Mascher and Damaschke[181] reported a threshold field of 3 V nm^{-1} for the Au−sample/Au−tip system for experiments performed in air. These workers showed that by applying a triangular pulse with amplitudes between 3.5 and 5 V and a duration of 1 s, the above mentioned erratic behavior of mound and pit formation was overcome: Triangular pulses with sample-(+) bias exclusively formed pits, whereas pulses with sample-(−) bias formed hillocks only.

The patterning of gold surfaces using Pt/Ir tips has also been reported by Bessho and Hashimoto.[182] In these experiments, a voltage threshold for pit formation in air was 2.2 V [sample-(+)], and a 90% success rate was obtained at 3 V. Mounds were obtained with sample-(−) pulses and the same voltage values for both threshold and 90% success rates were seen. Mounds, generated using sample-(−) pulses, could be removed by applying a second sample-(+) pulse in some cases. The authors attribute this behavior to characteristics of the Pt/Ir tips used in these experiments.

Lebreton and Wang[183] wrote letters (appearing as grooves) ~30 nm in height on gold surfaces using Pt/Ir tips in air. A humidity of at least 18% was required for successful patterning and the patterns written in the gold surface remained stable over several days in dry nitrogen environment.

Tungsten tips were employed by McBride and Wetsel.[184] They also were able to produce both pits and mounds depending on the polarity of the pulse. The mounds, however, adhered poorly to the surface.

Schaub *et al.*[185] further investigated hillocks created with STM tips made of Fe, Ni, and Pt.

Penner and co-workers[186] investigated lithographic processes at hydrogen-terminated Si(111) surfaces using gold and copper STM tips in air and in N_2 ambients. By means of scanning Auger microprobe analyses, it was demonstrated that for sample-(+) pulses, metallic structures having typical dimensions of 20-50 nm in diameter and 1−5 nm in height could be formed, as shown in Figure 13. Typical pulse parameters were 5−20 V (amplitude) and 2 μs to 2 ms (duration). Structures were also obtained using sample-(−) pulses; however, these protrusions were not stable to repeated STM imaging and Auger analysis did not indicate the presence of metal on the silicon surface. On the basis of the SAM analyses, the authors proposed that the structures obtained using sample-(−) pulses consisted either of contaminants or of oxidation products of the silicon surface.

Au STM tips were used by Hosaka *et al.*[187] to write "Tbit" onto SiO_2 with 0.5 μm gold letters consisting

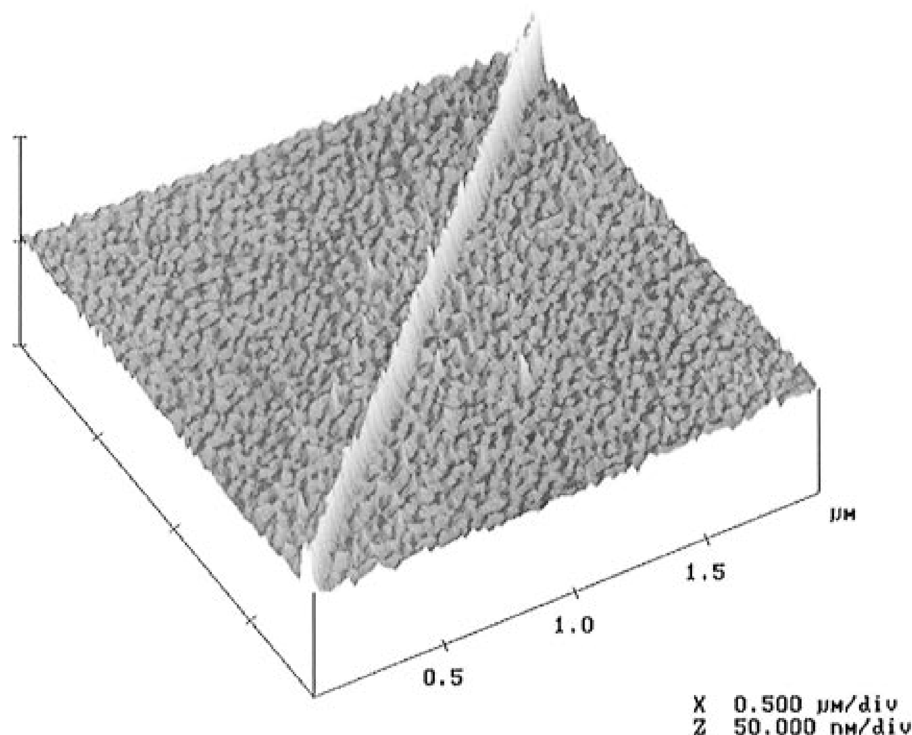

Figure 14. STM image of a nickel line on silicon which was fabricated using the CVD scheme with $Ni(CO)_4$ as precursor at a base pressure of 5×10^{-5} Torr. A writing bias of bias 15 V (sample-(+)), and current of 2.0 nA, were employed at a velocity of 190 nm s^{-1}. The tip was rastered several times along this line in order to produce a continuous line, resulting in a effective writing speed of 10 nm s^{-1}. The line is 14 nm high and 6.2 μm long with an apparent width 40 nm (measured as FWHF). (Reproduced with permission from ref 357.)

of mounds with a ~20 nm diameter. In contrast to the experiments described above, thresholds were sample-(+) 70 V and sample-(−) −40 V; values in agreement with theoretical values for field evaporation despite the fact that these experiments were also performed in air. In later work, these authors also showed that using smaller bias pulse amplitudes (10 V), the deposition of gold particles was possible.[127,188]

Hosaka and co-workers have also employed gold covered AFM tips to pattern gold surfaces in air. Reproducibility was similar to that seen in the prior STM experiments of this group.[189−191] In addition to gold surfaces, this group also deposited gold structures on the graphite basal plane using the same technique. For bias pulses having a small amplitude sample-(+) 5 V, pits in the graphite surface were obtained and, upon increasing this amplitude to 10−25 V, mounds were obtained.[192] A theoretical treatment of field emission confirmed the feasibility of this process. The threshold voltages predicted by this theory did not agree well with experiment, but these differences were attributed to the imprecision with which the tip−sample distance was known. This theory also predicts a lower threshold voltage for gold atom transfer using a negative tip bias as compared with a positive tip bias.

Lozovik and co-workers[193] suggested the following experiment for nanoscale lithography: In a STM configuration tips are employed made of a metal that is able to adsorb larger amounts of hydrogen, e.g., Pd. When a pulse is applied between sample and tip, hydrogen will be emitted from the tip and can cause local chemical and/or physical modification on the surface.

Pérez-Murano *et al.*[194] used tapping mode AFM with gold-coated tips to pattern silicon surfaces with small gold mounds by applying 5 V sample-(+) pulses. With a 100 kΩ resistor in series, current was limited and the authors observed mound formation but did not attribute these to gold deposits but to oxide formation. This was seen after subsequent etching that resulted in pits for this case, whereas when gold was deposited mounds would remain.

Shekhawat *et al.*[195] used Al STM tips to fabricated lines onto a hydrogen terminated p-type Si(100) substrate. Lines were generated in air by applying a bias of 3.5 V and current of 2 nA. The authors further claimed that tunneling spectroscopy revealed metallic characteristics of the lines and therefore suggested that these lines (10 nm wide and 21.5 nm high) consist of Al.

4. Chemical Vapor Deposition

The first SPL experiments in which gas-phase CVD-like precursors (volatile metal organic complexes) were reacted using an STM were reported by the research groups of de Lozanne[196] and McCord[197,198] in the late 1980s. A pervasive problem in the early experiments of this type was the high levels of carbon incorporated into metal nanostructures prepared by CVD. This contamination was derived from the organic ligands which are required to confer volatility in metal-containing precursors. As indicated in the synopses which follow, this problem has now been defeated for several metals. An example of structures obtained using this CVD scheme is depicted in Figure 14.

CVD deposition has been extended to reactive metals, including aluminum and tungsten.

Baba and Matsui[199] reported that sample-(−) pulses having a 4 V amplitude caused the precursor gas, WF_6 (4.5×10^{-6} Torr), adsorbed on a Si(111) surface, to be dissociated. Pulses having the opposite bias, on the other hand, produced only carbonaceous deposits derived, presumably, from contamination in the vacuum chamber.

Trimethylaluminum (TMA, 10^{-4} Torr) was employed by Yau *et al.*[200] to create Al deposits on graphite surfaces. A threshold voltage for this deposition was found at 3.5 V. At higher biases, pits were formed in the graphite (see b) and metal deposits were not observed.

De Lozanne and co-workers have refined their original CVD methodology and demonstrated that high purity metal nanostructures are accessible using this technique. For example, de Lozanne and Rubel *et al.*[201−204] investigated CVD processes with $NiCO_6$ as precursor. Typical parameters were 10^{-5} Torr $NiCO_6$, 15 V bias, and a writing speed of 10 nm s^{-1}. Lines with minimum dimensions of 24 nm wide and 4 nm high were obtained. Long lines, having uniform dimensions were reported to be difficult to obtain. Auger analyses revealed that the formed structures were up to 95% Ni. In order to investigate the electrical properties of lines fabricated with this technique, the authors attempted to draw lines between prefabricated contact pads. For this purpose a high-resolution tip positioning system was implemented, and for these experiments, a combined STM and SEM was used. Four probe resistance measurements were performed as a function of temperature, and an estimation for the resistance of a single Ni wire was 25 $\mu\Omega$ cm.[205]

Similar precursors were used by Kent *et al.*[206,207] to fabricate an array of several hundred iron structures on a silicon substrate using gaseous $Fe(CO)_5$. These particles were employed for investigations of the magnetic properties as a function of the particle size. Experimental parameters were as follows: $E_B = 15$ V (sample-(+)), $I_T = 50$ pA, $P_{Fe(CO)_5} = 3 \times 10^{-5}$ Torr. Auger spectroscopy revealed a minimum iron content of 50% in these structures. The application of sample-(−) pulses resulted in the deposition of structures having a composition of 10% iron and 90% carbon. This difference in composition suggested the existence of two different decomposition modes for the precursor: Electron bombardment of the precursor molecules for sample-(+) biases, versus field-induced reaction with sample-(−) polarity.

Iron-containing nanostructures have also been deposited using ferrocene as a precursor by Thibaudau *et al.*[208] The following experimental findings were reported: At a threshold bias of 1.7 V [sample-(−)], ferrocene pressure in the chamber could be varied between 10^{-4} and 10^{-3} Torr and the writing efficiency was found to be independent of the tunneling current within 0.04−4.0 nA. Letters, 30 nm high and 3 nm wide—consisting of a string of particles—were deposited. The authors predicted that the structures possessed a composition of ~1:1 Fe:Si, however experimental proof of the composition was not available.

Palladium was deposited onto p-Si(111) using allylcyclopentadienyl palladium ($Pd(C_3H_5)(C_5H_5)$) as a precursor by Saulys *et al.*[209] Deposition occurred on both tip and sample depending upon the polarity of the applied bias and was performed in an UHV chamber with 4×10^{-11} Torr base pressure and an estimated pressure of the precursor of 10^{-5} Torr. Deposition on the sample was seen when reimaging the surface, whereas Pd deposition on the tip was deduced to occur based on improvements to the imaging resolution. Line drawing was performed by means of rastering the tip along one line for several times at a 3−4 V bias. These lines, having apparent widths of 50 nm and heights of 10 nm, were found to be discontinuous (as was apparent from topographical images) and to consist of a series of dots.

In addition to metals, the nonmetals gallium and silicon have also been deposited using the CVD strategy in three previous instances:

Uesugi *et al.*[210] employed physisorbed gallium precursor to deposit Ga on Si(111) surfaces. Rather than maintaining the precursor gas in the UHV chamber at a certain pressure—the practice in all of the experiments involving metal deposition above—the authors exposed the H-terminated Si(111) surface to 10^4 Langmuirs of triethylgallium (TEG) and then evacuated the chamber. Dots with apparent diameters between 2 and 13 nm were produced by the application of sample-(−) pulses having an amplitude of at least 2.5 V. No structures were obtained for sample-(+) pulses. The authors suggest that under the influence of the electrical field the weak Ga−C bond of the TEG molecule breaks and reactive Ga atoms bond with Si atoms of the sample surface.

Rauscher *et al.*[211] operated a STM in field emission mode ($E_B = 40$ V, $I_T = 30$ pA) to crack SiH_4 precursor molecules at a Si(111)-(7×7) surface. The exact composition of the fabricated deposits was not reported in this paper, but the presence of Si−H species was expected. Structures with heights between 0.4 and 5 nm with apparent widths of 40 nm were observed. The site selectivity of the fabrication process was imperfect since deposited material was observed up to 200 nm from the position of the tip on the surface. This absence of site selectivity was attributed to the transport of "activated" SiH_4 molecules away from the tip−sample gap prior to deposition as a consequence of cracking. A rough calculation showed that the efficiency of the cracking process should at least be 15%. A linear relation between amount of deposited material and deposition time (bias at 40 V) was observed, indicating that the deposition rate is constant.

Nanolithography based on the decomposition of SiH_4 was also investigated by Wong *et al.*[212] who fabricated discontinuous lines 2−5 nm in width and ≤100 nm in length. These workers emphasized the importance of the tungsten tip in the process and suggested that SiH_4 is fragmented at the tungsten surface under the influence of the applied field. This field further induces surface diffusion of the silane fragments to the apex of the tip where they are field evaporated to the sample. Shielding effects of the tip were also reported.

5. In Situ SPL in Liquids

In situ SPL experiments in liquids usually involve either of two types of electrochemical processes which

can be directed in a localized fashion at a conductive surface using an STM (or AFM) tip: *Deposition reactions* involve the localized electrochemical synthesis of a material on the surface, whereas *etching reactions* are those which result in the localized removal of material from the surface.

The field-assisted etching of Si(100) and GaAs(100) surfaces was observed by Nagahara *et al.*[213] A STM was operated in the so-called two-electrode mode[214] with a bias of 1.4 V (tip-(+)) and a current of 1 nA in 0.05% HF (with a Pt/Ir tip). Etched scan windows could be observed in the repeated imaging of an area. The etch rate was observed to be dependent upon the scan speed, i.e., the dwell time of the tip over a particular region of the sample. The authors scanned varying areas with the same nominal scan rate of 10 Hz and found that when the "image acquisition rate" was greater than 28 000 $nm^2\ s^{-1}$, no modification of the sample surface could be discerned. The smallest etched structures had linewidths of 20 nm and depths were 1−5 nm. Mechanical ablation of the surface by the tip was ruled out as a mechanism for this lithography because etching was not observed in other electrolytes such as pure water or dilute H_2SO_4. The importance of the applied field was demonstrated using experiments in which the tip was retracted from the surface by 50 nm, thereby lowering the applied field by at least 1 order of magnitude. Under these circumstances, the etching of these surfaces was not observed.

The etching of Si(100) surfaces was also investigated by Ye *et al.*[215] using a four-electrode STM[214] operating in 10 mM HF. In these experiments, the silicon surface was modified using either anodic and cathodic positive potentials, i.e., below 1 V vs NHE or above −0.5 V. The authors assume that in the case of negative sample potentials, the surface gets attacked by the HF under the influence of the electric field between tip and sample causing localized dissolution of Si. With positive voltage pulses, apparent depressions were formed, but the authors assumed that these depressions were not purely topographic but also electronic in nature due to the formation of silicon oxide on the sample.

Li and Crooks *et al.*[216] observed the selective dissolution of a Au(111) surface in F^- and CN^- containing electrolytes. Using tunneling conditions of $E_B = 0.1$ V (tip-(+)) and $I_T \approx 0.5$ nA, etching was not observed in 0.1 M KF solutions at the open circuit potential (OCP) of the surface (ca. +200 mV vs Ag/AgCl). However, at −150 mV vs Ag/AgCl the nucleation and growth of monoatomic deep pits was observed. Imaging larger areas showed that pitting was confined to regions of the surface which had been previously imaged. In 0.001 M KCN, 0.1 M KOH solutions, and using similar tunneling conditions, the gold surface was stable at potentials below −770 mV vs Ag/AgCl, whereas at potentials above −520 mV, dissolution was again observed. The authors further observed that a positive bias (tip vs sample) accelerated the dissolution process, whereas a negatively biased tip locally retarded dissolution.

Using an AFM in contact mode, Chen and Guay[217] showed that aluminum surfaces could be locally dissolved. Both bulk polycrystalline Al surfaces, and Al films evaporated onto glass surfaces were employed for these studies. Upon repetitive scanning of the Al surface using a force of ~200 nN for 2 h in 0.1 M NaCl, depressions were formed in the sample which, for evaporated Al surfaces, extended to the underlying glass substrate surface. In pure water ambients, no modification of the aluminum surface was seen using identical imaging conditions, whereas in 1.0 M NaCl, the dissolution process was not spatially selective—corrosion of the entire aluminum surfaces was instead observed. The authors proposed that the AFM selective etching effect was induced by the dissipated energy from tip−sample frictional forces.

As first demonstrated by Albrecht *et al.*[101] (see the section on layered or van der Waals Materials), the application of an STM bias pulse while tunneling at a basal plane graphite surface can cause the formation of pits in the surface. The characteristics of this STM-induced pitting of graphite surfaces was studied in liquid ambients by Penner, Heben, *et al.*[218,219] In aqueous electrolyte solutions, a threshold level of 4 V for pit formation was seen, and this threshold was independent of the bias pulse polarity, and the tunneling conditions (within the range explored by the authors). This fact argues for a nonelectrochemical mechanism for this modification process. At the 4.0 V threshold required for pit formation, small mounds having dimensions of 0.7 nm wide and 0.22 nm deep were sometimes seen, whereas pulses with larger amplitudes formed pits with diameters of 2 nm or more. The depths of the pits was usually one or two graphite monolayers. Although the mechanism of this pitting reaction was incompletely understood, the presence of water was required: Attempts to effect pit formation in dry, nonaqueous solvents (including acetonitrile and methanol), and in dry N_2 gaseous ambients failed.

Metal plating is the most straightforward, and the most studied, type of deposition. It is therefore not surprising that most initial forays into the area of SPL electrochemical deposition by several groups has involved attempts to locally deposit metals using the STM.

Li and Penner *et al.*[220−223] have used the bias pulse-induced pitting of graphite to prepare nucleation sites which facilitate the deposition of metal (Ag and Cu) nanostructures. Silver and copper particles (having dimensions of 20−50 nm diameter × 1−7 nm height) were deposited at graphite surfaces immersed in dilute ($[M^{n+}] \approx 0.5$ mM) metal-plating solutions by applying bias pulses in a two-electrode STM configuration; an example is shown in Figure 15. *Ex situ* scanning Auger microprobe analyses confirmed that the nanostructures deposited using this method from silver electrolytes were composed of silver. The bias pulse consisted of an initial voltage spike (sample-(−), 6 V × 5 μs) which caused the formation of a pit on the surface, followed immediately by a 3 V × 50 μs pulse which induced metal deposition at this pit. By varying the concentration of the metal ion in the electrolyte, it was demonstrated that dissolved metal ions do not supply the growth of metal nanostructures in these experiments. Instead it was experimentally demonstrated that an under-potentially deposited (UPD) silver monolayer[224,225]—adsorbed at

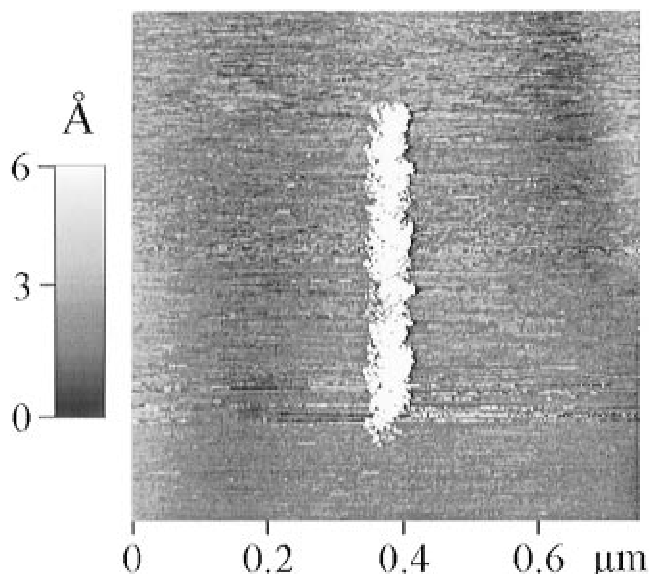

Figure 15. STM image of a silver line on graphite acquired in aqueous 0.1 M $AgNO_3$. This line was formed by applying a series of bias pulses between the platinum STM tip and the HOPG sample with a small lateral movement of the tip between each pulse. Each write pulse sequence consisted of a 6 V × 5.0 μs initial pulse (pit formation) followed immediately by a 3 V × 50 μs pulse (metal deposition) with the tip positively polarized in both cases. The height of the structure is about 1 nm.

the platinum STM tip—provided the precursor silver required for the creation of silver nanostructures in these experiments. The silver in this monolayer is alternatively stripped (during nanostructure growth), and replenished by adsorption of Ag^+ from the electrolyte solution (during the intervals between nanostructure deposition). Monte Carlo simulations of the deposition process confirmed the feasibility of this mechanism, and additional electrochemical experiments addressed issues relating to the kinetics of regeneration of the silver UPD layer, and the chemical nature of this layer at the surface of the platinum STM tip.

Will *et al.*[226–228] used a STM, operating in the four-electrode mode, to locally deposit copper nanostructures on gold surfaces from dilute copper plating solutions. Before applying a potential step to the substrate, the initial potentials of Au(111) sample and tip were chosen such that an UPD monolayer of Cu existed on the Au substrate (+9 mV vs Cu/Cu^{2+}). The tip bias relative to the sample was adjusted to insure that excess Cu also existed on the tip (−30 mV vs Cu/Cu^{2+}). From these initial conditions, the sample potential was stepped briefly by +50−90 mV causing a momentary inversion of the tunneling bias—and, of course, two excursions of the bias through 0.0V. These "zero crossings" are believed to provide the means by which the tip is moved gently, and momentarily, into contact with the sample surface allowing a cluster of copper atoms to be transferred from the tip to the surface. The electrochemical disposition of the tip and sample at the beginning of this experiment (specified above) are crucial to its success. If, for example, copper is not present on the STM tip, no clusters are deposited. It was further shown that the size of the clusters could be varied with varying the pulse amplitude; surprisingly with smaller pulse widths leading to larger structures. These clusters had heights of 0.4−1.5 nm, and apparent widths of 5−8 nm. Clusters could be produced in rapid succession (>10 Hz) and placed within 10 nm of each other.

In addition to the STM, the scanning electrochemical microscope (SECM[229]) has also been employed for the local electrochemical deposition on surfaces. Shohat and Mandler[230] used the SECM to create Ni-$(OH)_2$ nanostructures in a scheme involving the perturbation of the local pH. Methyl viologen (*N,N*′-dimethyl-4,4′-bipyridinium dichloride) was used as a redox couple in an aqueous nickel containing electrolyte buffered at pH 5.5. Feedback current—associated with the reversible oxidation of $MV^{\bullet +}$ to MV^{2+} at the platinum surface, and rereduction to $MV^{\bullet +}$ at the tip—permitted the operation of the SECM in the so-called positive feedback mode (see ref 231 and references cited therein). The oxidation reaction of $MV^{\bullet +}$ at the sample surface, however, also involves removal of a proton from the electrolyte (by hydrogen reduction), causing a local increase of the pH which was sufficient to promote deposition of Ni-$(OH)_2$. Lines roughly 80 and 150 μm wide were fabricated using a 50 μm tip and lateral scan rates between 0.1 and 1 $\mu m\ s^{-1}$, respectively. The platinum surface itself played a crucial role in this experiment—on glassy carbon surfaces, for example, no $Ni(OH)_2$ deposition was observed.

Meltzer and Mandler[232] used a SECM to locally deposit gold from a gold UME onto a indium tin oxide (ITO) substrate. The first step of this process involved the anodic dissolution of gold at the UME in the presence of Br^-. At the ITO surface, the gold complex $AuBr_4^-$ was reduced leading to a gold deposit. This deposit consisted of dots of roughly 1 μm diameter. If the tip was moved along the surface, lines with could be written. The resolution in this and other SECM experiments was believed to be limited by the size of the UME. The quantity of gold deposited per dot was sufficiently small (as calculated from the feedback current) to permit the UME to be used for lithography for an extended time.

LaGraff and Gewirth[233,234] described a fundamentally different approach involving the localized removal of a passivation layer on an immersed metal electrode surface using the tip of an AFM. The specific system of interest was a Cu(110) surface immersed in $HClO_4$ (pH 2.45)/10^{-5} M Cu and maintained at open circuit potential (280 mV vs NHE). Upon applying a higher imaging force of 25 nN (increased from 5 nN), a sample-(−) 70 mV pulse caused the localized deposition of Cu. In previous work by this same group,[235] the existence of an epitaxial oxide adlayer on the copper surface has been demonstrated under the conditions existing in the lithography experiments. This oxide adlayer apparently suppressed the deposition of copper which, at lower pHs where this layer is absent, occurs at small negative overpotentials. However when this adlayer was disrupted by imaging at an applied force of 25 ± 5 nN, copper electrodeposition promptly occurred within the scanned region and nanostructures, having heights of 40−60 nm, were obtained. Lateral dimensions could not be given precisely due to tip convolution.

In addition to metals and metal oxides, polymers have also been electrochemically synthesized in a localized fashion on surfaces using the STM. The focus in experiments of this type have been the electronically conductive polyheterocycles (e.g., polypyrrole, polythiophene). In principle, the synthesis of these polymers is easily implemented using the STM because polymerization is initiated and propagated simply by poising either the tip or sample potential sufficiently positive to cause the electrochemical oxidation of the appropriate monomer. The first experiment of this type—and the only example of SPM-induced localized polymerization prior to 1991—was an experiment in which an aniline-containing Nafion layer on a platinum surface was reacted using the tip of a SECM.[236]

Since 1991, many additional cases have been reported, and high resolution for this type of SPL process has been demonstrated. Polypyrrole (PPy) was singled out for investigation by Sasano *et al.*[237] In a pyrrole containing electrolyte (0.01 M pyrrole, 0.003 M $LiClO_4$ in propylene carbonate), structures 30 nm in diameter were formed on HOPG basal plane surfaces as follows: The sample was potentiostatted slightly negative of the polymerization threshold and the tip was poised at a potential slightly positive of this value for several minutes. Although these conditions would appear to favor electrochemical deposition of PPy *on the tip*, this difficulty was not reported. Instead, after applying these potentials for 5−15 min, cluster-like structures were found *on the sample*.

Yang *et al.*[238] applied pulses over a wide voltage range (3−7 V, 1−10 s) to effect the localized polymerization of pyrrole on Au(111) surfaces from solutions of aqueous 0.04−0.05 M pyrrole and 0.02−0.05 M $(C_2H_5)_4N\text{-}BF_4$. These workers also reported that upon application of a pulse with the opposite polarity, fabricated structures could be removed. Macroscopic analogies to this removal at positive potentials do not exist for PPy and the nature of the removal process is therefore unclear. A distinguishing characteristic of this work was the excellent reproducibility of the modification process which was demonstrated. In one case, the pulse-to-pulse reproducibility enabled the word "Science" to be spelled out on a gold surface.

A similar approach was undertaken by Yaniv and McCormick[239] who reported the use of sample-(+) bias pulses of 7.5 V amplitude and 250 ns duration to fabricate PPy structures having typical dimensions of 50 nm on the HOPG basal plane.

As already noted, the SECM has also been employed for localized polymerization experiments. PPy lines having a 50 μm width and a length of up to 1 mm were deposited on Au-coated glass surfaces from dilute pyrrole-containing electrolyte solutions by Kranz *et al.*[9,240] For polymerization, the SECM was operated with the probe—a 10 μm UME—as a counter electrode and a Ag/AgCl reference electrode. A programmed pulse sequence was applied that included first a 1.2 V × 2 s pulse that initialized pyrrole oxidation. This pulse was followed by a 0.85 V × 1 s pulse to complete oxidation, and a final 2 s period at the imaging bias (0.35 V vs Ag/AgCl) to allow reequilibration of the monomer concentration in the vicinity of the tip. The tip was moved during the application of this pulse train at a speed of 2.6 μm s^{-1} and lines having the above-mentioned dimensions were obtained by repeating each scan five times.

Borgwarth *et al.*[241] used SECM to locally polymerize a thiophene derivative (2,5-bis(1-methylpyrrol-2-yl)thiophene). The molecules were deposited as monomer onto an ITO surface by evaporation and then locally polymerized using the SECM in aqueous 0.1 M KBr/0.9 M Na_2SO_4. This was accomplished by electrochemically oxidizing bromide to bromine at the tip; this bromine then diffused to the surface and oxidized thiophene monomers to initialize the polymerization to polythiophene. Lines, approximately 20 μm in width and more than 100 μm in length, were fabricated with the 10 μm SECM tip. A distinguishing characteristic of this experiment was the fact that the sample surface played no role in the polymerization process. Oxidizing equivalents were delivered to the adsorbed thiophene via bromine which was created (from Br^-) at the tip. Following patterning experiments, residual (nonoxidized) monomer could be removed using either acetone or acetonitrile leaving PPy lines having a width of 20 μm. This resolution was attributed to diffusional broadening caused by the diffusion of the bromine away from the UME tip before reaction with the monomer.

The localized polymerization of aniline at graphite surfaces using an STM was investigated by Nyffenegger and Penner.[242] A sequence of two pulses were applied in order to generate each PANI nanostructure (~10−30 nm diameter × 0.5−5 nm height) in these experiments: An initial 6 V × 5 μs [sample-(+)] spike caused the formation of a pit on the graphite surface (see above) and a second 3 V × 50 μs pulse induced the polymerization of aniline at this pit. PANI is known[243,244] to exhibit an oxidation state dependent volume: The oxidized form of the polymer had a larger volume than the reduced form of the polymer. *In situ* measurement of the particle volume as a function of potential demonstrated that individual nanostructures prepared using this procedure also exhibited this property, indicating that these particles were, in fact, PANI. As in the case of the silver deposition experiment reported by this group (see above) it was demonstrated using Monte Carlo simulations that the flux of dissolved aniline molecules at the reaction site (i.e., the pit) integrated over the 50 μs duration of the experiment, was insufficient to supply the quantity of aniline required to support PANI nanostructure growth. On the basis of this analysis, and other experimental data for this system, a physisorbed layer of aniline at the graphite surface was postulated to provide the primary source for "precursor aniline" for nanostructure growth in these experiments. Qualitatively as expected, the success rate for STM-directed PANI deposition was observed to depend sensitively on the electrochemical potential of the graphite surface with a maximum in the success rate coinciding with the potential of zero charge of the graphite surface.

6. Atomic-Scale Modification Processes

In this section—for the reasons already discussed in the introduction—we briefly list work which has

been published without attempting a description of the experiments contained in each contribution. All of the following experiments were performed in UHV. A typical example is shown in Figure 4.

The low-temperature manipulation of atoms and molecules has been reported by Eigler *et al.*[7,8,245,246] and has been summarized, e.g., by Stroscio and Eigler.[247]

Meyer *et al.*[248−250] have also described the manipulation of single atoms at low temperatures and demonstrated writing capabilities.

Cesium structures on GaAs and InSb were fabricated by Whitman *et al.*[251]

Lyding and co-workers[252−254] desorbed hydrogen from the Si(100)2×1 monohydride surface at the near atomic level by applying 4.5 V [sample-(+)] pulses. No modification was observed with pulses up to 10 V having the opposite polarity. Line widths of less than 1 nm were obtained. Upon exposure to O_2, only the depassivated, i.e., hydrogen free, pattern was "affected", as seen by comparing the patterns before and after exposure. NH_3 was also found to repassivate the exposed area.

Lyo and Avouris[255−258] were able to remove a single silicon atom from the Si(111)7×7 surface by applying a voltage pulse between tip and sample in a STM configuration. A silicon atom could subsequently be reinserted into this vacancy by applying a second pulse having the opposite polarity. Hasegawa and Avouris[256,259] removed single atoms from a reconstructed Au(111) surface. The vacancies produced by this process caused both short-range and long-range modifications of the $22 \times \sqrt{3}$ reconstruction of this surface.

Also on the Si(111)7×7 surface, Aono and co-workers[260−264] investigated the influence of tip composition on the nature of the modification produced by bias pulses. These workers reported that the transfer of Si atoms from the surface to the tip occurs with an exponentially decreasing probability even after the bias pulse has been turned off.[261] A tip material dependence of the critical bias (field) was observed and correlated with the respective work function of the tip material: Low work function metals (Ag, W) exhibited a higher threshold than high work function materials such as Pt and Au.[262,263]

Komeda *et al.*[265] described a modification scheme involving a tip excursion toward the sample surface up to point contact. Jumps in the current response during this excursion were attributed to the removal of single atoms from the Si(111) surface.

Iwatsuki *et al.*[266,267] showed that relatively large (80 nm in diameter, 5−10 nm in height) but well-defined pyramids could be fabricated on Si by applying a small bias at either Si(111) or Si(100) surfaces held at 600 °C. Hexagonal pyramids were formed on Si(111) and square pyramids on Si(100).

Salling *et al.*[15,268,269] patterned the (100) surface of Si as well as antimony monolayers deposited on this surface.

Gu *et al.*[270,271] removed atoms from the Si(111)7×7 surface by altering the tunneling current from the 1 nA set point employed for imaging to 30−50 nA. Straight lines could be formed having the same width as the unit cell when scanning along low index directions of the surface. Scanning along other directions produced somewhat broader and less regular lines.

Tsong and Chang[272] observed that also during imaging, Si atoms previously desorbed from the sample could evaporate back. They obtained markedly different images of a previously formed structure depending on the imaging bias which probably caused a different flux of atoms back to the sample.

Hosaka *et al.*[187] removed single S atoms from a MoS_2 surface to obtain a pattern of sulfur vacancies arranged to spell the word "nanospace". The removal of each S atom was accomplished by the application of a sample-(+) 5.5 V × 70 ms pulse.

On InSb(110) surfaces, small pits were produced using imaging conditions of 3 V sample-(+) and 120 pA when the tip was maintained at a particular point on the surface or a very small area was rescanned several times. The dimensions of these pits depended on the "exposure" time. A 100 s exposure, for example, produced a pit having a 2.5 nm diameter.[273]

7. Applications

In the following section we review SPL experiments where the fabricated features were used as a part of a *device*. Within this section, we have not distinguished between various fabrication mechanisms.

The potential for obtaining very high information storage densities is often cited as motivation for pursuing SPM-based modification. Several papers have appeared which have specifically sought to demonstrate some of the capabilities required for a practical memory including pulse-to-pulse uniformity, high contrast, error checking, and correction (the ability to identify a modified region by more than topography alone), erasability, persistence, and last but not least high writing/reading speeds.

Vanadium-based glasses were investigated by Sato *et al.*[274−276] for applications as a SPM-addressable high density storage media. The application of a 4 V pulse between the tip and the glass (with V_2O_5 as electrical conduction component) in a STM configuration caused the appearance of hillocks having a diameter of ~15 nm in the current signal of the STM. These hillocks were explained in terms of a phase transformation from the amorphous into the crystalline phase. A negative pulse having the same amplitude caused this process to be reversed, and the crystallite to be erased. Up to 10 reversible cycles could be performed at a particular site on the surface; however, subsequent attempts to erase crystallites were unsuccessful. Current−voltage spectroscopic investigations of the glassy and of the crystalline forms of the vanadium glass revealed behavior characteristic of a semiconductor and a metal, respectively. Consequently, these two forms were distinguishable in a STM configuration because at a fixed bias voltage, the crystalline form exhibited higher conductivity.

AFM-induced local changes of conductivity in amorphous $GeSb_2Te_4$ films were demonstrated by Kado and Tohda.[277] An AFM in contact mode with a conducting probe was used to pattern and to measure both the topography and conductivity of a sputtered $GeSb_2Te_4$ film on gold that served as the underlying

electrode. After applying a 5 ms × 3 V pulse at certain locations on the sample, the current reading at these places changed from 10 pA to 1 nA (at 0.5 V bias). In the conductivity image a clear change could thus be seen, whereas in the topographic image no change between the modified and unmodified areas could be observed.

SPL has also been employed to fabricate transistors, or components of transistors such as gate electrodes, channels, etc.

Fayfield and Higman[278] used an AFM to pattern the channel area between the source and drain of a MOSFET. Patterning was achieved by oxidizing the Si substrate using sample-(+) biases of 4−5 V applied between silicon surface and the Ti-coated AFM tip. The thickness of the fabricated oxide structures was adjustable over the range from ~2 to 6 nm using the bias amplitude over the range from 4 to 7 V. Further increases in E_B or slower scan speeds did not further increase this height, but broader line widths were instead obtained. Lines were drawn parallel and perpendicular to the electron channel. After patterning, MOSFETs having patterns parallel to the channel exhibited a higher mobility for electrons, likely due to surface potential modulations induced by the grating. These potential modulations lowered the electron mobility in the direction perpendicular to the grating.

Minne *et al.*[279] used the AFM for an intermediate step in the fabrication of a MOSFET. This step consisted of patterning the gate area by selectively oxidizing selected parts of the hydrogen-terminated a-Si half-product. This was accomplished by applying a bias between 12 and 25 V between the sample and a Ti-covered AFM tip in contact mode.

A so-called side-gated field effect transistor was fabricated by Cambell *et al.*[280,281] The fabrication steps again included preforming of contacts pads by standard lithographic tools, passivation of the silicon with hydrogen and subsequent SPL patterning and post-processing. The authors pointed out that this type of FET may be advantageous for certain applications such as single electron tunneling structures because of its low gate channel capacitance.

The fabrication of a single electron transistor was described by Matsumoto *et al.*[282] On top of a 100 nm thick SiO_2 film, a layer of 3 nm Ti was sputtered. In air, the top 1 nm of Ti was partially oxidized and further oxidation of this layer using the STM operating with a sample-(+) bias of 5 V could be accomplished, as indicated by Auger analysis of patterned regions[283] (see also references by Sugimura and co-workers[59,60,62,64]). The spatially selective oxidation of this surface permitted the construction by SPL of very small (30 × 35 nm^2) tunneling junctions and a functional transistor. A Coulomb staircase (see e.g., refs 284 and 285), characteristic of a functioning single electron device, was observed at room temperature.

A similar device was operated at 0.3 K by Yamada and Yamamoto.[286] In this device, the SPL was employed to generate a nanostructure (70 nm diameter, 15 nm high) composed of tungsten. This was accomplished by applying a tip-(+) pulse of 15 V, 0.5 ms between a tungsten tip and the top layer (Si doped GaAs) of the substrate. Auger was used to confirm the presence of tungsten in the modified regions of the sample.

B. Mechanical SPL Methods

In this chapter we review SPL experiments in which modifications are produced by tip−surface contact. The organization of this section follows that of the Electrical Lithography section (4.1). As compared with electrical modification schemes, however, a broader range of surfaces are accessible because mechanical SPL schemes are usually implemented using an AFM which can be operated on nonconductive surfaces. An additional consideration in all such experiments, however, are such factors as degradation of the patterning resolution with time and tip durability. Applications of mechanical SPL are shown in Figures 16 and 17.

1. Direct Modification of the Surface

Because of the malleability of the coinage metals (including copper, nickel, gold, silver, and platinum), surfaces or films of these metals have been frequently used for modification experiments involving both STM and AFM.

Pits were produced in 3−15 nm thick sputtered polycrystalline gold surfaces using an STM by Roberts *et al.*[287] These pits, having typical dimensions of 30 nm diameter × 10 nm depth, were produced by operating the STM with a low tunneling resistance below 85 MΩ. On platinum/carbon films, in contrast, modifications were not seen even for gap resistances as low as 500 kΩ. Resistances below 50 MΩ also caused damage to PMMA film-modified Si surfaces. In these experiments, material was pushed to the edges of the scan window. The mechanism of modification in the case of gold surfaces was presumed to involve the mechanical transfer of gold to the tip.

Silva and co-workers[288] used a tungsten STM tip as a “cutting” tool to isolate selected areas of a thin gold film evaporated onto a mica surface. The procedure described by these authors required that the gold film thickness be determined by cutting through the film to the mica substrate with the tip by scanning the tip along one line and lowering the tip by 0.1 nm between each scan. Once the film thickness was determined using this procedure, the feedback was disabled, the tip was depressed into the gold film to a depth equaling the measured film thickness, and was then moved in a desired pattern parallel to the surface resulting in the removal of gold along these scan lines. Using this procedure, the authors inscribed lines with depths of 23 nm, widths of 70 nm, and lengths as great as 350 nm.

A diamond tip on a stiff cantilever (10.8 N m^{-1}) was used by Sumomogi *et al.*[50] to modify copper, gold, and nickel surfaces. Both, bulk metals and evaporatively deposited metal films were investigated. The machining was performed by scanning a square region using a scheme in which each line was repetitively scanned four times with forces of 1−20 μN. Particularly precise milling of Ni surfaces was possible resulting in well-defined square patterns with edge profiles in the range of the tip size; see Figure 16. The micromachining of gold samples was much less successful: Gold appeared to be pushed

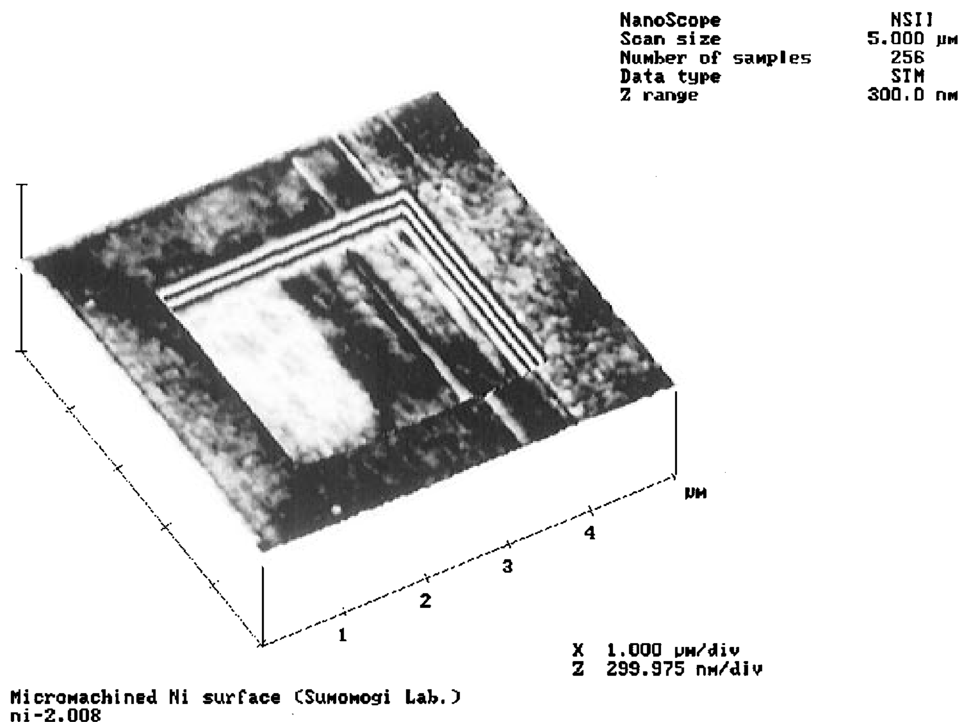

Figure 16. An AFM image of a nickel surface after scratching with a diamond AFM tip with a loading force of 7.84 μN. The area was scanned four times in total, and the scratch depth for each scan was about 80 nm. (Reproduced with permission from ref 50. Copyright 1994 American Vacuum Society.)

to the edges of the scanned area. Cu represented an intermediate case. In the cases of Ni and Cu, a roughly linear relationship between the depth of a milled area and the applied force was established. In a subsequent paper,[51] the parameter space in this experiment was further explored. Investigations of the relationships between the line depth, the number of scans, the density of scan lines, the scan rate, and the scan width were reported.

Wendel *et al.*[289] used an AFM tip to inscribe a line in a 30 nm thick gold stripe on a silicon oxide surface. Measurements of the conductivity through the gold showed that it was possible to completely remove the metal. However, the forces involved in removing the gold were more than 10 times higher than forces they applied to modify photoresists, and tip degradation was problematic under these conditions. By employing sharpened AFM tips, fabricated by e-beam deposition (EBD), the authors further reported the mechanical patterning of a resist (Shipley 1805, 3−15 nm film thickness) with inscribed lines having a minimum width of 9 nm. Surprisingly, although EBD-fabricated AFM tips appeared fragile by SEM inspection, 100 000 holes of similar size could be prepared using a single such tip. The patterns so prepared were transferred into the underlying GaAs−AlGaAs heterostructure by multistep development involving etching in $H_2O/NH_4OH/H_2O_2$ = 1000:3:1, removing of resist in acetone, and dry etch in oxygen plasma.[290,291]

Bouju *et al.*[292] calculated the time-dependent behavior of up to three gold atoms on a NaCl surface upon pushing one of the atoms with a diamond AFM tip. It was shown that by pushing, gold dimers and trimers can be formed. However, it is not possible to align three gold atoms in row on the NaCl(100) surface, as the gold atoms will preferentially form a triangular cluster.

In experiments similar to those anticipated by Bouju *et al.*, Schaefer *et al.*[293] arrange Au clusters with heights between 9 and 20 nm on flat substrates including HOPG or WSe_2.

Göbel and von Blanckenhagen[294] created regular patterns on bulk and thin film gold films using a conventional Si tip and forces in the 25 μN range. A series of grooves formed using this method were successively less deep, indicating wear of the probe. Tip degradation was confirmed by comparing SEM micrographs of the cantilever before and after the lithography experiment. The mechanism of this micromachining was not well understood. One hypothesis involved friction-induced local heating effects which might induced localized melting. However, the authors estimated a local temperature increase during the plowing to be ~0.6 μK, a value that does not support this model.

Goto and Hane[295] produced pits 9 nm deep in indium films having a thickness of 200 nm. Although the cantilevers used in these experiments were relatively soft (0.01 N m^{-1}), high forces could be applied by means of electrostatic forces: Between the sample and the gold-coated backside of the cantilever, a voltage pulse was applied which generated, for example, ~1.9 μN for a 200V pulse. A pronounced relation between the depths of pits obtained in the iridium surface, and the applied pulse amplitude was observed. Extrapolation of these data permitted a threshold of 160 V (1.2 μN) to be estimated for pit formation.

Substantial interest has focused on developing modification schemes which are applicable to the high T_c copper oxide based materials.

The STM etching of a high T_c superconductor, $YBa_2Cu_3O_{7-x}$, was investigated by Parkinson and coworkers.[296] The mechanism of the removal process in this case was attributed to the mechanical ablation of surface atoms by the tip. STM imaging using tunneling biases of 0.10 to 1.5 V (tip-(+)) and currents of <1.0 nA caused the removal of layers having a thickness of 1.2 nm; equal to the unit cell dimension along the *c* axis of this material. The removal of larger quantities of material from the surface was correlated with the observation of a stepped topography in which a series of layers, separated by 1.2 nm steps, were observed. Nanostructures consisting of linear troughs and square recesses were "milled" into the surface by repetitive STM imaging.

The etching of superconducting material was also observed by Virtanen *et al.*[297] Using Pt tips in STM in air, flat square patterns were "milled" into the surface of a YBCO surfaces. Again a threshold tunneling bias (~1.5 V) was observed above which no modification of the surfaces was seen.

Chen *et al.*[298] also suggested that mechanical processes—such as tip ablation—may also play a role during STM modification procedures in the case of YBCO surfaces. As one example they showed a series of STM images (100×100 nm^2, bias −0.75 V tip-(−), current 0.42 nA) of an YBCO surface: A pit was observed to grow from a diameter of 5 nm to more than 40 nm over the course of 13 scans. Concurrently, a degradation of the resolution was observed and attributed by the authors to a change of the tip morphology.

Mechanical superconductor modifications induced by STM were also reported by Volodin and Aarts[299] for superconducting $NbSe_2$ surfaces. Tungsten and platinum tips were employed in a STM at 4.2 K to both image and modify the surface of cleaved $NbSe_2$. No modifications were observed when the tunneling resistance was maintained above 6 MΩ; however, for lower gap resistances, etching of the surface was observed. The authors did not attribute the etching to electrical processes, but to "mechanical lithography" for the following reasons: No excess material (originating from the etched pits) was found at the edges of the pits and at low temperature, the diffusion of removed atoms should be very low, so it is unlikely that the debris diffused out of the scan window. In addition to etching, these workers also reported the deposition of material on the surface following the application of short voltage pulses between the tip and sample. Freshly prepared STM tips did not possess the ability to deposit material, and this fact suggests that the deposited material is actually derived from the surfaces of the superconductor by mechanical removal by the tip.

Bogy[300] demonstrated that doped diamond STM tips[49] could be employed to confirm the hardness of thin (30 nm) refractory carbon layers. Grooves and indentations were formed in a carbon-coated hard disk. Degradation of the diamond tip was not observed provided the applied force did not exceed a critical value (not measurable in this experiment). However, as the author points out, in the STM configuration, the applied force was not measurable during the indentation process and for this reason, only relative measurements of hardness were possible using this method.

Jung *et al.*[301] suggested a dynamical AFM method for effecting modifications at polycarbonate (PC) surfaces: With the Si_2N_3 tip in light contact with the polycarbonate sample ($F \approx 10$ nN), the force was modulated with a frequency of a up to 8 kHz and with a 500 nN amplitude. An advantage of this force modulation is that—in contrast to large constant forces sometimes required to cause modifications—torsion and stick−slip with the surface during scanning of the tip were reduced. With this method the authors wrote the word "HEUREKA" on a PC surface with letters roughly 50 nm high.

In a recent review, Wiesendanger[12] presented two examples of lithography involving an AFM operated in the above-mentioned "dynamic mode":[301] Into the surface of a compact disk (polycarbonate), letters were written or a constriction was fabricated in a 5 μm wide and 30 nm thick YBCO film on a MgO substrate.

Junno *et al.*[302] used the tip of the AFM to move 30 nm GaAs particles on a GaAs surface. Lines and letters were formed using these displaced particles. In addition, these authors noted that this technique could be used to estimate the real diameter, *d*, of a particle using the following procedure: First, a single particle would be imaged, and then two would be brought into contact using the tip and reimaged. For each particle, a contribution of $2w$ due to tip convolution is expected, thus for an isolated particle, the apparent diameter equals $w + d + w$, whereas if two particles in contact are imaged, the total apparent diameter should be $w + d + d + w$. Subtraction of the one-particle width from the total two-particle width therefore yields the real diameter, *d*.

At Si(111) surfaces on which layers of C_{60} molecules were deposited, Maruno *et al.*[303,304] varied the tunneling parameters to gradually lower the height of the tip in an attempt to determine the threshold distance at which C_{60} molecules adsorbed on the silicon surface are displaced by the tip. The height above the silicon surfaces was found to equal that of the C_{60} molecule—roughly 0.7 nm. This threshold distance was interpreted in terms of a mechanical mechanism for the displacement process.

The "nanostructuring" of porous silicon was reported by Dumas *et al.*[305] On porous silicon surfaces derived from Si(100), lowering of the STM imaging bias from 5 to 0.5 V, caused the tip to contact the surface and to compress the porous silicon layer. Apparently because of the porosity of this surface, compression was possible and grooves could be formed without extruding SiO_2 from the sample surface. Grooves having a depth of 8 nm and widths of 60 nm were fabricated in this way.

2. Organic Materials as Lithographically Active Layers

a. Organic Resists. We have already summarized SPL experiments in which thin organic resists have been modified using electrically based mechanisms. The mechanical modification of resists has also been demonstrated by Sohn and Willett[306] who generated a line pattern on a 24 nm thick PMMA film (on top of a 300 nm thick PMMA/MAA

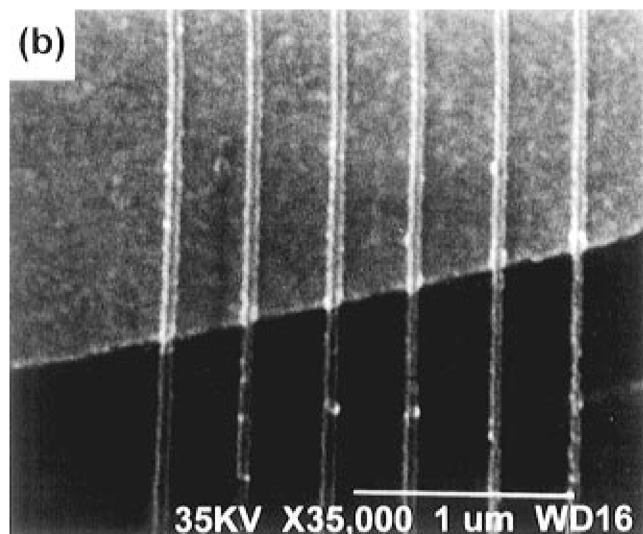

Figure 17. SEM micrograph of chromium lines at the boundary of a gold contact pad and the underlying GaAs substrate. These lines were obtained by mechanically patterning a PMMA/MMA resist layer with contact mode AFM using a loading force of 1.1 μN. After patterning, the resist was developed and used as a mask for the deposition of chromium. Finally, the mask was removed with acetone. These lines are 15 μm in length, and approximately 40 nm in width. (Reproduced with permission from ref 306. Copyright 1995 American Institute of Physics.)

film) using contact AFM. Forces higher than 1 μN were applied during the modification process. In effect, the tip "plowed" through the mask leaving trenches having a minimum width of 40 nm. The line width was found to be a linear function of the applied force and was dependent upon development time and resist thickness. Following the development of these AFM-patterned resists, height–width aspect ratios between 2:1 and 3:1 were achieved for the subsequently deposited structures into the resist pattern, as shown in Figure 17.

Yamamoto *et al.*[307] used a negative resist designed for e-beam lithography, poly(glycidyl methacrylate) (PGMA), in their SPL experiments. PGMA films (500 nm thick), spin coated on silicon, were at first employed. Grooves 10 nm deep could be fabricated at scan speeds of 1 μm s^{-1} and forces in the 300 nN range. Single indentations were obtained when the tip–sample force was increased to more than 70 nN. Square regions were milled using a force of 750 nN. However in these experiments, the excursion of the tip into the surface of the polymer film did not equal the film thickness, and the surface of the underlying silicon surface was therefore not exposed. On the basis of theoretical considerations, these authors estimated that using an applied force of 750 nN, a 17 nm thick film layer could be removed. On the basis of this prediction, the film thickness was decreased to 10 nm and the authors demonstrated that the polymeric material within the entire scanned area could be removed exposing the underlying silicon substrate.

b. Langmuir–Blodgett (LB) Films. Molecular layers prepared using the LB method are attractive candidates for mechanical modification schemes because the molecules within these films need not interact strongly with the substrate surface on which the LB film is deposited. In addition, in many instances, the amphiphilic molecules in these films are not significantly entangled. Thus, these molecules can relatively easily and cleanly be removed or displaced under the influence of an SPM tip.

Mechanical lithography on LB films of behinic acid ($CH_3(CH_2)_{20}COOH$) was reported by Garnaes *et al.*[308] Lithography was performed by scanning small squares of 30 × 30 nm^2 and using forces of ~70 nN with contact AFM. No change to the surface was observed when the force applied to the tip was kept below 10 nN. The depth of the resulting squares in the sample was approximately equal to the thickness of a behinic acid monolayer. Lines were written into the film by scanning a sequence of squares with a small offset between subsequent frames. These lines were stable in air for periods of 10 h.

Multilayered LB films of ω-tricosenoic acid (CH_2-$CH(CH_2)_{20}COOH$) were used by Fujihira and Takano[309] in their work. These workers fabricated monolayer- and bilayer-deep squares by scanning 1 × 1 to 3 × 3 μm^2 areas 2–3 times with 50 nN loading force. A damage threshold of 10 nN for these multilayers was estimated.

Demir *et al.*[310] prepared Langmuir–Schaefer (LS) films[311] on the (111) facets of Au droplets formed by melting the end of a Au wire.[312] By changing tunneling parameters these films could be imaged with an STM without visible damage. However, varying these parameters caused a modification of the surface. This way 1 × 1 μm^2 patterns were generated. Depending of the tunneling bias, the shape and the depth of these patterns varied markedly. The observed depth of the patterns which were obtained (up to 180 nm) was usually greater than the thickness of the LS film (~5 nm). This disparity indicated that the lithographic process might not involve simply the mechanical removal of material. In fact, in a paper by Kim and Bard,[159] it was suggested that modification of the underlying gold surface might occur during imaging of alkane thiols SAMs. The patterned LS film eventually was successfully employed as mask for localized electrodeposition of Cu into the fabricated squares.

c. Other Polymeric Materials. Very thin (4–10 nm) plasma-deposited polyacetylene films were patterned by Gorwadkar *et al.*[313] using contact AFM. Patterning was done by scanning once or several times over a small (100 × 100 nm^2) area at a defined force. They observed indentations even at very low forces of 5 nN, much lower than the forces employed for lithography by other groups (e.g., refs 309, 314, and 315). The shape of the indentations was found to be a function of the scan speed. Additionally, the applied force was varied by applying a bias between sample and tip.[316]

Polyimide (PI) films were patterned by Jin and Unertl.[314] The silicon-supported films employed for these studies were either commercial PI foils (thickness, d = 25 μm thick) or were prepared by spin coating (d = several micrometers). Rather high loads (up to 500 nN) were used to incribe grooves with apparent widths of 100 nm and depths of 5 nm. Two different patterning modes were observed: The application of forces below a certain threshold level produced patterns which appeared raised, whereas

forces above this threshold produced grooves or pits in the film with the removed material appearing at the edges of the pattern. Viscoelastic effects or morphological changes caused by sample heating during the scan process, were cited as possible contributing factors to the modification mechanism.

Khurshudov and Kato[315] observed a qualitatively similar effect—an apparent volume increase—on polycarbonate surfaces after "scratching" the surface with the tip of an AFM. The "scratching" was performed by scanning along one line with a nominal load of 44.5 nN, and modifications were obtained following at least five passes on a single line. Subsurface cracking of the polymer film was involved to explain the AFM-induced volume effect.

The physics of the deformation of polymer films with the tip of an AFM was probed by Boschung *et al.*[317] Polypropylene and poly(methyl methacrylate) films were investigated. Using unusually stiff STM cantilevers (125 N m^{-1}), plastic deformation and energy dissipation during the deformation of polymer surfaces with an AFM tip were measured. These workers discovered that a tip excursion of 75 nm into the surface of commercial, 0.1 mm thick PMMA foils produced 20 nm deep trenches. This mechanism permitted a micrometer-scale letter "T" to be inscribed. Force vs tip position curves were measured and—by defining the inelastic deformation as the area of the hystheresis loop in the tip position during penetration and retraction—the dissipated energy associated with the deformation process was calculated.

During the electropolymerization of poly(*N*-methylpyrrole) (PMeP) Yano *et al.*[318] observed *in situ* that the evolving polymer morphology could be modified by the applied forces of the contact AFM exceeded 10 nN. By repeatedly scanning areas of 2×2 μm^2 to 5×5 μm^2 with forces of 30 nN during film growth, square impressions of the image window were observed in the polymer film after the growth of the film was terminated. These depressed regions exposed the sample surface. Because PMeP exhibits a redox-switchable conductivity (the oxidized form is conductive; the reduced form insulating), the authors suggested that patterned PMeP films could serve as masks for the local electrochemical deposition of metals.

On a polymer blend of polystyrene (PS) and poly(ethylene oxide) (PEO), Nie *et al.*[319] observed that scanning with an applied force of 50 nN resulted in a lowering of the elasticity of PEO, but no modification of the elasticity of PS was observed. Furthermore, stripes perpendicular to the scanning direction were observed on PEO domains (15−20 nm periodicity, 3−5 nm in height). The observed decrease in the elasticity was explained in terms of a compacting effect of the AFM tip on this material.

d. Two Biological Examples. Garcia[320] has used a low current STM (<1 pA) in field emission mode to image purple membranes sprayed onto HOPG surfaces. By increasing the tunneling current to a few picoamps, a transition from field emission to tunneling was observed and, concurrently, the tip position above the purple membrane surface became unstable and an excursion of the tip toward the graphite surface (through the membrane) was observed. In this tunneling mode, irreversible modifications to the membrane were produced. For example, by repeatedly scanning across a membrane fragment on the HOPG surface, Garcia was able to cleanly "cut" the membrane.

Brandow *et al.*[321] used AFM to cut a model lipid membrane (1,2-bis(10,12-tricosadiynoyl)-*sn*-glycerol-3-phosphocholine) grown on HOPG. A fairly sharp damage threshold for the applied force (13 ± 1 nN) could be established. The cutting rate became significantly faster when forces slightly above the treshold level were used. When the lipid was polymerized (UV irradiation) forces up to 50 nN were applied without any visible damage.

C. Optical SPL Methods

In this section we present SPL experiments involving either the use of the scanning near-field optical microscopy (NSOM), or the application of an SPM in combination with external laser light sources. These experiments are closely related and the operational difference is that in case of the NSOM experiment, a transparent probe tip functions as a waveguide either to deliver light to the surface, or to detect scattered or fluorescence light from the surface in the near-field limit. In some NSOM experiments, interactions of light with the surface are used to establish the tip position above the surface (and, hence, the laser is an integral part of the microscope itself). More often, the tip position is established using a conventional noncontact AFM mode in which the transparent tip is vibrated either in the plane of the surface, or perpendicular to the surface.

1. Laser-Assisted Lithography

Using the AFM, Mamin and Rugar[23] were able to read and write information at frequencies in the range of 100 kHz. Writing involved a "thermomechanical" process in which an AFM, operating in contact mode, was used to pattern thin PMMA films. The AFM tip could also be illuminated using a diode laser (830 nm) from beneath the transparent sample surface. Writing was effected as follows: While operating with an applied force below the damage threshold for the PMMA film, the tip was illuminated by a laser pulse which heated the PMMA film above its heat deflection temperature. The locally heated PMMA film enabled the tip to transiently penetrate, producing a single pit or bit. By rotating the PMMA sample (as, for example, in conventional hard disks) these workers were able to write and read at rates (near 100 kHz) which were limited by the mechanical properties of the cantilever.

The system employed for this experiment was later refined by the same group.[322] In the improved apparatus, a sharpened optical fiber in contact (0.1−1 μN) with the polycarbonate sample was employed for both writing and reading—eliminating the requirement that the sample be transparent. An infrared laser pulse was coupled into the optical fiber to effect heating of the Au/Pd-coated tip apex and the sample. Reading was accomplished by detecting the movement of the fiber with a interferometer. Again, to facilitate fast data transfer during reading, the

sample was mounted on a rotating air spindle. Maximum writing speeds were limited by the cooling time for the tip/media system after each laser pulse; however, writing rates of 50 kHz and reading rates of 300 kHz were nevertheless obtained.

An even more recent refinement to this apparatus has been reported involving the thermal writing step.[28] The pulsed laser, which was used in previous work for heating, was replaced by a cantilever having an integral heating element. This cantilever consists of heavily boron doped (10^{20} cm^{-3}) "legs" terminated, at the apex of the tip, with a bridge having a much lower doping level of 10^{17} cm^{-3}. This bridge forms the "filament" of a resistive heater having a thermal time constant of just 40 μs. Typical pulse parameters for writing were 16 V and 20 μs, and a 11 kHz repetition rate was demonstrated.

A CVD-like deposition scheme has been described by Yau *et al.*[323] Like the CVD deposition schemes described earlier, the deposition of aluminum, for example, was performed using an STM located in a high vacuum chamber into which a volatile precursor (e.g., TMA, $Al_2(CH_3)_6$) was present at partial pressures of a few millitorr. However, in these experiments the STM was operated using conditions of imaging bias and current which did not induce the deposition of aluminum from TMA. Instead, deposition was induced by the illumination of the tunneling gap with a laser pulse which "activated" TMA molecules within the illuminated region (by photooxidation) causing these molecules to become more labile in the electron beam, flowing between the STM tip and sample. Following the application of a laser pulse, a small (16 nm diameter) deposit was found which, presumably, consisted of aluminum atoms. The authors also observed the reverse process (e.g., erasing) in cases where the sample was irradiated once more. Only those structures located underneath the tip disappeared, whereas other structures, also within the illuminated region, were not affected.[200,324]

Christenson *et al.*[325] described a patterning scheme in which a laser diode light source was employed in conjunction with an AFM. The sample involved was a proton-implanted multiple quantum well (MQW) InGaAs/GaAs light emitter. The proton bombardment increased the series resistance along the MQW junction and sensitized the surface to photons having subbandgap energies. By using W- or Au-covered Si_3N_4 AFM tips, voltage pulses—having an amplitude below that necessary to cause atom transfer between the tip and sample—were applied to the surface. Irradiation of the surface lowered the sample resistance (and the ohmic drop within the sample) increasing the bias pulse amplitude at the sample surface to values above the atom-transfer threshold, and causing either tungsten or gold from the tip to be transferred to the surface. The metal particles produced using this method were ~300−500 nm in diameter. These metal "bits" could be read using a scheme also based on the fact that the ohmic resistance between the tip and sample was decreased at locations where a metal mound was located. Again small amplitude (millivolt) tip−sample bias were applied while the surface was illuminated to optically activate it. As the tip encountered a metal particle on the surface, the improved electrical contact caused electron injection from the tip into the surfaces and the emission of light.

Gorbunov and Pompe[326] combined a STM together with a laser focused on the gap in the STM configuration. It has been theoretically established (in the context of the SERS enhancement, for example[327]) that the radiation field near metal particles having dimensions smaller than the wavelength of light can be strongly amplified. In an STM experiment, the optical properties of the tip—because of its small radius of curvature—can satisfy the conditions for "focusing" an incident radiation field having the correct wavelength. Under UHV conditions, the authors fabricated small hillocks on a gold surface by applying 5 ms pulses of laser light (800 nm, 0.8 W) to the tunneling gap existing between a silver tip and the gold surface. By applying 100 ms optical pulses, the formed hillocks could be erased. Without applying the second laser pulse, the hillocks were persistent for a few hours.

Jersch and Dickman[328] used the same approach in an air ambient environment. Using tungsten tips and irradiation by means of a Nd:YAG laser with 5 ns pulses at 532 nm and variable pulse energy, these workers produced pits and channels in a thin gold film in air ambients. When these tungsten tips were modified with a silver coating, the formation of hillocks instead of pits was reproducibly observed. The authors were also able to form hillocks using platinum/iridium tips; however, the threshold of the laser intensity would increase to 30−80 MW cm^{-2} compared to 10−20 MW cm^{-2} for silver or silver-coated tungsten tips.

2. Near-Field Optical Microscopy (NSOM)

The near-field scanning optical microscope (NSOM)[10,329] has been employed for lithographic purposes by several groups. A general overview of NSOM has been given by Heinzelmann and Pohl[330] and by van Hulst *et al.*[331] Using the NSOM, the resist-based optical lithographic method can, in principle, be employed without modification. A typical example is shown in Figure 6.

For example, films of the photoresist Shipley KTI 747 having a thickness of 0.2−0.5 μm thick on silicon were used in the NSOM patterning experiments of Smolyaninov *et al.*[332] By using 248 nm light (from a KrF excimer laser) and uncoated fibers, lithography at the 0.1 μm level was obtained. The light intensity (and not dosage) was found to be the most important factor determining the size of the exposed regions. These workers also observed nonlinear features ("donuts") in the linear resist, demonstrating that the radiation field near the tip has pronounced nonlinearities.

Krausch *et al.*[333] performed lithography with a NSOM on another standard photoresist—Hoechst Novolack AZ 6612—and obtained line widths of 200−80 nm for uncoated and Al-coated optical fiber tips respectively with a constant depth of about 15 nm. Because the photoresist reacts "linearly" to the irradiation, the shape of the formed lines represents the actual field of the irradiation. It was found that this field can best be fitted with a Gaussian-type

curve. For practical applications, this represents a major limitation where high aspect ratios are important.

The vibration of an optical fiber used in a NSOM with a shear force feedback system can impose a limitation on the resolution attainable in an NSOM experiment: When scanning the tip of a shear force NSOM, the tip may not only move along the scan direction but also slightly out of phase due to the vibration needed to establish the shear force feedback. The irradiation process is not instantaneous, thus during exposure the tip might expose a larger area than desired. Wegschneider *et al.*[334] investigated this possible limitation but found only a small influence on both shape and aspect ratio of the lines formed by the process described by Krausch *et al.*[333]

In addition to conventional photoresists, other photosensitive materials have been investigated for NSOM lithography applications.

Hosaka *et al.*[187,335−337] patterned unique layered samples using an NSOM. Photosensitive samples were prepared by rf sputtering a thin amorphous $Ge_2Sb_2Te_5$ layer onto a polycarbonate substrate and capping this layer with another of the optically transparent material $ZnS-SiO_2$. This capping layer also "insulated" the surface from possible topographical changes to the optically active $Ge_2Sb_2Te_5$ film. Upon irradiation through the Al-coated, optical fiber tip (785 nm, 7−8 mW, 0.5 −5 ms pulse length) the $Ge_2Sb_2Te_5$ layer became crystalline, and the reflectivity of this layer (upon irradiation with 0.2 mW, 785 nm) was altered—an optical effect which was readily observable using an NSOM. The estimated resolution of this method was 50 nm.

A NSOM using shear force feedback was used by Massanell *et al.*[338] to modify the surface of triglycine sulfate (TGS). Under illumination with increased laser power, lines could be written. Correcting for tip convolution the authors estimated the line width to be on the order of 60 nm. Very small lines were observed in the topographic image, whereas larger ones (obtained with higher laser power) were also visible in the optical image. The mechanism of the lithographic process was not well understood, possible explanations include charge removal, photochemistry, and local heating.

Froehlich *et al.*[339] used a modified STM in their work: The optical fiber as well as the photoresist on the substrate were coated with a thin (transparent) layer of gold in order that a tunnel junction could be established for distance control. A HeCd laser (λ = 442 nm) was then coupled into the optical fiber and used to expose the photoresist. Subsequent steps involved etching of the gold layer and standard development of the resist layer. Lines with a width of 200 nm were obtained. The authors claimed that by improving their instrumentation, e.g., the probe (currently 80 nm aperture) line width down to 20 nm should be achievable.

A photon scanning tunneling microscope (PSTM)[340] can also be employed to locally modify the optical properties of a resist material: Rather than using a regular HeNe (633 nm) laser as light source for the total internal reflection (TIR) in the resist-covered quartz sample, a more energetic HeCd (442 nm) was coupled onto the sample causing a bleaching of the resist. Lee *et al.*[341] found then that this photobleaching was enhanced in the proximity of the tip. By optimizing the exposure time a mirror image of the tip was thereby transferred into the resist material. The authors estimated an attainable resolution for line drawing using this method to be ~100 nm.

V. Conclusions and Outlook

Research in the area of SPL—published since 1991—has been surveyed in this review. We conclude in this section by providing a summary of the experimental observations and capabilities which have been demonstrated, by commenting briefly on possible technological applications for SPL, and by drawing attention to areas in which improvements to SPL methods appear to be possible. These are areas where forthcoming research in the area of SPL will likely be focused.

A. Summary of Experimental Observations

It is probably normal for research in a completely new area, such as SPL, to be somewhat phenomenological or descriptive during an initial discovery phase. This is an important period during which the limits of what is possible are probed, and after 10 years, SPL appears to be at the close of this period now. The papers reviewed here mostly belong to this descriptive phase although some systematic and thorough investigations of SPL mechanisms have recently been reported. One example is very quantitative work in the area of material transfer to/from the tip, reviewed in section IV.A.3.

In Tables 1 and 2 are tabulated typical modification dimensions and—where applicable—write rates for all of the SPL method reviewed in section 4 (Table 1), as well as the values of experimental parameters such as the bias pulse amplitude, and tip−sample force required to effect surface modification using a particular SPL technique (Table 2). Because in many proof-of-concept papers, the available parameter space (e.g., bias, force, etc.) has not been probed, these summaries are necessarily incomplete and frequently, "typical value ranges" are specified in place of more informative statistical data. Although it is premature (or presumptuous perhaps) to "rank" various SPL techniques, we have attempted to highlight advantages and disadvantages for many SPL methods, and to identify the SPL approaches which appear best suited to various applications.

From Table 1, it is apparent that the smallest characteristic dimensions which are routinely achievable are ~10 nm. Wang *et al.*[90] have suggested that this minimum value might be dictated by the chemical and physical phenomena involved in the lithographic process—independent of the technique which is employed. One instrumental source for this limiting value in STM-based experiments has been discussed by Dobisz *et al.*[147] who have calculated that for sharp STM tips, a minimum "electron beam" spot size of 5 nm is obtained.

One aspect which has not received adequate attention is the possibility that a functional lower limit for a particular system may exist which is not equal

Table 1. Summary of Write Rates and Attainable Resolutions for the Various SPL Methods Reviewed

technique[a]	section	write rate[b] (μm s^{-1})	resolution[c] (nm)
(a) electrical	IV.A		
Si:H	1.a	10	10−60
SiO_2/Si	1.a	23	10−40
layered materials	1.b		1−10
metals; metal films	1.c	10	30−50
organic resists	2.a	30 000	15−150
LB films	2.b	25	6−25
SAMs	2.c	3 000	15−70
transfer: mounds	3		10−20
transfer: pits	3		5−15
CVD	4	0.035	5−50
electrolyte; *in situ*	5	0.1	10−500
(b) mechanical	IV.B		
direct modification	1	1	100−200
using resists	2	0.2	10−50
(c) optical	IV.C		
NSOM	1	20	60−100
laser assisted	2	25 000	30−350

[a] Techniques and materials are listed according to their respective appearance in section 4. [b] These numbers represent fastest reported values for scan rates during the lithographic process. Unfortunately no typical values can be given as only a relatively small number of speeds were reported. In some cases "speed" was not even an issue, e.g., in studies of the mechanism of pit formation. [c] These values represent *typical* or average dimensions for the line width and/or the "dotsize" which was obtained.

to the smallest acheivable modification. From a technological standpoint, it may prove useless to fabricate features smaller than a certain size if, for example, surface diffusion, surface oxidation processes, etc., severely limit the stability of such features. It will likely prove necessary in the future to carefully identify this functional lower limit using careful stability studies lasting months. Once this functional lower limit is determined, subsequent research efforts should focus on achieving performance increases, i.e., speed and reliability. Surface diffusion rates, surface energies, and nanostructure dopant concentrations are possible starting points for the discussion of desirable, functional lower size limits.

No well-defined limit to the data transfer rate for SPL (at a single tip) has been demonstrated. In Table 1, a tremendous variation in the write rate from experiment to experiment is evident, and the experimental factors responsible for imposing this limit were also quite variable. As one example, Park *et al.*[146] reported a maximum scan rate of 3 mm s^{-1} which was limited by the positioner (i.e., the piezo tube). The resolution at this speed was 100 nm, i.e., 10 times more than the suggested lower limit. This tradeoff, in which higher fabrication speeds lead to larger feature size, has been commonly reported. At present, it is absolutely clear that instrumentation is the limiting factor for SPL read and write rates. Theoretical investigations of the kinetics of nanostructure formation are therefore not urgently needed—at least not from a purely technological standpoint. As it appears increasingly probable that fabrication speeds will be improved by means of parallel operation, rather than by further increasing the serial write rates at single tips, it appears that a technological motivation for kinetic studies of nanostructure growth may not exist for some time.

Table 2. Summary of SPM Modification Parameters

technique[c]	section	bias (V)	current (nA)	force (nN)
(a) electrical	IV.A			
Si:H	1.a	2−9	0.2−2	
SiO_2/Si	1.a	3−10	0.1−1	
layered materials	1.b	3.5−4.5	0.1−50	
metals; metal films	1.c	3.5−10	0.5−3	
organic resists	2.a	20−70	0.01−1	
LB films	2.b	4−8	0.5−10	
SAMs	2.c	8−25	0.01−6	
transfer: mounds	3	3.5−5	0.1−2	
CVD	4	3−40	0.05−30	
(b) mechanical	IV.B			
polymer films	1	1		30−100
metals	2	0.2		≥1000

[a] In most publications, the set force in experiments involving an AFM with a conducting tip has not been given.

In Table 2 are tabulated the parameters (current and voltage, or applied force) which have been employed to effect SPL modifications. At first glance, the "bandwidth" of these instrumental parameters is tremendous. However one trend at least is evident: For "direct" modification experiments involving STM, bias voltage thresholds in the 2−3 V range are common and probably correlate with dissociation energy of typical chemical bonds (typically 1−2 eV). At surfaces on which a relatively thick LB or SAM layers are disposed, or in experiments in which a field emission imaging or modification mode was involved, higher bias voltage requirements usually exist. In a few experiments, electron dose (i.e., the injected charge per unit surface area) has been isolated as a determinate. In several such cases, it has been observed that the minimum required dosages (e.g., to draw a line in a resist) are higher for the STM experiment than for the analogous experiment conducted using e-beam exposure of the same resist layer (see e.g., refs 140, 145, and 151). It has been suggested that this effect may derive from the relatively small flux of energetic electrons in the STM experiments.

A related, technologically crucial point which has so far received relatively little attention is reproducibility with respect to nanostructure formation, data readout, and where devices have been prepared, performance of SPL patterned devices in applications such as transistors.

B. Performance of the Different Techniques

A ranking of SPL methods based on criteria of write speed, minimum nanostructure dimension (information density), reproducibility, and the ease of experimental implementation has been attempted. Two separate rankings for device fabrication and data storage applications have been generated however from both of these lists, several new, and promising SPL methods (e.g., laser-assisted material transfer from the tip to the sample) have been omitted because only a small data set is available, and the merit of these methods cannot yet be fairly assessed.

1. Device Fabrication

The highest write rates have been obtained by patterning an organic resist using AFM.[146] The

largest "data set" written out in single experiments has again involved the AFM patterning of organic resists,[141,146] and the AFM patterning of Si:H surfaces.[65,66] An important consideration for device fabrication is the proximity with which successive lines can be drawn. The highest densities for arrays of lines have apparently been acheived using STM to expose passivated Si(100).[85] Pre- and postprocessing steps, such as sputtering of the resist layer and etch steps are required for all of these methods either to resolve or to increase the relief of patterns obtained directly using SPL. However, if only the SPL process is considered, Si:H patterning using the AFM appears to be the most straightforward (see section IV.A.1.a).

2. Data Storage Fabrication

The fastest data writing and reading rates, as high as 100 kHz s^{-1}, have been obtained using a hybrid laser heating/AFM method to generate bits by locally melting a polymer film.[322] The instrumentation for this "local melting" experiment is now highly developed including (nonstandard) cantilevers in which the heating function and motion actuators have been fully integrated. With these instrumental refinements, the implementation of this SPL experiment has apparently become very straightforward.[28] The largest data sets, however, have been obtained via the mechanical patterning of polymer resist with very sharp AFM tips[290]—a techqniue which is not explicitly intended for data storage. The ability to generate data densities of terabits cm^{-2} have been claimed for yet other SPL methods involving the transfer of from a Au covered AFM tip,[187] and the SPL induction of domains having discrete conductivities in $GeSb_2Te_4$[277] and $Na_xV_2O_5$.[274] It has been suggested that even higher bit densities—up to 10^{15} bits cm^{-2}—may be possible for truely atomic scale SPL processes, in particular, the removal of single sulfur atoms from a MoS_2 surface.[187]

A somewhat unexpected conclusion is that mechanical SPL techniques appear superior overall to SPL methods on the basis of electrical modification of a surface. This is surprising in view of the expected deletarious effects of wear on the performance of an AFM tip for SPL (see section III.). Smaller feature sizes are more readily obtained using electrical SPL, interest in these techniques will then endure if sizes below 50 nm are to be realized.

C. SPL Applications and the Future

Of the two applications which are most often cited for SPL, high-density information storage and nanometer-scale device fabrication, prospects for long-term commercial viability appear to be better for the former. In a recent overview article, Hosaka[335] described SPM-based storage techniques and wrote "We predict that they are positioned close to the future [of] data storage". Indeed, the theoretical capacity for SPL-based storage devices, employing existing reading and writing strategies—approaching 10^{10} bits cm^{-2}—is unmatched by magnetic or optical storage media. However, data transfer rates continue to be too slow. For an AFM based system, for example, the maximum speed can approximate the resonance frequency of the cantilever (several hundred kilohertz), while data transfer rates in the vicinity of 10 MHz are required for many practical industrial applications

The most encouraging progress in this direction comes from the Quate group who have pioneered the microfabrication of piezoresistive cantilever arrays as large as 5×1 [25,26] and demonstrated that these cantilever/tip arrays may be operated in parallel both to modify and to image at higher data transfer rates than are possible using a single cantilever and tip.[25] It is clear that the extraordinary information density which is possible using SPL provides plenty of motivation to improve data transfer rates and further work in this direction is clearly justified.

The advantages of SPL for device fabrication are less apparent. Dagata[342] observed that the direct modification of GaAs surfaces—achieved, for example, by locally modifying a thin, passivating a S or As layer using an STM—might constitute a case where SPM modification is commercially feasible. However, Pease[343] has dramatically put into perspective the technological challenges associated with achieving commercial viability with SPL methods: An array of 100×100 probes scanned at several cm s^{-1} but with independent control of each tip constitutes an example of a configuration which might achieve adequate throughput in an industrial application. On the basis of his analysis, Pease concludes that SPL-based device fabrication is a "very long term option at best".

The prospects for commercial SPL applications in the area of device fabrication grow even dimmer when it is considered that the optical lithographic state-of-the art continues to be a rapidly moving target. Currently 0.5 μm technology is standard for Si based ICs, while parts of the new Pentium Pro and PowerPC microprocessors are patterned with 0.35 μm lithography, and microprocessors prepared using 0.25 μm technology are 1−2 years in the future. Further refinements such as the use of even more energetic radiation,[344] improvements to phase shift mask technology,[345] and the development of better chemically amplified resists[346] have the potential to lower this size to 0.15 μm (probably within a few years) and an absolute lower limit is difficult to predict. Finally, SPL faces competition from three older technologies—e-beam, ion beam and X-ray lithography—all of which compete with SPL in terms of the accessible resolution. Proceedings from the *1995 International Conference on Electron, Ion, and Photon Beam Technology and Nanofabrication* give a broad overview of the state of the art of these "competitors".[347] In addition, de Lozanne *et al.*[348] have recently compared SPL with these alternative technologies.

Collectively these considerations make it increasingly difficult to identify a niche for SPL in the manufacture of integrated circuits in quantity. A viable niche, however, may exist for the fabrication of single devices or prototypes. The initial cost of fabricating such experimental devices by conventional lithographic means is high, and it is conceivable, at least, that SPL will provide a means of producing single devices at lower cost. With further advancements in

parallel SPL technology, it may prove to be the case that the capability of preparing single experimental devices will be extended to a larger community of researchers since the cost of SPL, relative to conventional e-beam lithography, is small.

SPL has unique capabilities for performing a variety of fundamental investigations involving surfaces, and in this capacity, many of the capabilities provided by SPL methods are unsurpassed. In many previous cases, for example, a single SPL experiment has functioned as a perturbation to the surface structure and the subsequent relaxation of the surface to equilibrium has afforded an opportunity to observe, by SPM, surface transport mechanisms, phase transitions, etc., which are difficult to discern at nonperturbed surfaces. Examples include the measurement of the surface diffusion coefficient for metal atoms on a surface,[259,349] measurements of the viscosity of a bilayer molecular assembly,[156] and the observation of electron standing waves in a corral.[246] In addition, SPL methods provide a means for synthesizing single nanoscopic domains of materials for subsequent investigation by SPM, and by other methods. An ensemble of nanoscopic particles—either on a surface, or suspended in solution—can be obtained using a variety of synthetic methods such as MBE,[350] arrested precipitation,[351,352] electrospray,[353] and pyrolysis methods,[354] but the synthesis of a single nanoscopic particle can so far only be accomplished using SPL. Single, SPL-synthesized particles have so far been employed to study, for example, single electron devices,[282,286] and molecular adsorption.[355] These two unique experiments, aimed at probing fundamental surface chemical and physical problems, are likely to sustain interest in SPL well into the future independent of the success of SPL as a technological tool.

VI. Glossary

AES	auger electron spectroscopy
AFM	atomic force microscope/microscopy
CMPTS	[4-(chloromethyl)phenyl]trichlorosilane
CVD	chemical vapor deposition
HMDS	hexamethyldisilazane
LB	Langmuir−Blodgett
LS	Langmuir−Schaefer
MAA	methacrylic acid
NCAFM	noncontact atomic force microscope/microscopy
NHE	normal hydrogen electrode
NSOM	near-field optical microscope/microscopy
PANI	polyaniline
PC	polycarbonate
PEDA	[[[(aminoethyl)amino]methyl]phenethyl]trimethoxysilane
PEO	polyethylene oxide
PGMA	polyglycidyl methacrylate
PMeP	poly(*N*-methylpyrrole)
PMMA	polymethylmethacrylate
PP	polypropylene
Ppy	polypyrrole
PS	polystyrene
PSTM	photon scanning tunneling microscope/microscopy
PVA	polyvinyl alcohol
OCP	open circuit potential
OTS	octadecyltrichlorosilane
SAM	self-assembled monolayer
SECM	scanning electrochemical microscope
SERS	surface enhanced Raman spectroscopy
SPL	scanning probe lithography
SPM	scanning probe microscope/microscopy
STM	scanning tunneling microscope/microscopy
TMA	trimethyl aluminum
TGS	triglycine sulfate
TIR	total internal reflection
UME	ultramicroelectrode
UPD	under potential deposition
YBCO	$YBa_2Cu_3O_{7-x}$

VII. Acknowledgments

We thank the contributing authors for providing us with preprints and picture files. The ongoing financial support of SPM-based lithography research in the authors' laboratory by the Office of Naval Research (#400×119YIP) and the National Science Foundation (#DMR-9257000) are gratefully acknowledged. R.M.N. thanks the Swiss National Science Foundation for generous financial support. R.M.P. acknowledges additional financial support as an A. P. Sloan Foundation Fellow, a Camille Dreyfus Teacher−Scholar, and an Arnold and Mabel Beckman Foundation Young Investigator.

VIII. References

(1) Binnig, G.; Rohrer, H. *Helv. Phys. Acta* **1982**, *55*, 726−735.
(2) Binnig, G.; Quate, C. F.; Gerber, C. *Phys. Rev. Lett.* **1986**, *56*, 930−933.
(3) Ringger, M.; Hidber, H. R.; Schlogl, R.; Oelhafen, P.; Guntherodt, H. J. *Appl. Phys. Lett.* **1985**, *46*, 832−4.
(4) Abraham, D. W.; Mamin, H. J.; Ganz, E.; Clarke, J. *IBM J. Res. Dev.* **1986**, *30*, 492−499.
(5) McCord, M. A.; Pease, R. F. W. *J. Phys. (Paris)* **1986**, *47*, 485−491.
(6) Quate, C. F. *Surf. Sci.* **1994**, *299*−300, 980−995.
(7) Eigler, D. M.; Schweizer, E. K. *Nature* **1990**, *344*, 524−526.
(8) Eigler, D. M.; Lutz, C. P.; Rudge, W. E. *Nature* **1991**, *352*, 600−603.
(9) Kranz, C.; Ludwig, M.; Gaub, H. E.; Schuhmann, W. *Adv. Mater.* **1995**, *7*, 38−40.
(10) Dürig, U.; Pohl, D. W.; Rohner, F. *J. Appl. Phys.* **1986**, *59*, 3318−3327.
(11) Mainsbridge, B. *Mater. Forum* **1994**, *18*, 77−84.
(12) Wiesendanger, R. *Jpn. J. Appl. Phys 1* **1995**, *34*, 3388−3395.
(13) Avouris, P. *Acc. Chem. Res.* **1995**, *28*, 95−102.
(14) Czajka, R. *Acta Phys. Pol. A* **1995**, *88*, 813−28.
(15) Salling, C. T. Materials - Fabrication and Patterning at the Nanoscale, San Francisco, 1995; p 143−151.
(16) Kern, D. P. *Microelectron. Eng.* **1994**, *23*, 41.
(17) Maivald, P.; Butt, H. J.; Gould, S. A. C.; Prater, C. B.; Drake, B.; Gurley, J. A.; Elings, V. B.; Hansma, P. K. *Nanotechnology* **1991**, *2*, 103−106.
(18) Mate, C. M.; McClelland, G. M.; Erlandsson, R.; Chiang, S. *Phys. Rev. Lett.* **1987**, *59*, 1942−1945.
(19) Morita, S.; Ishizaka, T.; Sugawara, Y.; Okada, T.; Mishima, S.; Imai, S.; Mikoshiba, N. *Jpn. J. Appl. Phys. 2* **1989**, *28*, L1634-L1636.
(20) van de Walle, G. F. A.; van Kempen, H.; Wyder, P.; Flipse, C. J. *Surf. Sci.* **1987**, *181*, 27−36.
(21) Bedzig, E.; Trautman, J. K.; Harris, T. D.; Weiner, J. S.; Kostelak, R. L. *Science* **1991**, *251*, 1468.
(22) For example, "Nanolithography" from Park Scientific Instruments, S., CA; "SPMTools" from Topometrix, Santa Clara, CA; "Lithography" submenu from Digital Instruments, Santa Barbara, CA; "Lithography" submenu from Omicron Vakuumphysik GmbH, Taunusstein, Germany.
(23) Mamin, H. J.; Rugar, D. *Appl. Phys. Lett.* **1992**, *61*, 1003−1005.
(24) Minne, S. C.; Manalis, S. R.; Atalar, A.; Quate, C. F. *J. Vac. Sci. Technol. B* **1996**, *14*, 2456−2461.
(25) Minne, S. C.; Flueckiger, P.; Soh, H. T.; Quate, C. F. *J. Vac. Sci. Technol. B* **1995**, *13*, 1380−1385.
(26) Minne, S. C.; Manalis, S. R.; Quate, C. F. *Appl. Phys. Lett.* **1995**, *67*, 3918−20.
(27) Manalis, S. R.; Minne, S. C.; Atalar, A.; Quate, C. F. *Rev. Sci. Instrum.* **1996**, *67*, 3294−3297.
(28) Chui, B. W.; Stowe, T. D.; Ju, Y. S.; Soh, H. T.; Minne, S. C.; Goodson, K. E.; Quate, C. F.; Kenny, T. W.; Mamin, H. J.; Terris,

B. D.; Pied, R. P.; Rugar, D. Solid-State Sensor and Actuator Workshop, Hilton Head Island, SC, 1996; p 219−224.
(29) Minne, S. C.; Manalis, S. R.; Atalar, A.; Quate, C. F. *Appl. Phys. Lett.* **1996**, *68*, 1427−9.
(30) Manalis, S. R.; Minne, S. C.; Quate, C. F. *Appl. Phys. Lett.* **1996**, *68*, 871−873.
(31) Fujii, T.; Watanabe, S. *Appl. Phys. Lett.* **1996**, *68*, 467−468.
(32) MacDonald, N. C.; Adams, S. G.; Ayon, A. A.; Bohringer, K. F.; Chen, L. Y.; Das, J. H.; Haronian, D.; Hofmann, W.; Huang, X. T.; Jazairy, A.; Mihailovich, R. E.; Miller, S. A.; Ogo, I.; Prasad, R.; Reed, B. W.; Saif, M. T. A.; Shaw, K. A.; Webb, R. Y.; Xu, Y. *Microelectron. Eng.* **1996**, *30*, 563−4.
(33) MacDonald, N. C. *IEEE Trans Electron Devices* **1993**, *40*, 2098−2099.
(34) Altman, E. I.; DiLella, D. P.; Ibe, J.; Lee, K.; Colton, R. J. *Rev. Sci. Instrum.* **1993**, *64*, 1239−1243.
(35) Lapshin, R. V.; Obyedkov, O. V. *Rev. Sci. Instrum.* **1993**, *64*, 2883−2887.
(36) Koops, R.; Sawatzky, G. A. *Rev. Sci. Instrum.* **1992**, *63*, 4008−4009.
(37) Barrett, R. C.; Quate, C. F. *J. Vac. Sci. Technol. B* **1991**, *9*, 302−306.
(38) Michel, B.; Novotny, L.; Dürig, U. *Ultramicroscopy* **1992**, *42*−44, 1647−1652.
(39) Mamin, H. J.; Birk, H.; Wimmer, P.; Rugar, D. *J. Appl. Phys.* **1994**, *75*, 161−168.
(40) Kuipers, L.; Loos, R. W. N.; H., N.; J., t. H.; Ruwiel, G. J.; Dejongh, A. P.; Frenken, J. W. M. *Rev. Sci. Instrum.* **1995**, *66*, 4557−4565.
(41) Nuzzo, R. G.; Allara, D. L. *J. Am. Chem. Soc.* **1983**, *105*, 4481−4483.
(42) Moreau, W. M. *Semiconductor Lithography, Principles, Practices and Materials*; Plenum Press: New York, 1988.
(43) Stuart, R. V. *Vacuum technology, thin films, and sputtering. An introduction*; Academic Press: London, 1983.
(44) Gaines, G. L. *Insoluble Monolayers at Liquid-Gas Interfaces*; Wiley-Interscience: New York, 1966.
(45) Roberts, G. G. *Langmuir-Blodgett Films*; Plenum Press: New York, 1990.
(46) Ulman, A. *An Introduction to ultrathin organic films: from Langmuir-Blodgett to self-assembly*; Academic Press: Boston, 1991.
(47) Dubois, L. H.; Nuzzo, R. G. *Annu. Rev. Phys. Chem.* **1992**, *43*, 437−463.
(48) Marrian, C. R. K.; Dobisz, E. A.; Colton, R. J. *J. Vac. Sci. Technol. A* **1990**, *8*, 3563−3569.
(49) Kaneko, R.; Oguchi, S. *Jpn. J. Appl. Phys 1* **1990**, *29*, 1854−1855.
(50) Sumomogi, T.; Endo, T.; Kuwahara, K.; Kaneko, R.; Miyamoto, T. *J. Vac. Sci. Technol. B* **1994**, *12*, 1876−1880.
(51) Sumomogi, T.; Endo, T.; Kuwahara, K.; Kaneko, R. *J. Vac. Sci. Technol. B* **1995**, *13*, 1257−1260.
(52) Niedermann, P.; Hanni, W.; Blanc, N.; Christoph, R.; Burger, J. *J. Vac. Sci. Technol. A* **1996**, *14*, 1233−6.
(53) Tortonese, M. Personal Communication.
(54) Thomson, R. E.; Moreland, J. *J. Vac. Sci. Technol. B* **1995**, *13*, 1123−1125.
(55) Dagata, J. A.; Schneir, J.; Harary, H. H.; Bennett, J.; Tseng, W. *J. Vac. Sci. Technol. B* **1991**, *9*, 1384−1388.
(56) Dagata, J. A.; Tseng, W.; Bennett, J.; Evans, C. J.; Schneir, J.; Harary, H. H. *Appl. Phys. Lett.* **1990**, *57*, 2437−2439.
(57) Snow, E. S.; Campbell, P. M.; McMarr, P. J. *Appl. Phys. Lett.* **1993**, *63*, 749−751.
(58) Snow, E. S.; Campbell, P. M.; Shanabrook, B. V. *Appl. Phys. Lett.* **1993**, *63*, 3488−3490.
(59) Sugimura, H.; Uchida, T.; Kitamura, N.; Masuhara, H. *Jpn. J. Appl. Phys. 2* **1993**, *32*, L553−L555.
(60) Sugimura, H.; Uchida, T.; Kitamura, N.; Masuhara, H. *Appl. Phys. Lett.* **1993**, *63*, 1288−1290.
(61) Sugimura, H.; Kitamura, N.; Masuhara, H. *Jpn. J. Appl. Phys. 2* **1994**, *33*, L143-L145.
(62) Sugimura, H.; Uchida, T.; Kitamura, N.; Masuhara, H. *J. Vac. Sci. Technol. B* **1994**, *12*, 2884−2888.
(63) Sugimura, H.; Yamamoto, T.; Nakagiri, N.; Miyashita, M.; Onuki, T. *Appl. Phys. Lett.* **1994**, *65*, 1569−1571.
(64) Sugimura, H.; Uchida, T.; Kitamura, N.; Masuhara, H. *J. Phys. Chem.* **1994**, *98*, 4352−4357.
(65) Sugimura, H.; Nakagiri, N. *J. Vac. Sci. Technol. B* **1995**, *13*, 1933−1937.
(66) Sugimura, H.; Nakagiri, N. *Jpn. J. Appl. Phys 1* **1995**, *34*, 3406−3411.
(67) Sugimura, H.; Nakagiri, N. *Jpn. J. Appl. Phys. 2* **1995**, *34*, L698-L700.
(68) Sugimura, H.; Nakagiri, N.; Ichinose, N. *Appl. Phys. Lett.* **1995**, *66*, 3686−3688.
(69) Sugimura, H.; Nakagiri, N. *Nanotechnology* **1995**, *6*, 29−33.
(70) Sugimura, H.; Nakagiri, N. *Appl. Phys. Lett.* **1995**, *66*, 1430−1431.
(71) Sugimura, H.; Nakagiri, N. *Langmuir* **1995**, *11*, 3623−3625.
(72) Sugimura, H.; Nakagiri, N. *Thin Sol. Films* **1996**, *273*, 245−249.
(73) Sugimura, H.; Nakagiri, N. *J. Vac. Sci. Technol. A* **1996**, *14*, 1223−1227.
(74) Sugimura, H.; Nakagiri, N. *Thin Sol. Films* **1996**, *281*−282, 572−575.
(75) Sugimura, H.; Okiguchi, K.; Nakagiri, N. *Jpn. J. Appl. Phys 1* **1996**, *35*, 3749−53.
(76) Fay, P.; Brockenbrough, R. T.; Abeln, G.; Scott, P.; Agarwala, S.; Adesida, I.; Lyding, J. W. *J. Appl. Phys.* **1994**, *75*, 7545−7549.
(77) Urban, J.; Brauer, S.; McKinnon, A. W.; Horn, J. *Microelectron. Eng.* **1995**, *27*, 113−116.
(78) Pérez-Murano, F.; Barniol, N.; Abadal, G.; Ye, J. H.; Aymerich, X.; Cane, C. *Mater. Sci. Technol.* **1995**, *11*, 85−89.
(79) Barniol, N.; Pérez-Murano, F.; Abadal, G.; Ye, J. H.; Aymerich, X. *Microelectron. Eng.* **1995**, *27*, 27−30.
(80) Pérez-Murano, F.; Barniol, N.; Aymerich, X. *J. Vac. Sci. Technol. B* **1993**, *11*, 651−657.
(81) Barniol, N.; Perez-Murano, F.; Aymerich, X. *Appl. Phys. Lett.* **1992**, *61*, 462−4.
(82) Kramer, N.; Jorritsma, J.; Birk, H.; Schönenberger, C. *J. Vac. Sci. Technol. B* **1995**, *13*, 805−811.
(83) Kramer, N.; Birk, H.; Jorritsma, J.; Schönenberger, C. *Appl. Phys. Lett.* **1995**, *66*, 1325−1327.
(84) Snow, E. S.; Campbell, P. M. *Appl. Phys. Lett.* **1994**, *64*, 1932−1934.
(85) Campbell, P. M.; Snow, E. S.; McMarr, P. J. *Solid-State Electron.* **1994**, *37*, 583−586.
(86) Snow, E. S.; Juan, W. H.; Pang, S. W.; Campbell, P. M. *Appl. Phys. Lett.* **1995**, *66*, 1729−1731.
(87) Teuschler, T.; Mahr, K.; Miyazaki, S.; Hundhausen, M.; Ley, L. *Appl. Phys. Lett.* **1995**, *66*, 2499−2501.
(88) Teuschler, T.; Mahr, K.; Miyazaki, S.; Hundhausen, M.; Ley, L. *Appl. Phys. Lett.* **1995**, *67*, 3144−3146.
(89) Gordon, A. E.; Fayfield, R. T.; Litfin, D. D.; Higman, T. K. *J. Vac. Sci. Technol. B* **1995**, *13*, 2805−2808.
(90) Wang, D.; Tsau, L.; Wang, K. L. *Appl. Phys. Lett.* **1994**, *65*, 1415−1417.
(91) Tsau, L.; Wang, D.; Wang, K. L. *Appl. Phys. Lett.* **1994**, *64*, 2133−2135.
(92) Hattori, T.; Ejiri, Y.; Saito, K.; Yasutake, M. *J. Vac. Sci. Technol. A* **1994**, *12*, 2586−2590.
(93) Yasutake, M.; Ejiri, Y.; Hattori, T. *Jpn. J. Appl. Phys. 2* **1993**, *32*, L1021−L1023.
(94) Whidden, T. K.; Allgair, J.; Jenkins-Gray, A.; Kozicki, M. N. *J. Vac. Sci. Technol. B* **1995**, *13*, 1337−1341.
(95) Enachescu, M.; Hartmann, E.; Koch, F. *Appl. Phys. Lett.* **1994**, *64*, 2253−2255.
(96) Hartmann, E.; Enachescu, M.; Koch, F.; Behm, R. J. *Phys. Rev. B* **1994**, *50*, 17172−17179.
(97) Ostrom, R. M.; Tanenbaum, D. M.; Gallagher, A. *Appl. Phys. Lett.* **1992**, *61*, 925−927.
(98) Yau, S.-T.; Zheng, X.; Nayfeh, M. H. *Appl. Phys. Lett.* **1991**, *59*, 2457−2459.
(99) Zheng, X.; Hetrick, J.; Yau, S.-T.; Nayfeh, M. H. *Ultramicroscopy* **1992**, *42*−44, 1303−1308.
(100) Hetrick, J. M.; Zheng, X.; Nayfeh, M. H. *J. Appl. Phys.* **1993**, *73*, 4721−4723.
(101) Albrecht, T. R.; Dovek, M. M.; Kirk, M. D.; Lang, C. A.; Quate, C. F.; Smith, D. P. E. *Appl. Phys. Lett.* **1989**, *55*, 1727−1729.
(102) Terashima, K.; Kondoh, M.; Yoshida, T. *J. Vac. Sci. Technol. A* **1990**, *8*, 581−584.
(103) Moriaty, P.; Hughes, G. *Appl. Phys. Lett.* **1992**, *60*, 2338−2340.
(104) Abe, T.; Hane, K.; Okuma, S. *Jpn. J. Appl. Phys 1* **1996**, *35*, 1850−6.
(105) Abe, T.; Hane, K.; Okuma, S. *Intl. J. Jpn. Soc. Precis. Eng.* **1995**, *29*, 123−127.
(106) Abe, T.; Hane, K.; Okuma, S. *J. Appl. Phys.* **1994**, *75*, 1228−30.
(107) Kondo, S.; Lutwyche, M.; Wada, Y. *Appl. Surf. Sci.* **1994**, *75*, 39−44.
(108) Kondo, S.; Heike, S.; Lutwyche, M.; Wada, Y. *J. Appl. Phys.* **1995**, *78*, 156−160.
(109) Uesugi, K.; Yao, T. *Ultramicroscopy* **1992**, *42*−44, 1443−1445.
(110) Wang, Z. H.; Dai, C. C.; Zhang, P. C.; Huang, G. Z.; Li, R. L.; Guo, Y.; Bai, C. L. *Chin. Phys. Lett.* **1993**, *10*, 535−538.
(111) Parkinson, B. A. *J. Am. Chem. Soc.* **1990**, *112*, 7498.
(112) Akari, S.; Möller, R.; Dransfeld, K. *Appl. Phys. Lett.* **1991**, *59*, 243.
(113) Schimmel, T.; Fuchs, H.; Lux-Steiner, M. *Phys. Stat. Sol. A* **1992**, *131*, 47−57.
(114) Schimmel, T.; Fuchs, H.; Akari, S.; Dransfeld, K. *Appl. Phys. Lett.* **1991**, *58*, 1039−1041.
(115) Fuchs, H.; Schimmel, T. *AIP Conf. Proc.* **1991**, *241*, 480−489.
(116) Permana, H.; Lee, S.; Ng, K. Y. S. *J. Vac. Sci. Technol. B* **1992**, *10*, 2297.
(117) Heckl, W. M.; Ohnesorge, F.; Binnig, G.; Specht, M.; Hashmi, M. *J. Vac. Sci. Technol. B* **1991**, *9*, 1072.
(118) Schimmel, T.; Kemnitzer, R.; Küppers, J.; Fuchs, H.; Lux-Steiner, M. *Thin Sol. Films* **1995**, *254*, 147−152.

(119) Huang, J. L.; Sung, Y. E.; Lieber, C. M. *Appl. Phys. Lett.* **1992**, *61*, 1528–1530.
(120) Rabe, J. P.; Buchholz, S. *Appl. Phys. Lett.* **1991**, *58*, 702–704.
(121) Casillas, N.; Snyder, S. R.; White, H. S. *J. Electrochem. Soc.* **1991**, *138*, 641–642.
(122) Song, H. J.; Rack, M. J.; Abugharbieh, K.; Lee, S. Y.; Khan, V.; Ferty, D. K.; Allee, D. R. *J. Vac. Sci. Technol. B* **1994**, *12*, 3720–3724.
(123) Wang, D.; Tsau, L.; Wang, K. L.; Chow, P. *Appl. Phys. Lett.* **1995**, *67*, 1295–1297.
(124) Fukuzawa, H.; Kimijima, H.; Yoshikawa, N.; Sugahara, M. *Jpn. J. Appl. Phys. 2* **1995**, *34*, L1221–L1223.
(125) Rosolen, G. C.; Hoole, A. C. F.; Welland, M. E.; Broers, A. N. *Appl. Phys. Lett.* **1993**, *63*, 2435–2437.
(126) Taylor, M. E.; Golon, B.; McKinnon, A. W.; Rosoloen, G. C.; Gray, S. M.; Welland, M. E. *Appl. Surf. Sci.* **1993**, *67*, 228–234.
(127) Hosaka, S.; Koyanagi, H.; Kikukawa, A.; Miyamoto, M.; Imura, R.; Ushiyama, J. *J. Vac. Sci. Technol. B* **1995**, *13*, 1307–1311.
(128) Nakamura, J.; Miyamoto, M.; Hosaka, S.; Koyanagi, H. *J. Appl. Phys.* **1995**, *77*, 779–81.
(129) Yang, X.; Rosner, K.; Winzer, K.; von Minnigerode, G. *Ann. Phys.* **1992**, *1*, 575–583.
(130) Bertsche, G.; Clauss, W.; Kern, D. P. *Appl. Phys. Lett.* **1996**, *68*, 3632–4.
(131) Heyvaert, I.; Osquiguil, E.; Van Haesendonck, C.; Bruynseraede, Y. *Appl. Phys. Lett.* **1992**, *61*, 111–13.
(132) Thomson, R. E.; Moreland, J.; Roshko, A. *Nanotechnology* **1994**, *5*, 57–69.
(133) Terashima, K.; Kondoh, M.; Takamura, Y.; Komaki, H.; Yoshida, T. *Appl. Phys. Lett.* **1991**, *59*, 644–646.
(134) Dagata, J. A.; Tseng, W.; Bennett, J.; Schneir, J.; Harary, H. H. *J. Appl. Phys.* **1991**, *70*, 3661–3665.
(135) Sinnott, S. B.; Colton, R. J.; White, C. T.; Brenner, D. W. *Surf. Sci.* **1994**, *316*, L1055-L1060.
(136) Perkins, F. K.; Dobisz, E. A.; Marrian, C. R. K. *J. Vac. Sci. Technol. B* **1993**, *11*, 2597–2602.
(137) Marrian, C. R. K.; Dobisz, E. A.; Dagata, J. A. *J. Vac. Sci. Technol. B* **1992**, *10*, 2877–2881.
(138) Marrian, C. R. K.; Dobisz, E. A. *Ultramicroscopy* **1992**, *42*–44, 1309–1316.
(139) Marrian, C. R. K.; Dobisz, E. A.; Dagata, J. A. *Proc. SPIE* **1992**, *1671*, 166–176.
(140) Dobisz, E. A.; Marrian, C. R. K. *J. Vac. Sci. Technol. B* **1991**, *9*, 3024–3027.
(141) Dobisz, E. A.; Marrian, C. R. K. *Appl. Phys. Lett.* **1991**, *58*, 2526–2528.
(142) Marrian, C. R. K.; Dobisz, E. A.; Peckerar, M. C. *Proc. IEEE* **1991**, *79*, 1149–1158.
(143) Dobisz, E. A.; Marrian, C. R. K.; Colton, R. J. *J. Vac. Sci. Technol. B* **1990**, *8*, 1754–1758.
(144) Archer, A.; Hetrick, J. M.; Nayfeh, M. H.; Adesida, I. *J. Vac. Sci. Technol. B* **1994**, *12*, 3166–3170.
(145) Kragler, K.; Günther, E.; Leuschner, R.; Falk, G.; Hammerscmidt, A.; von Seggern, H.; Saemann-Ischenko, G. *Appl. Phys. Lett.* **1995**, *67*, 1163–1165.
(146) Park, S. W.; Soh, H. T.; Quate, C. F.; Park, S.-I. *Appl. Phys. Lett.* **1995**, *67*, 2415–2417.
(147) Dobisz, E. A.; Koops, H. W. P.; Perkins, F. K. *Appl. Phys. Lett.* **1996**, *68*, 3653–5.
(148) EO-3D, 2, Munro's Electron Beam Software, London, England, 1994.
(149) Perkins, F. K.; Dobisz, E. A.; Brandow, S. L.; Calvert, J. M.; Kosakowski, J. E.; Marrian, C. R. K. *Appl. Phys. Lett.* **1996**, *68*, 550–552.
(150) Bruynseraede, Y.; Gielen, L.; Strunk, C.; Neuttiens, C.; Stockman, L.; Van Haesendonck, C.; Moshchalkov, V. V. *Nanostruc. Mater.* **1995**, *6*, 169–78.
(151) Van Haesendonck, C.; Stockman, L.; Neuttiens, G.; Strunk, C.; Bruynseraede, Y. *J. Vac. Sci. Technol. B* **1995**, *13*, 1290–1293.
(152) Van Haesendonck, C.; Stockman, L.; Bruynseraede, Y.; Langer, L.; Bayot, V.; Issi, J.-P.; Heremans, J. P.; Olk, C. H. *Phys. Scr.* **1994**, *T55*, 86–89.
(153) Stockman, L.; Neuttiens, G.; Van Haesendonck, C.; Bruynseraede, Y. *Appl. Phys. Lett.* **1993**, *62*, 2935–7.
(154) Xu, L. S.; Allee, D. R. *J. Vac. Sci. Technol. B* **1995**, *13*, 2837–2840.
(155) Day, H. C.; Allee, D. R.; George, R.; Burrows, V. A. *Appl. Phys. Lett.* **1993**, *62*, 1629–1631.
(156) Virtanen, J. A.; Lee, S.; Li, W.; Penner, R. M. *J. Phys. Chem.* **1994**, *98*, 2663–2667.
(157) Lee, S.; Virtanen, J. A.; Virtanen, S. A.; Penner, R. M. *Langmuir* **1992**, *8*, 1243.
(158) Yano, K.; Kyogaku, M.; Kuroda, R.; Shimada, Y.; Shido, S.; Matsuda, H.; Takimoto, K.; Albrecht, O.; Eguchi, K.; Nakagiri, T. *Appl. Phys. Lett.* **1996**, *68*, 188–190.
(159) Kim, Y.-T.; Bard, A. J. *Langmuir* **1992**, *8*, 1096–1102.
(160) Ross, C. B.; Sun, L.; Crooks, R. M. *Langmuir* **1993**, *9*, 632–636.
(161) Corbitt, T. S.; Crooks, R. M.; Ross, C. B.; Hampden-Smith, M. J.; Schoer, J. K. *Adv. Mater.* **1993**, *5*, 935–938.
(162) Schoer, J. K.; Ross, C. B.; Crooks, R. M.; Corbitt, T. S.; Hampden-Smith, M. J. *Langmuir* **1994**, *10*, 615–618.
(163) Perkins, F. K.; Dobisz, E. A.; Brandow, S. L.; Koloski, T. S.; Calvert, J. M.; Rhee, K. W.; Kosakowski, J. E.; Marrian, C. R. K. *J. Vac. Sci. Technol. B* **1994**, *12*, 3725–3730.
(164) Marrian, C. R. K.; Perkins, F. K.; Brandow, S. L.; Koloski, T. S.; Dobisz, E. A.; Calvert, J. M. *Appl. Phys. Lett.* **1994**, *64*, 390–392.
(165) Müller, H. U.; David, C.; Völkel, B.; Grunze, M. *J. Vac. Sci. Technol. B* **1995**, *13*, 2846–2849.
(166) Lercel, M. J.; Redinbo, G. F.; Craighead, H. G.; Sheen, C. W.; Allara, D. L. *Appl. Phys. Lett.* **1994**, *65*, 974–976.
(167) Lercel, M. J.; Redinbo, G. F.; Pardo, F. D.; Rooks, M.; Triberio, R. C.; Simpson, P.; Graighead, H. G.; Sheen, C. W.; Parikh, A. N.; Allora, D. L. *J. Vac. Sci. Technol. B* **1994**, *12*, 3663–3667.
(168) Tang, S. L.; McGhie, A. J.; Lewittes, M. E. *Appl. Phys. Lett.* **1992**, *60*, 1821–1823.
(169) Bashkin, M. O.; Bespalov, V. A.; Emelyanov, A. V.; Inkin, V. N.; Portnov, S. M.; Zimin, A. V.; Kharkevich, S. I.; Menshikov, O. D. *Ultramicroscopy* **1992**, *42*–44, 977–982.
(170) Müller, E. W.; Tsong, T. T. *Field ion microscopy; principles and applications*; American Elsevier Pub. Co.: New York, 1969.
(171) Tsong, T. T. *Phys. Rev. B* **1991**, *44*, 13703–10.
(172) Lang, N. D. *Phys. Rev. B* **1992**, *45*, 13599–13606.
(173) Gratzke, U.; Simon, G. *Phys. Rev. B* **1995**, *52*, 8535–40.
(174) Mamin, H. J.; Chiang, S.; Birk, P. H.; Guethner, P. H.; Rugar, D. *J. Vac. Sci. Technol. B* **1991**, *2*, 1398.
(175) Mamin, H. J.; Guethner, P. H.; Rugar, D. *Phys. Rev. Lett.* **1990**, *65*, 2418–21.
(176) Binh, V. T.; Garcia, N. *Ultramicroscopy* **1992**, *42*, 80–90.
(177) Chang, C. S.; Su, W. B.; Tsong, T. T. *Phys. Rev. Lett.* **1994**, *72*, 574–577.
(178) Xu, J. B.; Lauger, K.; Moller, R.; Dransfeld, K.; Wilson, I. H. *Appl. Phys. A* **1994**, *A59*, 155–161.
(179) Ohi, A.; Mizutani, W.; Tokumoto, H. *J. Vac. Sci. Technol. B* **1995**, *13*, 1252–1256.
(180) Pascual, J. I.; Mendez, J.; Gomez-Herrero, J.; Baro, A. M.; Garcia, N.; Binh, V. T. *Phys. Rev. Lett.* **1993**, *71*, 1852–1855.
(181) Mascher, C.; Damaschke, B. *J. Appl. Phys.* **1994**, *75*, 5438–40.
(182) Bessho, K.; Hashimoto, S. *Appl. Phys. Lett.* **1994**, *65*, 2142–2144.
(183) Lebreton, C.; Wang, Z. Z. *Scanning Microsc.* **1994**, *8*, 441–448.
(184) McBride, S. E.; Wetsel, G. C., Jr. *Appl. Phys. Lett.* **1990**, *57*, 2782–2784.
(185) Schaub, T.; Wiesendanger, R.; Güntherodt, H.-J. *Nanotechnology* **1992**, *3*, 77–83.
(186) Hsiao, G. S.; Penner, R. M.; Kingsley, J. *Appl. Phys. Lett.* **1994**, *64*, 1350–1352.
(187) Hosaka, S.; Hosoki, S.; Hasegawa, T.; Koyanagi, H.; Shintani, T.; Miyamoto, M. *J. Vac. Sci. Technol. B* **1995**, *13*, 2813–2818.
(188) Hosaka, S.; Koyanagi, H.; Kikukawa, A.; Maruyama, Y.; Imura, R. *J. Vac. Sci. Technol. B* **1994**, *12*, 1872–1875.
(189) Imura, R.; Koyanagi, H.; Miyamoto, M.; Kikukawa, A.; Shintani, T.; Hosaka, S. *Microelectron. Eng.* **1995**, *27*, 105–108.
(190) Hosaka, S.; Koyanagi, H. *Jpn. J. Appl. Phys. 2* **1994**, *33*, L1358–61.
(191) Imura, R.; Koyanagi, H.; Miyamoto, M.; Shintani, T.; Nakamura, K.; Kikukawa, A.; Hosaka, S. *Proc. SPIE* **1994**, *2338*, 56–64.
(192) Hosaka, S.; Koyabagi, H.; Kikukawa, A. *Jpn. J. Appl. Phys. 2* **1993**, *32*, L464-L467.
(193) Lozovik, Y. E.; Merkulova, S. P.; Sekatskii, S. K.; Letokhov, V. S. *Phys. Lett. A* **1994**, *189*, 131–133.
(194) Pérez-Murano, F.; Abadal, G.; Barniol, N.; Aymerich, X.; Servat, J.; Gorostiza, P.; Sanz, F. *J. Appl. Phys.* **1995**, *78*, 6797–6801.
(195) Shekhawat, G. S.; Gupta, R. P.; Agarwal, A.; Garg, K. B.; Vyas, P. D. *J. Appl. Phys.* **1995**, *78*, 127–131.
(196) Silver, R. M.; Ehrichs, E. E.; de Lozanne, A. L. *Appl. Phys. Lett.* **1987**, *51*, 247.
(197) McCord, M. A.; Awschalom, D. D. *Appl. Phys. Lett.* **1990**, *57*, 2153.
(198) McCord, M. A.; Kern, D. P.; Chang, T. H. P. *J. Vac. Sci. Technol. B* **1988**, *6*, 1877.
(199) Baba, M.; Matsui, S. *Jpn. J. Appl. Phys 1* **1990**, *29*, 2854–2857.
(200) Yau, S.-T.; Saltz, D.; Wriekat, A.; Nayfeh, M. H. *J. Appl. Phys.* **1991**, *69*, 2970–2974.
(201) Rubel, S.; Wang, X. D.; de Lozanne, A. L. *J. Vac. Sci. Technol. B* **1995**, *13*, 1332–1336.
(202) de Lozanne, A. *Jpn. J. Appl. Phys 1* **1994**, *33*, 7090–7093.
(203) Rubel, S.; Trochet, M.; Ehrichs, E. E.; Smith, W. F.; de Lozanne, A. *J. Vac. Sci. Technol. B* **1994**, *12*, 1894–1897.
(204) de Lozanne, A.; Ehrichs, E. E.; Smith, W. F. *J. Phys.: Condens. Matter* **1993**, *5*, A409–A410.
(205) Ehrichs, E. E.; Smith, W. F.; de Lozanne, A. L. *Ultramicroscopy* **1992**, *42*–44, 1438–1442.
(206) Kent, A. D.; von Molnár, S.; Gider, S.; Awschalom, D. D. *J. Appl. Phys.* **1994**, *76*, 6656–6660.
(207) Kent, A. D.; Shaw, T. M.; von Molnar, S.; Awschalom, D. D. *Science* **1993**, *262*, 1249–1252.
(208) Thibaudau, F.; Roche, J. R.; Salvan, F. *Appl. Phys. Lett.* **1994**, *64*, 523–525.

(209) Saulys, D. S.; Ermakov, A.; Garfunkel, E. L.; Dowben, P. A. *J. Appl. Phys.* **1994**, *76*, 7639−7641.
(210) Uesugi, K.; Sakata, K.; Kawano, S.; Yoshimura, M.; Yao, T. *Jpn. J. Appl. Phys 1* **1993**, *32*, 2814−2817.
(211) Rauscher, H.; Memmert, U.; Behm, R. J. *J. Vac. Sci. Technol. B* **1995**, *13*, 1216−1220.
(212) Wong, T. M. H.; O'Shea, S. J.; McKinnon, A. W.; Welland, M. E. *Appl. Phys. Lett.* **1995**, *67*, 786−788.
(213) Nagahara, L. A.; Thundat, T.; Lindsay, S. M. *Appl. Phys. Lett.* **1990**, *57*, 270−272.
(214) Siegenthaler, H. In *Scanning tunneling microscopy II: further applications and related scanning techniques*; Wiesendanger, R., Güntherodt, H.-J., Eds.; Springer Verlag: Berlin, 1992; Vol. 28.
(215) Ye, J. H.; Pérez-Murano, F.; Barniol, N.; Abadal, G.; Aymerich, X. *J. Vac. Sci. Technol. B* **1995**, *13*, 1423−1428.
(216) Li, Y.-Q.; Chailapakul, O.; Crooks, R. M. *J. Vac. Sci. Technol. B* **1995**, *13*, 1300−6.
(217) Chen, L.; Guay, D. *J. Electrochem. Soc.* **1994**, *141*, L43−L45.
(218) Penner, R. M.; Heben, M. J.; Lewis, N. S.; Quate, C. F. *Appl. Phys. Lett.* **1991**, *58*, 1389−1391.
(219) Blumenthal, R.; Penner, R. M.; Heben, M. J.; Lewis, N. S. *AIP Conf. Proc.* **1991**, *241*.
(220) Li, W.; Hsiao, G. S.; Harris, D.; Nyffenegger, R. M.; Virtanen, J. A.; Penner, R. M. *J. Phys. Chem.* **1996**, *100*, 20103−20113.
(221) Li, W. J.; Virtanen, J. A.; Penner, R. M. *J. Phys. Chem.* **1992**, *96*, 6529−6532.
(222) Penner, R. M. *Scanning Microsc.* **1993**, *7*, 805−813.
(223) Li, W. J.; Virtanen, J. A.; Penner, R. M. *Appl. Phys. Lett.* **1992**, *60*, 1181−1183.
(224) Vaskevich, A.; Rosenblum, M.; Gileadi, E. *J. Electroanal. Chem.* **1995**, *383*, 167−174.
(225) Aberdam, D.; Salem, C.; Durand, R.; Faure, R. *Surf. Sci.* **1990**, *239*, 71−84.
(226) Ullmann, R.; Will, T.; Kolb, D. M. *Ber. Bunsen-Ges. Phys. Chem.* **1995**, *99*, 1414−20.
(227) Ullmann, R.; Will, T.; Kolb, D. M. *Chem. Phys. Lett.* **1993**, *209*, 238−42.
(228) Stimming, U.; Vogel, R.; Kolb, D. M.; Will, T. *J. Power Sources* **1993**, *43*, 169−180.
(229) Bard, A. J.; Denuault, G.; Lee, C. M.; Mandler, D.; Wipf, D. O. *Acc. Chem. Res.* **1990**, *23*, 357−363.
(230) Shohat, I.; Mandler, D. *J. Electrochem. Soc.* **1994**, *141*, 995−999.
(231) Bard, A. J.; Mirkin, M. V.; Unwin, P. R.; Wipf, D. O. *J. Phys. Chem.* **1992**, *96*, 1861−1868.
(232) Meltzer, S.; Mandler, D. *J. Electrochem. Soc.* **1995**, *142*, L82−L84.
(233) LaGraff, J. R.; Gewirth, A. A. *Mater. Res. Soc.* **1995**, 247−252.
(234) LaGraff, J. R.; Gewirth, A. A. *J. Phys. Chem.* **1994**, *98*, 11246.
(235) LaGraff, J. R.; Gewirth, A. A. *Surf. Sci.* **1995**, *326*, L461−6.
(236) Wuu, Y.-M.; Fan, R.-R.; Bard, A. J. *J. Electrochem. Soc.* **1989**, *136*, 885.
(237) Sasano, K.; Nakamura, K.; Kaneto, K. *Jpn. J. Appl. Phys. 2* **1993**, *32*, L863-L865.
(238) Yang, R.; Evans, D. F.; Hendrickson, W. A. *Langmuir* **1995**, *11*, 211−213.
(239) Yaniv, D. R.; McCormick, L. D. *Nanotechnology* **1992**, *3*, 44−47.
(240) Kranz, C.; Hiller, M.; Bauerle, P.; Gaub, H. E.; Schuhmann, W. 8th International Conference on Solid-State Sensors and Actuators and Eurosensors IX. *Dig. Tech. Pap.* **1995**, 506−8 (Vol. 1, (IEEE Cat. no.95TH8173).
(241) Borgwarth, K.; Ricken, C.; Ebling, D. G.; Heinze, J. *Ber. Bunsen-Ges. Phys. Chem.* **1995**, *99*, 1421−6.
(242) Nyffenegger, R. M.; Penner, R. M. *J. Phys. Chem.* **1996**, *100*, 17041−17049.
(243) Nyffenegger, R.; Ammann, E.; Siegenthaler, H.; Kötz, R.; O., H. *Electrochim. Acta* **1995**, *40*, 1411−1415.
(244) Barbero, C.; Kötz, R. *J. Electrochem. Soc.* **1994**, *141*, 859−865.
(245) Zeppenfeld, P.; Lutz, C. P.; Eigler, D. M. *Ultramicroscopy* **1992**, *42*−44, 128−133.
(246) Crommie, M. F.; Lutz, C. P.; Eigler, D. M. *Science* **1993**, *262*, 218−220.
(247) Stroscio, J. A.; Eigler, D. M. *Science* **1991**, *254*, 1319−1326.
(248) Meyer, G.; Neu, B.; Rieder, K. H. *Appl. Phys. A* **1995**, *A60*, 343−345.
(249) Meyer, G.; Neu, B.; Rieder, K. H. *Phys. Stat. Sol. B* **1995**, *192*, 313−24.
(250) Neu, B.; Meyer, G.; Rieder, R. H. *Mod. Phys. Lett. B* **1995**, *9*, 963−969.
(251) Whitman, L. J.; Stroscio, J. A.; Dragoset, R. A.; Celotta, R. J. *Science* **1991**, *251*, 1206−1210.
(252) Abeln, G. C.; Shen, T.-C.; Tucker, J. R.; Lyding, J. W. *Microelectron. Eng.* **1995**, *27*, 23−26.
(253) Shen, T.-C.; Wang, C.; Lyding, J. W.; Tucker, J. R. *Appl. Phys. Lett.* **1995**, *66*, 976−978.
(254) Lyding, J. W.; Abeln, G. C.; Shen, T.-C.; Wang, C.; Tucker, J. R. *J. Vac. Sci. Technol. B* **1994**, *12*, 3735−3740.
(255) Avouris, P. *Acc. Chem. Res.* **1994**, *27*, 159−165.
(256) Avouris, P.; Lyo, I.-W.; Hasegawa, Y. *J. Vac. Sci. Technol. A* **1993**, *11*, 1725−1732.
(257) Avouris, P.; Lyo, I.-W. *Appl. Surf. Sci.* **1992**, *60*−61, 426−436.
(258) Lyo, I.-W.; Avouris, P. *Science* **1991**, *253*, 173−176.
(259) Hasegawa, Y.; Avouris, P. *Science* **1992**, *258*, 1763−1765.
(260) Huang, D.; Uchida, H.; Aono, M. *Jpn. J. Appl. Phys. 2* **1994**, *33*, L190−L193.
(261) Grey, F.; Huang, D. H.; Kobayashi, A.; Snyder, E. J.; Uchida, H.; Aono, M. *J. Vac. Sci. Technol. B* **1994**, *12*, 1901−1905.
(262) Aono, M.; Kobayashi, A.; Grey, F.; Uchida, H.; Huang, D.-H. *Jpn. J. Appl. Phys. 1* **1993**, *32*, 1470−1477.
(263) Kobayashi, A.; Grey, F.; Williams, R. S.; Aono, M. *Science* **1993**, *259*, 1724−1726.
(264) Huang, D.; Uchida, H.; Aono, M. *Jpn. J. Appl. Phys. 1* **1992**, *31*, 4501−4503.
(265) Komeda, T.; Hasunuma, R.; Mukaida, H.; Tokumoto, H. *Appl. Phys. Lett.* **1996**, *68*, 3482−4.
(266) Iwatsuki, M.; Kitamura, S.; Sato, T.; Sueyoshi, T. *Appl. Surf. Sci.* **1992**, *60*, 580−6.
(267) Iwatsuki, M.; Kitamura, S.; Sato, T.; Sueyoshi, T. *Nanotechnology* **1992**, *3*, 137−141.
(268) Salling, C. T.; Kravchenko, I. I.; Lagally, M. G. *J. Vac. Sci. Technol. B* **1995**, *13*, 2828−2831.
(269) Salling, C. T.; Lagally, M. G. *Science* **1994**, *265*, 502−506.
(270) Gu, Q. J.; Liu, N.; Zhao, W. B.; Ma, Z. L.; Xue, Z. Q.; Pang, S. J. *Appl. Phys. Lett.* **1995**, *66*, 1747−1749.
(271) Ma, Z. L.; Liu, N.; Zhao, W. B.; Gu, Q. J.; Ge, X.; Xue, Q.; Pang, S. J. *J. Vac. Sci. Technol. B* **1995**, *13*, 1212−1215.
(272) Tsong, T. T.; Chang, C.-S. *Jpn. J. Appl. Phys. 1* **1995**, *34*, 3309−3318.
(273) Yong, L.; Packard, W. E.; Dow, J. D. *Superlattices Microstruct.* **1992**, *11*, 461−463.
(274) Sato, A.; Momose, S.; Tsukamoto, Y. *J. Vac. Sci. Technol. B* **1995**, *13*, 2832−2836.
(275) Sato, A.; Tsukamoto, Y. *Adv. Mater.* **1994**, *6*, 79−80.
(276) Sato, A.; Tsukamoto, Y. *Nature* **1993**, *363*, 431−432.
(277) Kado, H.; Tohda, T. *Appl. Phys. Lett.* **1995**, *66*, 2961−2962.
(278) Fayfield, T.; Higman, T. K. *J. Vac. Sci. Technol. B* **1995**, *13*, 1285−1289.
(279) Minne, S. C.; Soh, H. T.; Flueckiger, P.; Quate, C. F. *Appl. Phys. Lett.* **1995**, *66*, 703−705.
(280) Snow, E. S.; Campbell, P. M. *Science* **1995**, *270*, 1639−1641.
(281) Campbell, P. M.; Snow, E. S.; McMarr, P. J. *Appl. Phys. Lett.* **1995**, *66*, 1388−1390.
(282) Matsumoto, K.; Ishii, M.; Segawa, K.; Oka, Y.; Harris, J. S.; Vartanian, B. J. *Appl. Phys. Lett.* **1996**, *68*, 34−36.
(283) Matsumoto, K.; Takahashi, S.; Ishii, M.; Hoshi, M.; Kurokawa, A.; Ichimura, S.; Ando, A. *Jpn. J. Appl. Phys. 1* **1995**, *34*, 1387−1390.
(284) Barner, J. B.; Ruggiero, S. T. *Phys. Rev. Lett.* **1987**, *59*, 807−10.
(285) Van Bentum, P. J. M.; Smokers, R. T. M.; van Kempen, H. *Phys. Rev. Lett.* **1988**, *60*, 2543−6.
(286) Yamada, S.; Yamamoto, M. *Appl. Phys. Lett.* **1994**, *65*, 2600−2602.
(287) Roberts, C. J.; Wilkins, M. J.; Beamson, G.; Davies, M. C.; Jackson, D. E.; Scholes, P. D.; Tendler, S. J. B.; Williams, D. M. *Nanotechnology* **1992**, *3*, 98−110.
(288) Silva, L. A.; Laitenberger, P.; Palmer, R. E. *J. Vac. Sci. Technol. B* **1993**, *11*, 1992−1999.
(289) Wendel, M.; Kuhn, S.; Lorenz, H.; Kotthaus, J. P.; Holland, M. *Appl. Phys. Lett.* **1994**, *65*, 1775−1777.
(290) Wendel, M.; Lorenz, H.; Kotthaus, J. P. *Appl. Phys. Lett.* **1995**, *67*, 3732−3734.
(291) Wendel, M.; Lorenz, H.; Kotthaus, J. P.; Holland, M. *Solid-State Electron.* **1996**, *40*, 25−8.
(292) Bouju, X.; Joachim, C.; Girard, C. *Phys. Rev. B* **1994**, *50*, 7893−7902.
(293) Schaefer, D. M.; Reifenberger, R.; Patil, A.; Andres, R. P. *Appl. Phys. Lett.* **1995**, *66*, 1012−1014.
(294) Göbel, H.; van Blanckenhagen, P. *J. Vac. Sci. Technol. B* **1995**, *13*, 1247−1251.
(295) Goto, K.; Hane, K. *Rev. Sci. Instrum.* **1996**, *67*, 397−400.
(296) Harmer, M. A.; Fincher, C. R.; Parkinson, B. A. *J. Appl. Phys.* **1991**, *70*, 2760.
(297) Virtanen, J. A.; Suketu, P.; Huth, G. C.; Cho, Z. H. *J. Appl. Phys.* **1991**, *70*, 3376−3378.
(298) Chen, S.; Wang, L. M.; Jian, W. B.; Wang, S. Y.; Yang, H. C.; Horng, H. E. *J. Appl. Phys.* **1994**, *76*, 2535−2537.
(299) Volodin, A. P.; Aarts, J. *Physica C* **1994**, *235*−240, 1909−1910.
(300) Bogy, D. B. *J. Tribol.-Trans. ASME* **1992**, *114*, 493−398.
(301) Jung, T. A.; Moser, A.; Hug, H. J.; Brodbeck, D.; Hofer, R.; Hidber, H. R.; Schwarz, U. D. *Ultramicroscopy* **1992**, *42*−44, 1446−1451.
(302) Junno, T.; Deppert, K.; Montelius, L.; Samuelson, L. *Appl. Phys. Lett.* **1995**, *66*, 3627−3629.
(303) Maruno, S.; Inanaga, K. *Microelectron. Eng.* **1995**, *27*, 39−42.
(304) Maruno, S.; Inanaga, K.; Isu, T. *Appl. Phys. Lett.* **1993**, *63*, 1339−1341.

(305) Dumas, P.; Gu, M.; Syrykh, C.; Hallimaoui, A.; Salvan, F.; Gimzewski, J. K. *J. Vac. Sci. Technol. B* **1994**, *12*, 2067–2069.
(306) Sohn, L. L.; Willett, R. L. *Appl. Phys. Lett.* **1995**, *67*, 1552–1554.
(307) Yamamoto, S.-I.; Yamada, H.; Tokumoto, H. *Jpn. J. Appl. Phys. 1* **1995**, *34*, 3396–3399.
(308) Garnaes, J.; Bjørnholm, T.; Zasadzinski, J. A. N. *J. Vac. Sci. Technol. B* **1994**, *12*, 1839–1842.
(309) Fujihira, M.; Takano, H. *J. Vac. Sci. Technol. B* **1994**, *12*, 1860–1865.
(310) Demir, U.; Balasubramanian, K. K.; Cammarata, V.; Shannon, C. *J. Vac. Sci. Technol. B* **1995**, *13*, 1294–1299.
(311) Langmuir, I.; Schaefer, V. J. *J. Am. Chem. Soc.* **1937**, *59*, 1762–1763.
(312) Clavilier, J.; Faure, R.; Guinet, G.; Durand, R. *J. Electroanal. Chem.* **1980**, *107*, 205–209.
(313) Gorwadkar, S.; Vinogradov, G. K.; Senda, K.; Morita, S. *J. Appl. Phys.* **1995**, *78*, 2242–2247.
(314) Jin, X.; Unertl, W. N. *Appl. Phys. Lett.* **1992**, *61*, 657–659.
(315) Khurshudov, A.; Kato, K. *J. Vac. Sci. Technol. B* **1995**, *13*, 1938–1944.
(316) Vinogradov, G. K.; Gorwadkar, S.; Senda, K.; S., M. *Jpn. J. Appl. Phys. 1* **1994**, *33*, 6410–6414.
(317) Boschung, E.; Heuberger, M.; Dietler, G. *Appl. Phys. Lett.* **1994**, *64*, 3566–3568.
(318) Yano, T.; Nagahara, L. A.; Hashimoto, K.; Fujishima, A. *J. Vac. Sci. Technol. B* **1994**, *12*, 1596–1599.
(319) Nie, H.-Y.; Motomatsu, M.; Mizutani, W.; Tokumoto, H. *J. Vac. Sci. Technol. B* **1995**, *13*, 1163–1166.
(320) Garcia, R. *Appl. Phys. Lett.* **1994**, *64*, 1162–1164.
(321) Brandow, S. L.; Turner, D. C.; Ratna, B. R.; Gaber, B. P. *Biophys. J.* **1993**, *64*, 898–902.
(322) Hoen, S.; Mamin, H. J.; Rugar, D. *Appl. Phys. Lett.* **1994**, *64*, 267–269.
(323) Yau, S.-T.; Saltz, D.; Nayfeh, M. H. *Appl. Phys. Lett.* **1990**, *57*, 2913–2915.
(324) Yau, S.-T.; Saltz, D.; Nayfeh, M. H. *J. Vac. Sci. Technol. B* **1991**, *9*, 1371–1375.
(325) Christenson, G. L.; Miller, S. A.; Zhu, Z. H.; MacDonald, N. C.; Lo, Y. H. *Appl. Phys. Lett.* **1995**, *66*, 2780–2.
(326) Gorbunov, A. A.; Pompe, W. *Phys. Stat. Sol. A* **1994**, *145*, 333–338.
(327) *Surface enhanced Raman scattering*; Plenum Press: New York, 1982.
(328) Jersch, J.; Dickmann, K. *Appl. Phys. Lett.* **1996**, *68*, 868–870.
(329) Pohl, D. W.; Denk, W.; Lanz, M. *Appl. Phys. Lett.* **1984**, *44*, 651–653.
(330) Heinzelmann, H.; Pohl, D. W. *Appl. Phys. A* **1994**, *59*, 89–101.
(331) van Hulst, N. F.; Moers, M. H. P.; Bölger, B. *J. Microsc.* **1993**, *171*, 95–105.
(332) Smolyaninov, I. I.; Mazzoni, D. L.; Davis, C. C. *Appl. Phys. Lett.* **1995**, *67*, 3859–3861.
(333) Krausch, G.; Wegscheider, S.; Kirsch, A.; Bielefeldt, H.; Meiners, J. C.; Mlynek, J. *Opt. Commun.* **1995**, *119*, 283–8.
(334) Wegscheider, S.; Kirsch, A.; Mlynek, J.; Krausch, G. *Thin Sol. Films* **1995**, *264*, 264–7.
(335) Hosaka, S. *IEEE Trans. Magn.* **1996**, *32*, 1873–7.
(336) Hosaka, S.; Shintani, T.; Miyamoto, M.; Hirotsune, A.; Terao, M.; Yoshida, M.; Fujita, K.; Kammer, S. *Jpn. J. Appl. Phys 1* **1996**, *35*, 443–7.
(337) Imura, R.; Shintani, T.; Nakamura, K.; Hosaka, S. *Microelectron. Eng.* **1996**, *30*, 387–90.
(338) Massanell, J.; García, N.; Zlatkin, A. *Opt. Lett.* **1996**, *21*, 12–14.
(339) Froehlich, F. F.; Milster, T. D.; Uber, R. *Proc. SPIE* **1993**, *1751*, 312–320.
(340) Reddick, R. C.; Warmack, R. J.; Ferrell, T. L. *Phys. Rev. B* **1989**, *39*, 767–770.
(341) Lee, I.; Warmack, R. J.; Ferrell, T. L. *AIP Conf. Proc.* **1993**, *288*, 544–549.
(342) Dagata, J. A. Materials - Fabrication and Patterning at the Nanoscale, San Francisco, 1995; p 153–162.
(343) Pease, R. F. W. *Mater. Sci. Eng.* **1995**, *B35*, 188–191.
(344) Stulen, R. H. *IEEE J. Sed. Top. Quantum Electron.* **1995**, *1*, 970–975.
(345) Levenson, M. D. *Proc. SPIE* **1991**, *1496*, 544–551.
(346) Reichmanis, E.; Houlihan, F. M.; Nalamasu, O.; Neenan, T. X. *Adv. Mater. Opt. Elec.* **1994**, *4*, 83–93.
(347) *J. Vac. Sci. Technol. B* **1995**, *13*.
(348) de Lozanne, A. L.; W. F., S.; E. E., E. In *Nanolithography: a borderland between STM, EB, IB, and X-ray lithographies*; Gentili, M., Giovannella, C., Selci, S., Eds.; Kluwer Academic Publishers: Dordrecht, Boston, 1994.
(349) Jaklevic, R. C.; Elie, L. *Phys. Rev. Lett.* **1988**, *60*, 120–3.
(350) *Mater. Sci. Eng. B (Solid-State Mater. Adv. Technol.)* **1995**, *35*.
(351) Fendler, J. H.; Meldrum, F. C. *Adv. Mater.* **1995**, *7*, 607–32.
(352) Alivisatos, A. P. *Science* **1996**, *271*, 933–7.
(353) Danek, M.; Jensen, K. F.; Murray, C. B.; Bawendi, M. G. *Appl. Phys. Lett.* **1994**, *65*, 2795–7.
(354) Murray, C. B.; Nirmal, M.; Norris, D. J.; Bawendi, M. G. *Z. Phys. D: At., Mol. Clusters* **1993**, *26*, 231–3.
(355) Li, W. J.; Virtanen, J. A.; Penner, R. M. *J. Phys. Chem.* **1994**, *98*, 11751–11755.
(356) Lyding, J. W.; Shen, T.-C.; Hubacek, J. S.; Tucker, J. R.; Abeln, G. C. *Appl. Phys. Lett.* **1994**, *64*, 2010–2012.
(357) Wang, X.-D.; Rubel, S.; Purbach, U.; de Lozanne, A. To be submitted for publication.

CR960069I